

# Characterisation of the multi-scheme chemical ionisation inlet-2 and the detection of gaseous iodine species using bromide and nitrate chemical ionisation methods

Xu-Cheng He<sup>1,2</sup>, Jiali Shen<sup>1</sup>, Siddharth Iyer<sup>3</sup>, Paxton Juuti<sup>4</sup>, Jiangyi Zhang<sup>1</sup>, Mrisha Koirala<sup>5</sup>, Mikko M. Kytökari<sup>5</sup>, Douglas R. Worsnop<sup>1,6</sup>, Matti Rissanen<sup>3,5</sup>, Markku Kulmala<sup>1,7,8,9</sup>, Norbert M. Maier<sup>5</sup>, Jyri Mikkilä<sup>4</sup>, Mikko Sipilä<sup>1</sup>, and Juha Kangasluoma<sup>1,4</sup>

<sup>1</sup>Institute for Atmospheric and Earth System Research/Physics, Faculty of Science, University of Helsinki, 00014 Helsinki, Finland

<sup>2</sup>Finnish Meteorological Institute, 00560 Helsinki, Finland

<sup>3</sup>Aerosol Physics Laboratory, Faculty of Engineering and Natural Sciences, Tampere University, 33014 Tampere, Finland

<sup>4</sup>Karsa Ltd., 00560 Helsinki, Finland

<sup>5</sup>Department of Chemistry, Faculty of Science, University of Helsinki, 00014 Helsinki, Finland

<sup>6</sup>Aerodyne Research, Inc., Billerica, 01821 MA, USA

<sup>7</sup>Helsinki Institute of Physics, University of Helsinki, 00014 Helsinki, Finland

<sup>8</sup>Joint International Research Laboratory of Atmospheric and Earth System Sciences, School of Atmospheric Sciences, Nanjing University, 210023 Nanjing, China

<sup>9</sup>Aerosol and Haze Laboratory, Beijing Advanced Innovation Center for Soft Matter Science and Engineering, Beijing University of Chemical Technology, 100029 Beijing, China

**Correspondence:** Jiali Shen (jiali.shen@helsinki.fi) and Xu-Cheng He (xucheng.he@helsinki.fi)

**Abstract.** The multi-scheme chemical ionisation inlet 1 (MION1) ~~allows fast switching between measuring~~ enables rapid switching between the measurement of atmospheric ions without chemical ionisation and neutral molecules ~~by multiple using various atmospheric pressure~~ chemical ionisation methods. In this study, ~~the upgraded we introduce the upgraded version, the multi-scheme chemical ionisation inlet 2 (MION2) is presented.~~ The new design ~~features improved ion optics that increase the~~ incorporates enhanced ion optics, resulting in increased reagent ion concentration, ~~a generally more robust operation and the possibility to run ensuring a robust operation, and enabling the use of~~ multiple chemical ionisation methods with the same ionisation time.

~~To~~ In order to simplify the regular calibration of MION2, we developed an open-source flow reactor chemistry model ~~(MARFORCE) to quantify~~ called MARFORCE. This model enables quantification of the chemical production of sulfuric acid (H<sub>2</sub>SO<sub>4</sub>), hypiodous acid (HOI), and hydroperoxyl radical (HO<sub>2</sub>). MARFORCE simulates the convection-diffusion-reaction processes ~~inside occurring within~~ typical cylindrical flow reactors with uniform inner diameters. The model also ~~provides~~ includes options to simulate ~~the chemical processes~~ chemical processes in two scenarios: 1) when two flow reactors with different inner diameters are connected ~~together,~~ and 2) when two flows are merged into one ~~(connected by using a Y-shape tee), but,~~ although with reduced accuracy. ~~Additionally~~ Furthermore, the chemical mechanism files in the model are compatible ~~with the widely-used Master Chemical Mechanism,~~ thus allowing (MCM), allowing for future adaptation to simulate other chemical processes in flow reactors.

~~We further carried out detailed~~ Furthermore, we conducted a comprehensive characterisation of the bromide ( $\text{Br}^-$ ) and nitrate ( $\text{NO}_3^-$ ) chemical ionisation methods with different ionisation times. We ~~calibrated~~ performed calibration experiments for  $\text{H}_2\text{SO}_4$ ,  $\text{HOI}$ , and  $\text{HO}_2$  by combining gas kinetic experiments with the MARFORCE model. ~~Sulfur~~ The evaluation of sulfur dioxide ( $\text{SO}_2$ ), water ( $\text{H}_2\text{O}$ ), and molecular iodine ( $\text{I}_2$ ) ~~were evaluated using~~ involved dilution experiments from a gas cylinder ( $\text{SO}_2$ ), dew point mirror measurements ( $\text{H}_2\text{O}$ ), and a derivatization approach ~~in combination~~ combined with high-performance liquid chromatography quantification ( $\text{I}_2$ ), respectively. ~~We find~~

Our findings indicate that the detection limit is ~~negatively~~ inversely correlated with the fragmentation enthalpy of the analyte-reagent ion ( $\text{Br}^-$ ) cluster, ~~i. e., a~~. In other words, stronger binding (resulting in a larger fragmentation enthalpy) leads to a lower detection limit. Additionally, a moderately longer ~~reaction~~ ionisation time enhances the detection sensitivity ~~thus decreasing~~, thereby reducing the detection limit. For ~~example, the instance, when using the~~  $\text{Br}^-$  chemical ionisation method with a 300 ms ionisation time, the estimated detection limit for  $\text{H}_2\text{SO}_4$  is ~~estimated to be~~  $2.9 \times 10^4 \text{ molec. cm}^{-3}$  ~~with a 300 ms ionisation time. A direct comparison suggests that this is even better than~~. Notably, this detection limit is even superior to that achieved by the widely-used Eisele-type chemical ionisation inlet, ~~as revealed by direct comparisons~~.

While the  $\text{NO}_3^-$  chemical ionisation method ~~is generally more robust, we find~~ remains stable in the presence of high humidity, we have observed that the  $\text{Br}^-$  chemical ionisation method ( $\text{Br}^-$ -MION2) is significantly affected by air water content. Higher ~~air water content results in lower levels of air water lead to reduced~~ sensitivity for  $\text{HO}_2$  and  $\text{SO}_2$  ~~within under~~ the examined conditions. ~~On the other hand, a steep sensitivity drop of~~ However, we have found that a sharp decline in sensitivity for  $\text{H}_2\text{SO}_4$ ,  $\text{HOI}$ , and  $\text{I}_2$  ~~is only observed occurs only~~ when the dew point ~~is greater than exceeds~~  $0.5\text{-}10.5 \text{ }^\circ\text{C}$  (equivalent to ~~20-40 % RH; calculated at 25 °C hereafter~~). ~~Future studies utilising throughout this manuscript~~. For future studies utilising the atmospheric pressure  $\text{Br}^-$  chemical ionisation method, including  $\text{Br}^-$ -MION2, ~~should carefully address the humidity effect on a molecular basis it is crucial to carefully consider the molecular-level effects of humidity~~. By combining ~~methods such as approaches such as the~~ water-insensitive  $\text{NO}_3^-$ -MION2 with  $\text{Br}^-$ -MION2, MION2 ~~should be able to provide greater details of air composition than either of these methods can offer more comprehensive insights into the composition of atmospheric air than what can be achieved by either method alone~~.

~~Combining~~ By employing instrument voltage-scanning, chemical kinetic experiments, and quantum chemical calculations, we ~~find that the detection is not interfered with by iodine oxides under atmospherically relevant conditions. The~~ have conclusively established that the presence of iodine oxides does not interfere with the detection of  $\text{HIO}_3$ . Our comprehensive analysis reveals that the ions  $\text{IO}_3^-$ , ~~and ions measured~~  $\text{HIO}_3 \cdot \text{NO}_3^-$ , and  $\text{HIO}_3 \cdot \text{Br}^-$ , which are detected using the  $\text{Br}^-$  and  $\text{NO}_3^-$  chemical ionisation methods, are primarily, if not exclusively, ~~produced~~ generated from gaseous  $\text{HIO}_3$  molecules ~~within atmospherically relevant conditions~~.

## 1 Introduction

Chemical ionisation mass ~~spectrometer~~ spectrometry (CIMS) has been widely used in atmospheric chemistry and aerosol formation studies due to its versatility and high sensitivity in measuring trace level gaseous species (see e.g., Eisele and Tanner

50 (1993); Munson and Field (1966); Hansel et al. (1995); Huey (2007); Kirkby et al. (2011); Ehn et al. (2014); Lee et al. (2014); Berndt et al. (2016); Sipilä et al. (2016); Laskin et al. (2018); He et al. (2021b)). With chemical ionisation methods, an analyte is charged either by 1) receiving charge (proton, electron or ion) from the reagent ion or 2) forming a relatively stable cluster with the reagent ion. Mass spectrometers further measure the charged analyte-containing ions to obtain their molecular information.

55

Various chemicals have been ~~used to produce reagent ions; the most~~ employed as reagent ions in chemical ionisation methods. The commonly used reagent ions include nitrate ( $\text{NO}_3^-$ , Eisele and Tanner (1993)), acetate ( $\text{C}_2\text{H}_3\text{O}_2^-$ , Veres et al. (2008)), iodide ( $\text{I}^-$ , Caldwell et al. (1989)), hydronium ( $\text{H}_3\text{O}^+$ , Lagg et al. (1994)), and sporadically ~~also e.g.,~~ bromide ( $\text{Br}^-$ , Caldwell et al. (1989)) and ammonium ( $\text{NH}_4^+$ , Westmore and Alauddin (1986)). These reagent ions transfer charges to or form clusters with distinct subsets of ~~analytes of interest. The trace gases.~~ However, the detection of an analyte-containing ion is ~~additionally limited influenced~~ by its transmission through the ion optics of the mass spectrometers, since mass spectrometer's ion optics, as collision-induced cluster fragmentation ~~may remove the signature of the original analyte. A strongly bonded analyte-reagent ion cluster has a substantially higher chance to reach~~ can diminish the analyte's signature. Analyte-reagent ion clusters with strong bonds have a higher likelihood of reaching the detector compared to weakly bonded ones (Passananti et al., 2019) ~~Therefore, a smart selection of a clusters (Passananti et al., 2019). Hence, it is crucial to select a~~ chemical ionisation method that can maintain the signature of the analyte is desired ~~preserves the analyte's signature.~~ For example, the  $\text{NO}_3^-$ -CIMS has been widely used to detect sulfuric acid ( $\text{H}_2\text{SO}_4$ ) (Eisele and Tanner, 1993) and highly oxygenated organic molecules (Ehn et al., 2014).  $\text{I}^-$ -CIMS is regularly used to detect semi-volatile organic compounds (Lee et al., 2014), bromine and chlorine-containing species (Liao et al., 2014; Wang et al., 2019) and e.g., dinitrogen pentoxide ( $\text{N}_2\text{O}_5$ ) (Thornton et al., 2010).  $\text{C}_2\text{H}_3\text{O}_2^-$ -CIMS was used to detect small organic acids (Veres et al., 2008) and highly oxygenated organic compounds (Berndt et al., 2016). The bromide chemical ionisation method has recently been used to detect species such as  $\text{HO}_2$  (Sanchez et al., 2016) and  $\text{H}_2\text{SO}_4$  (Wang et al., 2021a). The detection of a series of halogenated species by the  $\text{Br}^-$  chemical ionisation method was first demonstrated by He (2017). Detailed characterisation of the  $\text{Br}^-$  chemical ionisation method utilising the multi-scheme chemical ionisation inlet 1 (MION1) was presented in several of our earlier studies (Wang et al., 2021a; Tham et al., 2021; He et al., 2021b). Multiple species were successfully calibrated using either analytical methods or inter-instrument comparison, including  $\text{H}_2\text{SO}_4$ ,  $\text{I}_2$ ,  $\text{Cl}_2$  and  $\text{HOI}$  (Tham et al., 2021; Wang et al., 2021a). Among the calibrated species,  $\text{H}_2\text{SO}_4$  and  $\text{I}_2$  were shown to be detected at the collision limit (highest sensitivity). Although  $\text{H}_2\text{SO}_4$  has been quantified using standard methods (Kürten et al., 2012), the quantification of the measured  $\text{I}_2 \cdot \text{Br}^-$  signal remains challenging. This is primarily contributed by two factors: 1) the current  $\text{Br}^-$ -MION1/2 have a detection upper limit of a few hundred pptv of  $\text{I}_2$ , beyond which the reagent ions get depleted and the measurement is non-linear, 2) on the contrary, spectroscopic and other methods could be limited by their high detection limits and may not be able to detect  $\text{I}_2$  at appropriate levels. Therefore, the key is to find sensitive methods to quantify gaseous  $\text{I}_2$  at tens to hundreds of pptv levels.

Ideally, ~~all of simultaneous measurement of all~~ the mentioned analytes ~~can be measured simultaneously by utilising all~~  
85 ~~of the could be achieved by employing their~~ corresponding CIMS methods ~~at the same time concurrently~~ in ambient obser-  
vations or ~~in~~ complex laboratory experiments. However, CIMS instruments are ~~expensive costly~~, and research institutes ~~are~~  
~~regularly limited by available instrumentation. An alternative approach is using often face limitations due to the availability of~~  
~~such instrumentation. As an alternative approach,~~ chemical ionisation inlets ~~capable of switching reagent ions that have the~~  
~~capability to switch between different reagent ions can be employed.~~ Many switchable systems have been developed previously,  
90 such as for proton transfer reaction mass spectrometers (Jordan et al., 2009; Breitenlechner et al., 2017; Pan et al., 2017) and  
other chemical ionisation mass spectrometers (Hearn and Smith, 2004; Smith and Španěl, 2005; Agarwal et al., 2014; Brophy  
and Farmer, 2015). A common feature of these techniques is using a reduced-pressure ion-molecule reaction chamber, thus  
unavoidably diluting the gas molecules of interest by orders of magnitude. While the detection limit of an instrument is also  
affected by other factors, it is commonly observed that chemical ionisation inlets operating at reduced pressures have higher  
95 limits of detection compared to atmospheric pressure chemical ionisation inlets. For instance, reduced pressure inlets reported  
detection limits of various organic compounds from sub-pptv (parts per trillion by volume) to hundreds of pptv levels (Lee  
et al., 2014; Brophy and Farmer, 2015), while the best-performing atmospheric pressure chemical ionisation inlets regularly  
detect vapours at ppqv (parts per quadrillion by volume) levels for selected acids and highly oxygenated organic vapours using  
the same time-of-flight mass spectrometer (Jokinen et al., 2012; Ehn et al., 2014; He et al., 2021b).

100

To ~~lower the limit of detection of~~ ~~reduce the detection limit of~~ switchable reagent ion chemical ionisation systems, we devel-  
oped the MION1 inlet, ~~which allows~~ for fast switching of reagent ion chemistry ~~operating~~ at atmospheric pressure (Rissanen  
et al., 2019). This technique has ~~mostly been deployed to detect~~ ~~predominantly been employed for the detection of~~ sulfuric  
acid and halogenated species using either ~~the~~  $\text{NO}_3^-$  or  $\text{Br}^-$  chemical ionisation methods (Rissanen et al., 2019; Tham et al.,  
105 2021; He et al., 2021b; Wang et al., 2021a; Finkenzeller et al., 2022).

~~However, the remaining problems of~~ ~~However, there are some remaining issues with the MION1 include 1) the~~. ~~Firstly, its~~  
limit of detection ~~of the MION1 is lower is higher~~ compared to another ~~widely commonly~~ used atmospheric pressure chemical  
ionisation inlet (~~noted as referred to as the~~ "Eisele inlet" ~~hereafter~~) (Eisele and Tanner, 1993; Jokinen et al., 2012; Wang et al.,  
2021a) ~~and 2) the ion-molecule reaction~~. ~~Secondly, the ionisation~~ times for different chemical ionisation methods ~~had have~~  
110 to be different ~~owing due~~ to the design ~~that~~, ~~which involves aligning and attaching~~ the chemical ionisation units ~~are aligned~~  
~~and attached at varying distances~~ on a cylindrical tube ~~at varying distances~~. ~~These problems could limit its applicability to the~~  
~~detection of~~. ~~These challenges may restrict its suitability for detecting~~ vapours at extremely low concentrations (e.g., at  $10^5$  to  
 $10^6$  molec.  $\text{cm}^{-3}$  or ~~5 to 50~~ ~~4 to 40~~ ppqv) and ~~the interpretation of the~~ ~~interpreting the~~ species detected by different chemical  
ionisation methods.

115

In this study, we ~~present an upgraded MION inlet (noted~~ ~~introduce an upgraded version of the MION inlet, referred to~~  
as "MION2" ~~hereafter~~) ~~which addresses these problems. Laboratory experiments were carried out to characterise~~, ~~which~~  
~~specifically addresses these issues. We conducted laboratory experiments to characterise the performance of~~ this inlet using

analytical methods and a newly-developed open-source kinetic model. As ~~halogen-anion-based~~ chemical ionisation methods (e.g., based on halogen anions (such as  $I^-$ )) are commonly ~~affected by air water content~~ influenced by the water content in the air (Kercher et al., 2009; Mielke et al., 2011; Woodward-Massey et al., 2014; Lee et al., 2014), we ~~additionally performed systematic examinations of~~ also systematically examined the impact of air water content on the detection of  $Br^-$ -MION2.

## 2 Methods

### 125 2.1 Characterisation of the MION2 inlet

The ionisation inlet ~~used in this paper~~ utilised in this study is the upgraded multi-scheme chemical ionisation inlet, MION2 (~~developed by~~ Karsa Ltd. ). ~~The inlet is designed to be capable of measuring~~ This inlet is specifically designed to enable the measurement of neutral molecules using chemical ionisation methods ~~and detecting~~ while also facilitating the detection of atmospheric ions by disabling chemical ionisation. It ~~allows fast~~ offers the capability of rapid switching between two or more (~~up to six~~) chemical ionisation methods ~~to selectively measure~~ , allowing for selective measurement of gaseous species at ambient pressure. ~~The inlet accommodates three bipolar ion sources per reaction time, which~~ Currently, the MION2 inlet supports up to six ion sources.

Due to the geometric limitations of the previous MION1 inlet, the different ionisation sources in MION1 have to employ different ionisation times. The ionisation time is defined by the sample flow rate and the distance ~~from~~ between the ion injection port ~~to and~~ the instrument pinhole (refer to Figure 1). ~~For the longer reaction~~ The improved geometry of the MION2 inlet overcomes this limitation, allowing for the operation of three bipolar ion sources per ionisation time, all positioned at the same distance from the pinhole. Additionally, for the longer ionisation time, the length of the connecting pipe between the sources can be adjusted, i.e., providing flexibility in modifying the ionisation time can be modified. Therefore, the new design of MION2 allows it to operate two chemical ionisation methods with the same ionisation time to allow a direct comparison which was not possible with the MION1.

In this study, we ~~deployed the~~ employed the MION2 inlet with two chemical ionisation methods (namely  $NO_3^-$  and  $Br^-$ ) ~~and two reaction times to understand the inlet characteristics~~ . ~~To clarify the different positions of the ionisation inlet, we refer to~~ , along with two different ionisation times (35 and 300 milliseconds, ms, respectively). This configuration was chosen to investigate the characteristics of the inlet. To facilitate clear referencing, we designate the ion source positioned 3 cm away from the mass spectrometer as tower 1 (T1), and the source while the source located 25 cm away from the mass spectrometer is referred to as tower 2 (T2) throughout the paper (this paper (see Figure 1).

150 ~~Supplementary Figure A1 presents~~ Figure A1 illustrates the conceptual schematic ~~for of~~ one of the ion sources ~~with~~ depicting the airflow and ion paths. The ~~whole entire~~ source is attached to ~~an electrically grounded a~~ 24 mm inner diame-

155 ter tube ~~with~~ that is electrically grounded. The sample flow, which is provided by a mass flow controller (MFC) connected to a vacuum pump, is set at a rate of 22.5 standard litres per minute (slpm) ~~sample flow, where the target molecules are charged.~~ The target molecules undergo ionisation by reacting with the reagent ions ( $\text{NO}_3^-$  or  $\text{Br}^-$ ). ~~In this case, the reaction time of the targeted~~

~~In this configuration, the ionisation time for the target molecules and charged reagent ions for tower 1 was ea-~~ is approximately 35 ms ~~, and for tower 2, for tower 1 and 300 ms -for tower 2.~~ A neutral reagent inflow is ~~a stream~~ introduced, which consists of nitrogen or air enriched with reagent vapour ~~(or~~. The reagent vapour is generated by passing nitrogen or air over liquid reagent (nitric acid,  $\text{HNO}_3$  ~~in this paper~~), which, or dibromomethane,  $\text{CH}_2\text{Br}_2$ , in this study). The resulting mixture is then fed into the ion source ~~and~~, where it is ionised by a soft ~~x-ray~~ X-ray source (Hamamatsu L12535, 4.9 keV). The charged reagent ions are ~~then guided by an electric field~~ guided into the sample flow ~~. The electric field inside by an electric field within the ion source is created with.~~ This electric field is generated using concentric stainless steel electrode plates with ~~different size orifices (diameters between orifices of different sizes (ranging from 5-10 mm ), added resistances between every two plates, and two~~ in diameter), with resistances placed between each pair of plates. Two high voltages (~~ea-~~ approximately 2500 V and 250 V) are used in the inlet. The lower of ~~these the~~ two voltages determines ~~if whether~~ the reagent ions pass through the ~~last final~~ orifice in the deflector electrode ~~into the sample flow, effectively turning the ionisation on and off, and enabling the fast,~~ effectively controlling the ionisation process and enabling the rapid switching between ion sources.

170 ~~Compared with~~ In contrast to the MION1 (Rissanen et al., 2019), ~~where the source reagent flow was defined by the neutral reagent inflow and the outflow (i.e., exhaust), design (Rissanen et al., 2019), which relied on the reagent inflow and exhaust flow to define the source reagent flow,~~ MION2 ~~has~~ incorporates an additional purge flow to prevent the sample flow from entering the ion source. The purge flow consists of the same nitrogen ~~, or synthetic air, that is used to create or air used to generate~~ the reagent flow. ~~The purge flow splits in two upon~~ Upon entering the ion source: ~~one preventing the sample from entering and the other keeping,~~ the purge flow splits into two streams: one stream prevents the sample flow from entering, while the other stream ensures that the neutral reagent ~~from entering does not enter~~ the sample flow. ~~With the~~

180 In MION2, the typical flow rates for the reagent, purge, and exhaust are 10, 100, and 50 standard cubic centimetres per minute (sccm), respectively. The reagent concentration in the ion source is estimated to be  $2 \times 10^{17} \text{ cm}^{-3}$ . This design ~~effectively addresses the challenges faced in MION1, one had to choose between possibly~~ where a compromise had to be made between the risk of contaminating the sample pipe with ~~the neutral reagent, or pulling neutral reagent or introducing~~ sample air into the ion source ~~potentially contaminating the ion source, e. g., it sometimes results in salt formation in the ion source or potentially results in uncontrolled ion chemistry within the inlet leading to detection biases, potentially leading to contamination or uncontrolled ion chemistry and resulting in detection biases.~~ In MION2, the water vapour and other contaminants in the sample flow do not have the opportunity to oxidise the surfaces of the electrodes inside the ion source. Such oxidation would result in reduced ion transmission from the ion source to the sample flow. Operational testing ~~in ambient~~

~~measurements indeed showed during ambient measurements has demonstrated~~ that MION2 ~~is significantly more stable than~~ exhibits significantly improved stability compared to MION1. ~~The~~ For example, recent measurements conducted at a coastal site in Finland involved the uninterrupted operation of MION2 for at least two months.

190

~~Additionally, the upgraded ion optics inside the ion sources in-of~~ MION2 have ~~been upgraded which increase the reagent ion transmission compared to the MION1 by about an~~ increased the transmission of reagent ions and the observed reagent ion concentration at the mass spectrometer by approximately one order of magnitude ~~-compared to MION1~~. This improvement was achieved by modifying the last electrode within the ion source to minimize ion residence time and reduce diffusion losses ~~of ions~~.

195

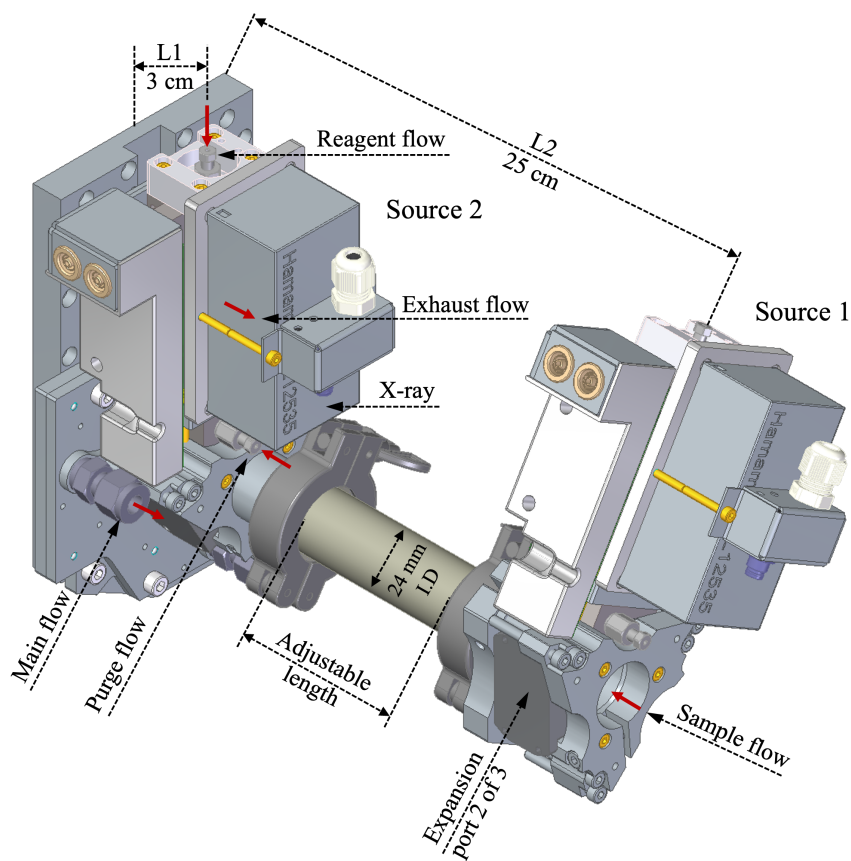


**Figure 1.** Schematic of the MION2 inlet illustrating its gas flows and ion paths. The new design increases the primary ion concentration and allows the operation of multiple chemical ionisation methods with the same ionisation time. L1 and L2 refer to the distances between the ion sources and the pinhole of the mass spectrometer. The exhaust flows are connected to two ports in the middle of the ion source.

## 2.2 Experimental setup

### 2.2.1 Calibration of inorganic species

~~In order to characterise~~ The experimental setup used for characterising the MION2 inlet ~~, we utilised an experimental setup~~  
200 ~~as shown is illustrated~~ in Figure A2, ~~which comprises three~~. It consists of three main sections: the flow reactor section, the  
MION2 chemical ionisation inlet (MION2)-section, and an Atmospheric Pressure interface Time-of-Flight mass spectrometer  
(APi-TOF, Aerodyne Inc., Junninen et al. (2010)).

The flow reactor section ~~consists of~~ includes a calibration source and ~~various~~ several gas feeds. Synthetic air (Woikoski OY,  
205 Finland; purity  $\geq 99.999\%$  with  $20.9\%$   $O_2$ ), nitrogen ( $N_2$ , Woikoski OY, Finland; purity  $\geq 99.999\%$ ), and sulfur dioxide  
( $SO_2$ , Air Products, USA;  $99.5\%$  purity) were injected by into the system using mass flow controllers (MFCs)-connected to  
standard gas cylinders or tanks ~~and they~~. These gases were pre-mixed before reaching the calibration source. ~~Molecular iodine~~  
~~(I<sub>2</sub>) was produced~~

210 I<sub>2</sub> was generated either from a homemade permeation tube or a commercial permeation tube (VICI Metronics) by blowing a  
A stream of nitrogen (50 millilitres-per-minute, mlpm) sccm) was passed over the permeation tube at controlled temperatures  
(ranging from 120 to 140 °C). The temperature of the permeation tubes was controlled by regulated using an electronically con-  
trolled heating mantle ~~to enable~~, allowing for adjustable yet stable iodine concentrations. Water vapour (H<sub>2</sub>O) was controlled  
by ~~an adjustable stream of nitrogen passing adjusting the flow of nitrogen~~ through a water bubbler, providing a controllable  
215 source of humidity.

The calibration source was mainly used to calibrate  $H_2SO_4$ ,  $HO_2$  and  $HOI$ . The  $H_2SO_4$  calibration ~~has been was~~ detailed in  
Kürten et al. (2012) and the  $HOI$  calibration ~~has been was~~ presented in Tham et al. (2021) and Wang et al. (2021a). ~~Briefly, a~~  
~~known amount of radical is produced by a mercury lamp (UVP Pen-Ray) in~~ The calibration source in the experimental setup  
220 was constructed using an aluminum box that encloses a 3-quarter-inch quartz tube. The quartz tube was chosen for its high  
transmission properties for ultra-violet (UV) light emitted from a mercury lamp. Adjacent to the quartz tube, the mercury  
lamp is housed in an aluminum block that contains a filter-covered hole. The filter used in the aluminum block allows for  
high transmission of 185 nm light emitted from the lamp. This specific wavelength of light is effective in photolysing H<sub>2</sub>O  
molecules, generating OH radicals.

225  
Before conducting the calibration experiment, a mixed flow of nitrogen (N<sub>2</sub>), oxygen (O<sub>2</sub>), H<sub>2</sub>O, and either SO<sub>2</sub> or I<sub>2</sub> was  
continuously passed through the calibration source ~~which further reacts with~~. This flow ensures that the source is thoroughly  
flushed with the desired gases and vapours, creating a controlled environment for subsequent calibration measurements. The  
produced OH radicals from the calibration source then undergo reactions with an excess amount of  $SO_2$  or a moderate amount  
230 of  $I_2$  to produce ~~either~~  $H_2SO_4$  or  $HOI$  as the final products. ~~As~~, respectively. Additionally, the  $HO_2$  radical is produced as a



by-product of the  $\text{H}_2\text{SO}_4$  calibration, calibration was simultaneously carried out at the calibration. The measured process.

To quantify the concentrations of  $\text{H}_2\text{SO}_4$ ,  $\text{HOI}$ , and  $\text{HO}_2$  were predicted using a numerical model adopting, an open-source Python library based on two-dimensional convection-diffusion-reaction equations was developed (Marine Atmospheric paRticle FORMation and ChEmistry, MARFORCE, Shen and He (2023)). This library aims to provide a framework for performing similar calibration tasks. Furthermore, it also allows users to simulate and predict concentrations of other chemical species by adopting different chemical reaction schemes. The MARFORCE library can be used as a tool in future research endeavours involving flow reactor chemistry simulations. As the numerical model needed to do the calibration is not yet available to the public, this study further develops an open-source Python library for such tasks (Shen and He, 2023).

240

The  $\text{SO}_2$  calibration is relatively straightforward and the calibrator source is not needed straightforward. The  $\text{SO}_2$  flow from the  $\text{SO}_2$  gas cylinder was diluted with humidified nitrogen and the mixed sample was fed into the inlet. The measured normalised  $\text{SO}_2 \cdot \text{Br}^-$  signal is was further compared with the estimated  $\text{SO}_2$  concentration to derive a calibration factor.

245

Absolute concentration was calibrated using To calibrate the absolute concentration of  $\text{H}_2\text{O}$ , a dew point mirror hygrometer (DewMaster Chilled Mirror Hygrometer, EdgeTec) was employed. The dew point mirror drew and measured a hygrometer drew a sample from a branch of the humidified flow before it entered the MION2 inlet tube. By measuring the dew point temperature, the dew point mirror hygrometer provides an accurate and reliable determination of the absolute  $\text{H}_2\text{O}$  concentration in the sample. This calibration method ensures precise measurement of  $\text{H}_2\text{O}$  concentration, which is important for accurate analysis and interpretation of the experimental data.

250

## 2.2.2 Calibration of molecular iodine

Although chemical ionisation method has been shown to be extremely sensitive in the molecular iodine ( $\text{I}_2$ ) detection (He, 2017; Wang et al., 2021), the quantification of the measured  $\text{I}_2 \cdot \text{Br}^-$  signal remains challenging. This is primarily contributed by two factors: 1) the current in  $\text{Br}^-$ -MION1/2 have a detection upper limit of a few hundred pptv of, beyond which the reagent ions get depleted and the measurement is non-linear, 2) on the contrary, spectroscopic and other methods could be limited by their high detection limits and may not be able to detect  $\text{I}_2$  at appropriate levels. Therefore, the key is to find sensitive methods to quantify gaseous at tens to hundreds of pptv level emitted from a permeation tube, which was regulated at a constant temperature and subjected to a continuous nitrogen stream (50 sccm).

260

The key to this calibration is determining the quantities of  $\text{I}_2$  emitted from the permeation tube. We have previously calibrated the  $\text{I}_2$  measurement of  $\text{Br}^-$ -MION1 using a cavity-enhanced differential optical absorption spectroscopy (CE-DOAS) instrument (Wang et al., 2021a), an UV/Vis spectrophotometer and an inductively coupled plasma mass spectrometer (ICP-MS) (Tham et al., 2021; Wang et al., 2021a). As none of these instruments is was available for this study, we further adapted

265 an alternative method.

The collection of the I<sub>2</sub> sample followed exactly the same procedure as described in our previous studies (Tham et al., 2021; Wang et al., 2021a). Briefly, 50 ~~standard cubic centimetres per minute (sccm)~~ sccm nitrogen carrier gas flow was passed through an I<sub>2</sub> permeation tube for 300 ~~min~~ minutes, under 120-140 °C. The nitrogen carrier stream containing the released I<sub>2</sub> was bubbled through an Schlenk-type impinger charged with 20 mL of hexane kept at -70 °C by a dry ice/acetone bath. After completion of the sampling process, the absorption flasks were allowed to warm to the ambient temperature and sealed with a Teflon-coated glass stopper. The solution was stored at 4 °C until further processing.

Inspired by Mishra et al. (2000), I<sub>2</sub> was converted into ~~an essentially a~~ non-volatile and stable derivative, followed by quantification of the latter using gas or liquid chromatography. Mishra et al. (2000) quantified I<sub>2</sub> in aqueous matrices by gas chromatography-mass spectrometry (GC/MS) after I<sub>2</sub> reacting with 2,6-dimethylaniline to form the corresponding 4-iodo-derivative.

An adaptation of this method was required as the iodine to be determined was diluted in hexane. Specifically, the iodine ~~derivatisation-derivatization~~ reaction was conducted directly with the hexane solutions in the presence of an aqueous buffer, to reduce losses associated with a hexane-to-water transfer. To avoid any losses of the volatile I<sub>2</sub> through evaporation, the reaction was conducted in hermetically sealed headspace vials, with efficient phase mass transfer being facilitated by vigorous magnetic stirring.

Control of the pH of the buffer was crucial for achieving high ~~derivatisation-derivatization~~ yields, with pH at 7.00 providing the most favourable level of conversion after 2 hours. Attempts to perform the ~~derivatisation-derivatization~~ reaction under homogeneous conditions in hexane in the presence of a variety of soluble organic bases (e.g., tertiary amines) returned poor yields and led to the formation of several side products, most probably due to iodine oxidation. Experiments using 1.00 mL aliquots of the I<sub>2</sub> sample solutions under investigation produced the derivative at the limit of detection, precluding a reliable quantification of the derivative by the reverse phase high-performance liquid chromatography (RP-HPLC/UV).

To improve the analytical sensitivity, 10 mL aliquots of the iodine sample solution were employed for ~~derivatisation-derivatization~~. To boost the sensitivity further, a high volume (15 μL) of the concentrated ~~derivatisation-derivatization~~ solution was injected into the HPLC system. Unfortunately, the hexane in the injection solution and the high injection volume gave rise to retention time instability and peak distortion. Subsequent optimisation of the chromatographic method provided robust reverse phase chromatographic conditions. Specifically, this was achieved by using relatively weakly eluting isocratic conditions for sample elution, followed by strongly eluting conditions for column cleaning and reconditioning. Using the fully optimised protocol, the derivative could be readily quantified for 0.17 to 11.05 μg mL<sup>-1</sup> initial iodine concentrations, with the LOD (limit of detection) and LOQ (limit of quantification) being 0.012 μg mL<sup>-1</sup> and 0.035 μg mL<sup>-1</sup>. Using this method, the hexane solution obtained

300 by absorption of iodine from the permeation tube was found to contain  $0.26 \mu\text{g iodine mL}^{-1}$ . Considering a total sample volume of 20 mL, the iodine output rate of the permeation tube under the employed conditions was calculated to be  $17.3 \text{ ng min}^{-1}$ .

It is worth noting that the sensitivity of the current method can be further improved by employing more sensitive separation and/or detection techniques, e.g., [liquid chromatography–mass spectrometry \(LC/MS\)](#) or GC/MS.

305

### 2.2.3 Humidity dependence of analyte detection

An ~~important part integral aspect~~ of the characterisation ~~is examining the impact~~ ~~involves investigating the influence~~ of water on the detection of MION2 when ~~utilising employing~~ the bromide chemical ionisation method. ~~Since is needed~~ ~~As water is essential~~ in the calibration source to ~~produce generate~~ OH radicals ~~which in turn produce~~, which subsequently yield either H<sub>2</sub>SO<sub>4</sub> or HOI, we ~~additionally added a dilution flow which joins after~~ ~~incorporated an additional dilution flow that merges with~~ the calibration source ~~using through~~ a Y piece (~~see refer to~~ Figure A3). This experimental ~~design enables changing the sample absolute humidity configuration allows for the alteration of the absolute humidity of the sample~~, independent of the OH production rate in the calibration source. During the experiments with varying humidity, the total flows of the dilution part and the flow reactor section were kept constant, while the relative humidity of the dilution flow was varied by mixing different combinations of dry and humidified flows. ~~In this way, we were able to keep the systematic errors, resulting from the mixing~~ ~~By employing this approach, we maintained a consistent level of systematic errors arising from the blending~~ of the dilution and sample flows, ~~constant~~. By comparing the relative signal intensities of analyte-containing ions, we could examine the influence of water on the detection of different analytes (e.g., H<sub>2</sub>SO<sub>4</sub>, HOI and HO<sub>2</sub>).

310  
315  
320

### 2.2.4 Quartz flow reactor setup

In order to study the sensitivity of Br<sup>-</sup>-MION2 to other oxidised iodine species, e.g., IO, OIO, HIO<sub>3</sub>, I<sub>2</sub>O<sub>3</sub>, I<sub>2</sub>O<sub>4</sub> and HIO<sub>2</sub>, a quartz flow reactor with an ~~outer diameter of 2.54~~ ~~inner diameter of 2.4~~ cm and a length of 94 cm was used. ~~The residence time inside the quartz tube was 8.5 s~~. A green LED, ~~with a wavelength of 528 nm~~, was hung on top and in parallel to the quartz flow reactor to initiate iodine ~~photo-chemistry~~ ~~photochemistry~~. In order to keep the temperature and light uniformity in the quartz flow reactor, the flow reactor was wrapped together with the green LED light by aluminium foil. The schematics of the setup are shown in ~~supplementary~~ Figure A4.

325

## 2.3 MARFORCE model description

As described above, calibration of H<sub>2</sub>SO<sub>4</sub>, HO<sub>2</sub>, and HOI requires a numerical model to simulate the chemical dynamics in the calibration source and inlet tube. This process can be simplified into a two-dimensional convection-diffusion-reaction prob-

330

lem. The concept of such a model was illustrated elsewhere (Kürten et al., 2012), specifically for the calibration of H<sub>2</sub>SO<sub>4</sub>. Our earlier studies also presented a numerical model for HOI calibration with similar principles but a simplified iodine chemistry scheme was instead implemented (Tham et al., 2021; Wang et al., 2021a). ~~However~~ Nevertheless, neither of these studies made ~~the calibration scripts openly available~~ their calibration scripts publicly accessible, and the scripts ~~are not flexible in~~ adopting ~~lack adaptability for~~ different chemistry schemes. ~~Therefore, we~~ Consequently, we have developed an open-source two-dimensional flow reactor model (~~MARFORCE~~, ~~Marine Atmospheric paRticle FORmation and ChEmistry~~) ~~for these tasks~~. ~~MARFORCE was named~~ MARFORCE to address these limitations. MARFORCE is built in Python and ~~is hosted in~~ GitHub (Shen and He, 2023). ~~Thus it can be freely accessed~~. ~~The model has two major~~ hosted on GitHub (Shen and He, 2023), allowing free access to interested users. The model comprises two main components: 1) the fluid dynamics simulation module and 2) the gas-phase ~~photo-chemistry module~~: photochemistry module.

### 2.3.1 Convection-diffusion-reaction equation

The ~~MARFORCE model utilises a two-dimensional~~ convection-diffusion-reaction equation ~~to simulate the fluid dynamics, photo-chemistry and chemical reactions in a cylindrical flow reactor~~. ~~The convection-diffusion-reaction equation~~ has been derived and discussed extensively in the literature (Gormley and Kennedy, 1948; Kürten et al., 2012) and is only briefly discussed here:

$$\frac{\partial c_i}{\partial t} = D_i \left( \frac{1}{r} \frac{\partial c_i}{\partial r} + \frac{\partial^2 c_i}{\partial r^2} + \frac{\partial^2 c_i}{\partial z^2} \right) - \frac{2Q}{\pi R^2} \left( 1 - \frac{r^2}{R^2} \right) \frac{\partial c_i}{\partial z} + P \quad (1)$$

where  $i$  corresponds to a specific chemical (e.g., H<sub>2</sub>SO<sub>4</sub>), the  $c_i$  is the concentration,  $D_i$  is the diffusion coefficient,  $r$  is the distance in the radial direction,  $R$  is the radius of the flow reactor,  $Q$  is the total flow in the flow reactor,  $z$  is the distance in the axial direction and  $P$  shows the production (positive values) or loss (negative values) rate due to chemical reactions. As the flow in tangential direction is symmetrical, the  $\frac{1}{r^2} \frac{\partial^2 c_i}{\partial \theta^2}$  term has been ignored.

The diffusion coefficient in the model can be defined in ~~two~~ three ways: 1) manually defined using experimental values ~~or~~ 2) calculated by kinetic theory or 3) calculated based on elemental composition using Fuller's method (Fuller et al., 1966).

The convection and diffusion processes were validated against a theoretical prediction by Alonso et al. (2016). A fixed amount of H<sub>2</sub>SO<sub>4</sub> was set at the first cross-section of the MARFORCE simulation and H<sub>2</sub>SO<sub>4</sub> was further carried to the outlet of a cylinder only by convection and diffusion processes. Comparing the H<sub>2</sub>SO<sub>4</sub> profiles at the outlet yields on average a 0.4 % difference between the MARFORCE model and the theoretical prediction by Alonso et al. (2016) (~~supplementary~~-Figure A5). This suggests that the convection and diffusion processes in the MARFORCE model are well simulated.

### 2.3.2 Gas-phase ~~photo-chemistry~~photochemistry

The photolysis and chemical reactions in the H<sub>2</sub>SO<sub>4</sub>, HO<sub>2</sub> and HOI calibrations can be simulated by a set of differential equations which describe the production and loss of various species. To make the MARFORCE model more versatile, the model was designed to accommodate the input file format from the Master Chemical Mechanism (MCM) (Jenkin et al., 1997; Saunders et al., 2003), a near-explicit chemistry mechanism for numerous organic precursors. The scripts used to compile and interpret MCM mechanisms were adapted from O'Meara et al. (2021). The input file extracted from MCM is reshaped and the reaction equations, reaction rate coefficients, reactants, products, their indices, and stoichiometric numbers are generated accordingly. The temperature and pressure dependence of reaction rate coefficients are taken into consideration. Finally, differential equations for each species based on its production and loss processes are produced and solved. Additionally, the MARFORCE model leaves an option to set abundant species as constants, so their concentrations are assumed uniform and homogeneous in the flow reactor. These species include, for example, (~~O<sub>2</sub>~~), N<sub>2</sub>, SO<sub>2</sub>, I<sub>2</sub>, and H<sub>2</sub>O in the H<sub>2</sub>SO<sub>4</sub> and HOI calibration experiments. With its flexibility, the MARFORCE model can be readily adapted to simulate organic oxidation or any other experiments using a laminar flow reactor.

375

There are two default chemistry schemes provided in the MARFORCE model and they are used for the H<sub>2</sub>SO<sub>4</sub> calibration and ~~the~~HOI calibration, respectively. The reaction rate coefficients utilised in these two schemes are tabulated in ~~supplementary~~ Table A1. The most important procedure of these calibration experiments is to ~~calculate~~obtain the OH concentration. The OH concentration is determined by the photon intensity produced by the calibration source (~~It-product~~~~, amount of photons per cross-section~~) and the absolute water content in the air passing through the calibration source. It-product refers to the product of UV light intensity at 185 nm and effective illumination time. In this study, we derived the It-product from the N<sub>2</sub>O experiment, which was conducted under the same conditions as the H<sub>2</sub>SO<sub>4</sub> calibration experiments. The details of the ~~It-product~~It-product determination can be found in Kürten et al. (2012). ~~Briefly~~In brief, the chemical actinometry method ~~utilising was employed, which involves~~ the conversion of N<sub>2</sub>O to NO<sub>x</sub> (primarily NO)~~is carried out,~~ to determine the light intensity. ~~As the~~Since NO is ~~less reactive compared with~~exhibits lower reactivity compared to OH and ~~it can easily be measured with~~can be conveniently measured using commercial NO<sub>x</sub> monitors, the ~~"It-product can therefore be derived."~~can be derived accordingly. Considering that the calibration experiment duration is relatively short (a few hours) compared to the potential lifetime of the mercury lamp, it is reasonable to assume that the attenuation of the It-product over time is negligible.

390 The OH initial concentration is further defined as

$$[\text{OH}] = \text{ItIt} \times \sigma_{\text{H}_2\text{O}} \times \Phi_{\text{H}_2\text{O}} \times [\text{H}_2\text{O}] \quad (2)$$

where  $\sigma_{\text{H}_2\text{O}}$  is the absorption cross-section of water vapour,  $7.22 \times 10^{-22} \text{ cm}^2$  (Creasey et al., 2000), and  $\Phi_{\text{H}_2\text{O}}$  is the quantum yield (unity in this case).

~~On top of the regular simulation of a~~ In addition to its ability to simulate a standard cylindrical flow reactor with a uniform size, the MARFORCE model also ~~has limited skills in~~ possesses limited capabilities in two specific conditions: 1) simulating ~~connected two two interconnected~~ flow reactors with ~~different sizes and varying sizes~~; the model is capable of simulating scenarios where two flow reactors of different sizes are connected. 2) simulating reactions when a dilution flow is merged with the sample flow through a ~~Y-shape tee~~. Y-shaped tee. These additional features enhance the versatility of the MARFORCE model, allowing for a more comprehensive analysis of complex flow reactor systems.

The first design aims to cope with the different sizes of the chemical ionisation inlet and the calibration source itself. For example, the MION2 inlet utilises a KF25 connector with an inner diameter of 24 mm while the ~~calibrator~~ calibration source utilises a 3/4" tube with an inner diameter of 15.6 mm. Our model considers an instantaneous transition between the tubes of different sizes, i.e., the chemical distributions at the last ~~grid~~ cross-section of the first cylinder are copied into the first ~~grid~~ cross-section of the second cylinder while the axial flow speed is adjusted to the cross-section of the second cylinder. As this simplification ignores the convective transport of species to the walls at the transition region, it likely gives the concentration upper limit at the pinhole of the mass spectrometer. Since the inner diameter difference between the calibration source and the MION2 inlet is relatively small in this study, we expect that the resulting uncertainty is well within the overall systematic uncertainty of -50/+100 %.

The second design considers that an additional dilution flow is utilised to reduce the sample water content when entering the Br<sup>-</sup>-MION2 inlet. Similarly, we assume an instantaneous transition at the spot where the dilution flow is added. In this case, both the chemical distribution and axial flow speed are changed since a new branch of flow is added. The simulation is carried out with a two-process procedure: before and after the dilution. First, we carry out a standard simulation before adding the dilution flow. Once the flow is fully developed and the chemical distribution reaches a steady state in the simulation, the last cross-section at the grid right before adding the dilution flow is stored and recalculated into the first cross-section of the next simulation. The second simulation is further carried out after considering the dilution flow, together with the changes in chemical distribution and axial flow speed.

It should be noted that the fluid dynamics processes are overly simplified in the second design and therefore, this option should be used with caution. In this study, this option is necessary only because investigating the detection humidity effect of e.g., H<sub>2</sub>SO<sub>4</sub>, HO<sub>2</sub> and HOI requires adding a dilution flow after the calibration source. In order to estimate the magnitude of error caused by the simplification of fluid dynamics, we carried out experiments comparing calibration results obtained with the first design (straight tube) and the second design (Y piece) and the results are shown in ~~supplementary~~ Figure A6. We find that the second design additionally introduces a 12 % higher calibration factor in the H<sub>2</sub>SO<sub>4</sub> calibration and a 27 % higher calibration factor in the HOI calibration, compared with the calibrations using the first design. Therefore, the application of

the second design for the purpose of this study is reasonable and does not introduce an excess amount of uncertainties. This  
430 mainly concerns the  $\text{H}_2\text{SO}_4$ ,  $\text{HO}_2$  and HOI calibration experiments.

## 2.4 Quantum chemical calculations

Cluster fragmentation enthalpies were calculated using quantum chemical methods. The initial conformational sampling was performed using the Spartan'18 program. The cluster geometry was then ~~optimized~~optimised using density function theory  
435 (DFT) methods at the  $\omega\text{B97X-D/aug-cc-pVTZ-PP}$  level of theory (Chai and Head-Gordon, 2008; Kendall et al., 1992). Iodine and bromine pseudopotential definitions were taken from the Environmental Molecular Sciences Laboratory (EMSL) basis set library (Feller, 1996; Peterson et al., 2003). Calculations were carried out using the Gaussian 16 program (Frisch et al., 2016). An additional coupled-cluster single-point energy correction at the DLPNO-CCSD(T)/def2-QZVPP (Riplinger and Neese, 2013; Riplinger et al., 2013; Weigend and Ahlrichs, 2005) level of theory was carried out on the lowest energy conformers to  
440 refine the DFT calculated enthalpies. The coupled-cluster calculation was performed using the ORCA program version 4.2.1 (Neese, 2012).

The master equation solver for multi-energy well reactions (MESMER) program was used to investigate the ionisation chemistry of  $\text{I}_2\text{O}_3 \cdot \text{HNO}_3\text{NO}_3^-$ . For the  $\text{I}_2\text{O}_3 \cdot \text{HNO}_3\text{NO}_3^-$  complex, Lennard-Jones potentials of  $\sigma = 6.5 \text{ \AA}$  and  $\epsilon = 300 \text{ K}$  were  
445 used, which are identical to those used previously for similar iodine systems (Gálvez et al., 2013). The MesmerILT method was used with a pre-exponential value of  $1.26 \times 10^{-9} \text{ cm}^3 \text{ molec}^{-1} \text{ s}^{-1}$ , which is equal to the  $\text{I}_2\text{O}_3 + \text{HNO}_3\text{NO}_3^-$  collision rate calculated using the average dipole orientation (ADO) method. ~~The method is described in detail by He et al. (2021a).~~ Varying the collision rate by a factor of 3 has no effect on the MESMER results, indicating that the reported final fragmentation rate coefficients of  $\text{I}_2\text{O}_3 \cdot \text{HNO}_3\text{NO}_3^-$  are not sensitive to the accuracy of the computed collision rate.

450

## 3 Results and Discussion

### 3.1 Calibration of $\text{H}_2\text{SO}_4$ , HOI and $\text{HO}_2$ using MARFORCE

Gaseous  $\text{H}_2\text{SO}_4$  concentration is regularly measured around the globe using the nitrate chemical ionisation method. In this study, a direct  $\text{H}_2\text{SO}_4$  calibration has been carried out for the MION2 inlet at tower 1 using either  $\text{Br}^-$  ( $\text{Br}^-$ -MION2-T1,  
455 [Figure A3](#)) or  $\text{NO}_3^-$  ( $\text{NO}_3^-$ -MION2-T1) chemical ionisation methods, and additionally at tower 2 with  $\text{Br}^-$  ( $\text{Br}^-$ -MION2-T2,  
[Figure A7](#)) chemical ionisation method. The MARFORCE model is utilised to simulate the evolution of various species at the cross-section of the inlet tube as shown in Figure 2. The predicted  $\text{H}_2\text{SO}_4$  concentrations are further compared with the measured normalised ratios to derive ~~calibrator~~calibration factors (Table 1).

**Table 1.** Calibration coefficients and detection limits for selected species measured by the MION2 inlet and Eisele-type inlet. It should be noted that ~~these~~ the reported numbers are specific to the experimental conditions and instrument tuning in our experiments. Different instrument tuning can ~~also~~ result in different calibration coefficients and detection limits. Undesired impurities may result in elevated detection limits despite the calibration coefficients being the same for the analytes. Therefore, these numbers should not be applied to another study without carrying out the same calibration experiments described in this study.

Species	Calibration coefficients (MION2)			Detection limit		Eisele inlet
	Tower 1		Tower 2	MION2 (Br <sup>-</sup> )	Tower 2 (160 ms)	
	(Ionisation Time = 35 ms)		(300 ms)	<u>Tower 1</u>		
	NO <sub>3</sub> <sup>-</sup>	Br <sup>-</sup>	Br <sup>-</sup>	<del>APi2(RH &lt; 0.1%)</del> <u>APi1(RH = 3.7%)</u>	<del>APi1(RH &lt; 0.1%)</del>	<del>APi1</del>
H <sub>2</sub> SO <sub>4</sub>	1.3 × 10 <sup>10</sup>	8.1 × 10 <sup>9</sup> (RH = 0.2-23.3%)	9.8 × 10 <sup>8</sup> (RH = 0.3-11.6%)	<del>a 8.5 × 10<sup>4</sup></del> <u>e 1 × 10<sup>5</sup></u>	<del>i f 2.9 × 10<sup>4</sup></del>	<del>l</del>
HOI	n/a	1.8 × 10 <sup>10</sup> (RH = 3-17%)	5.1 × 10 <sup>9</sup> (RH = 3-17%)	<del>a 2.2 × 10<sup>5</sup></del> <u>f b 5.9 × 10<sup>5</sup></u>	<del>i g 1.6 × 10<sup>5</sup></del>	
HIO <sub>3</sub>	n/a	n/a	n/a	<del>a 8.0 × 10<sup>4</sup></del> <u>e 1.3 × 10<sup>5</sup></u>	n/a	<del>l</del>
HO <sub>2</sub>	n/a	2.8 × 10 <sup>11</sup> (RH = 2.5%)	1.2 × 10 <sup>11</sup> (RH = 2.7%)	<del>b 5.2 × 10<sup>5</sup></del> <u>g c 3.3 × 10<sup>6</sup></u> (RH = 2.7%)	<del>h k 5.7 × 10<sup>5</sup></del> (RH = 0.3%)	
SO <sub>2</sub>	n/a	2.6 × 10 <sup>16</sup> (RH = 10%)	2.1 × 10 <sup>16</sup> (RH = 9.9%)	<del>c 9.4 × 10<sup>7</sup></del> <u>h d 1.8 × 10<sup>9</sup></u> (RH = 0.5%)	n/a	
I <sub>2</sub>	n/a	8.2 × 10 <sup>9</sup> (RH = 26-37%)	n/a	<del>d 6.7 × 10<sup>5</sup></del> <u>e 3.3 × 10<sup>5</sup></u>	n/a	
IO	n/a	n/a	n/a	<del>a 3 × 10<sup>4</sup></del> <u>e 1.6 × 10<sup>5</sup></u>	<del>i f 2.5 × 10<sup>4</sup></del>	
OIO	n/a	n/a	n/a	<del>a 3.4 × 10<sup>5</sup></del> <u>b 2.0 × 10<sup>5</sup></u>	<del>e 2 × 10<sup>5</sup></del> <u>i f 3.1 × 10<sup>4</sup></u>	
I <sub>2</sub> O <sub>2</sub>	n/a	n/a	n/a	<del>a 7.9 × 10<sup>4</sup></del> <u>e 1.9 × 10<sup>5</sup></u>	<del>i f 3.5 × 10<sup>4</sup></del>	
I <sub>2</sub> O <sub>3</sub>	n/a	n/a	n/a	<del>a 4.9 × 10<sup>4</sup></del> <u>e 1.9 × 10<sup>5</sup></u>	<del>i f 4.2 × 10<sup>4</sup></del>	
I <sub>2</sub> O <sub>4</sub>	n/a	n/a	n/a	<del>a 5.1 × 10<sup>4</sup></del> <u>e 1.9 × 10<sup>5</sup></u>	<del>i f 3.0 × 10<sup>4</sup></del>	
I <sub>2</sub> O <sub>5</sub>	n/a	n/a	n/a	<del>a 2.5 × 10<sup>5</sup></del> <u>b 2 × 10<sup>5</sup></u>	<del>e 2.0 × 10<sup>5</sup></del> <u>i f 3.7 × 10<sup>4</sup></u>	

Unit: molec. cm<sup>-3</sup> cps cps<sup>-1</sup>; "n/a" refer to "not available"; Experiments were conducted at room temperature. H<sub>2</sub>SO<sub>4</sub> calibration factor is applied to estimate the detection limits for the species w. Since other molecules may not be detected at the kinetic limit, their LODs are mere estimations. The detection limits are estimated with 1-min data and one-hour data collection time. The RH reported at 25 °C. The calibration factors and LODs have a systematic error of a factor of two (-50 %/+100 %).

Calibration factors used for the LOD calculation are: a. 8.1 × 10<sup>9</sup>, b. 1.8 × 10<sup>10</sup>, c. 2.8 × 10<sup>11</sup>, d. 1.03 × 10<sup>14</sup>, e. 8.2 × 10<sup>9</sup>, f. 9.8 × 10<sup>8</sup>, g. 5.1 × 10<sup>9</sup>, h. 4.1 × 10<sup>10</sup>, i. 3.5 × 10<sup>9</sup>.



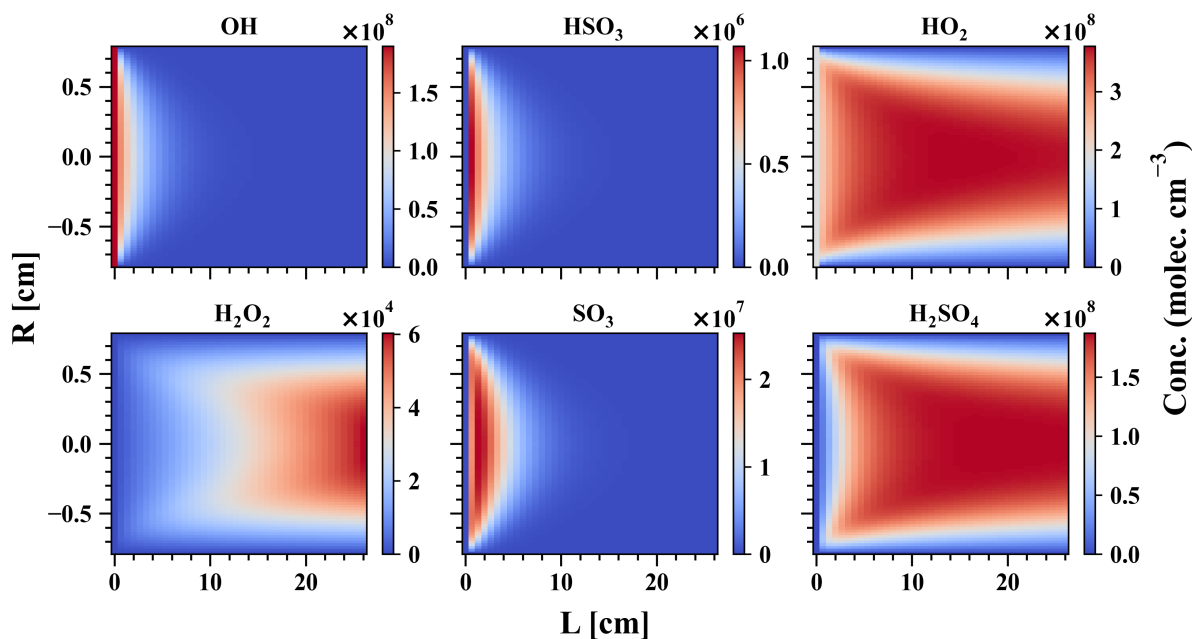


**Figure 2.** MARFORCE simulation results of the a  $\text{H}_2\text{SO}_4$  calibration experiment. The x-axis shows the distance from the UVP pen-ray lamp to the instrument pinhole-entrance of the chemical ionisation chamber and the y-axis shows the distance in the radial direction. Conditions for the simulation:  $R = 0.78$  cm,  $L = 26$  cm, sample flow = 10.6 slpm,  $[\text{SO}_2] = 5.78 \times 10^{13} \text{ cm}^{-3}$ ,  $[\text{O}_2] = 2.42 \times 10^{16} \text{ cm}^{-3}$  and  $[\text{H}_2\text{O}] = 2.8 \times 10^{16} \text{ cm}^{-3}$ .

460 The derived calibration factor of for  $\text{Br}^-$ -MION2-T1 ( $8.1 \times 10^9$ ) is roughly-approximately eight times higher than that of  $\text{Br}^-$ -MION2-T2 ( $9.8 \times 10^8$ ). This observation is consistent with the fact that the ionisation time from tower 2 to the pinhole (ea-around 300 ms) is approximately-roughly 8.6 times longer than that of tower 1 (35 ms). Longer ionisation time results in a larger fraction-A longer ionisation time leads to a greater conversion of  $\text{Br}^-$  and  $\text{H}_2\text{O} \cdot \text{Br}^-$  being converted to-into  $\text{H}_2\text{SO}_4 \cdot \text{Br}^-$  or  $\text{HSO}_4^-$ , thus-resulting in a lower calibration factor.As for the-

465

In the case of  $\text{NO}_3^-$ -MION2-T1, it achieves-exhibits a similar sensitivity as-the-to  $\text{H}_2\text{SO}_4$  detection as  $\text{Br}^-$ -MION2-T1 for detection-This-. This similarity is likely due to the fact-that-the ionisation time was kept constant-(consistent ionisation time (using tower 1 was used)-and-both-) for both methods, since both the  $\text{NO}_3^-$  and  $\text{Br}^-$  chemical ionisation methods measure  $\text{H}_2\text{SO}_4$  at the collision limit, as mentioned in previous studies (Kürten et al., 2012; Wang et al., 2021a).

470

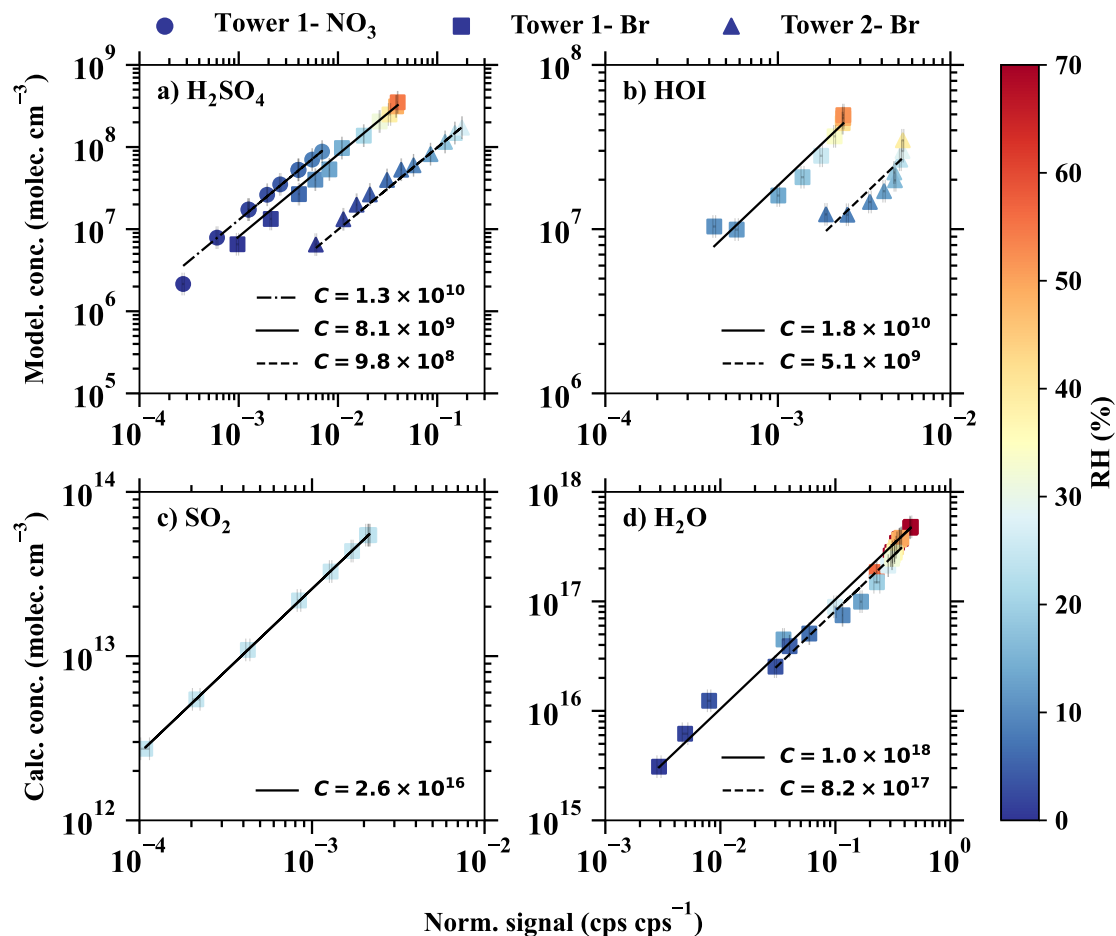


**Figure 3.** The modelled or calculated vapour concentrations vs. the normalised signals for a) H<sub>2</sub>SO<sub>4</sub>, b) HOI, c) SO<sub>2</sub>, d) H<sub>2</sub>O. The dashed-dotted, solid, and dashed lines are the linear fits of the results from different inlet modes: 1) tower 1 with the NO<sub>3</sub><sup>-</sup> chemical ionisation method, 2) tower 1 with the Br<sup>-</sup> chemical ionisation method, and tower 2 with the Br<sup>-</sup> chemical ionisation method. The slopes of the fitted lines represent the calibration coefficients, shown in the legend. The colour bar shows the relative humidity in the calibration experiments.

Sanchez et al. (2016) has reported that the [bromide chemical ionisation mass spectrometer \(Br<sup>-</sup>-CIMS\)](#) is capable of detecting HO<sub>2</sub> radicals at ambient relevant concentrations. In this study, we calibrated HO<sub>2</sub> together with H<sub>2</sub>SO<sub>4</sub>, as HO<sub>2</sub> is a by-product in the chemical production of H<sub>2</sub>SO<sub>4</sub> (see [supplementary-Table A1](#)). As the binding of HO<sub>2</sub> with Br<sup>-</sup> is significantly weaker than that of H<sub>2</sub>SO<sub>4</sub> with Br<sup>-</sup>, the collision induced fragmentation of HO<sub>2</sub>·Br<sup>-</sup> in the ion-optics of the mass spectrometer is larger (Passananti et al., 2019). Additionally, as the humidity effect of HO<sub>2</sub> will be shown to be strong in [a section below section 3.3](#), the calibration coefficient of HO<sub>2</sub> has to be derived with respect to a specific humidity level. The derived HO<sub>2</sub> calibration factors at 2.5 - 2.7 % RH (25 °C) are 2.8 × 10<sup>11</sup> and 1.2 × 10<sup>11</sup>, respectively, for Br<sup>-</sup>-MION2-T1 and

Br<sup>-</sup>-MION2-T2 (Table 1).

480 The HOI calibration was also carried out using the H<sub>2</sub>SO<sub>4</sub> calibration source, except that the SO<sub>2</sub> source was replaced with an I<sub>2</sub> source. ~~The calibration procedure was described in greater detail in our earlier studies (Tham et al., 2021; Wang et al., 2021a) . While the calibration experiment remains the same, the MARFORCE model in this study utilises a complete set of iodine chemistry thus producing a more accurate calibration factor for HOI (supplementary Table A1). We estimate that the HOI concentration using the MARFORCE model is only 0.1–0.7% lower compared to our earlier model which only considers the~~  
485 ~~essential steps of the HOI formation.~~ As can be seen in Figure 3 and Table 1, the calibration factor for HOI is roughly two times that of H<sub>2</sub>SO<sub>4</sub>. This suggests that HOI is detected at close to the collision limit. It is worth noting that we find instrument setting affects HOI detection significantly since HOI is not strongly bonded to Br<sup>-</sup>. The preferred fragmentation pathway is HOI·Br<sup>-</sup> → HOI + Br<sup>-</sup> (Table 2), and thus a fraction of HOI·Br<sup>-</sup> ~~lose the signature of dissociates into~~ HOI and Br<sup>-</sup> after passing the ion optics of ~~our the~~ mass spectrometer. A more fragmentation-oriented setting can result in a higher fraction of  
490 HOI·Br<sup>-</sup> getting lost in the ion optics, thus resulting in a higher calibration factor, i.e., lower sensitivity. As an example, in our earlier studies (Tham et al., 2021; Wang et al., 2021a), we used a relatively fragmenting setting ~~was used in our earlier studies compared to the one used in this study~~ in an attempt to reduce (H<sub>2</sub>O)<sub>n</sub>·Br<sup>-</sup> clusters and other water-associated clusters ~~which complicated the mass spectra (Tham et al., 2021; Wang et al., 2021a). Such a setting resulted in an eight times higher . This experimental setup led to a~~ calibration factor for HOI ~~than that for and it cannot be explained by iodine chemistry schemes used~~  
495 ~~in the calibration scripts nor by any differences in the experimental conditions. that was eight times higher than the calibration factor for H<sub>2</sub>SO<sub>4</sub>.~~

### 3.2 Calibration of H<sub>2</sub>O and SO<sub>2</sub>

H<sub>2</sub>O·Br<sup>-</sup> is a regular peak and one of the primary ions measured by the Br<sup>-</sup>-~~CIMS-MION2~~. Br<sup>-</sup>-~~CIMS-MION2~~ is, therefore,  
500 able to measure absolute water content if the H<sub>2</sub>O·Br<sup>-</sup> signal is calibrated against a dew point mirror instrument. Such a calibration has at least two purposes: 1) the calibrated H<sub>2</sub>O·Br<sup>-</sup>:Br<sup>-</sup> can be used as an indicator of the fragmentation level of the Br<sup>-</sup>-~~CIMS-MION2~~ and 2) ~~CIMS can be more sensitive to compared with~~ compared to regular relative humidity sensors and dew point mirrors, Br<sup>-</sup>-MION2 exhibits higher sensitivity towards H<sub>2</sub>O. In this study, the calibration of H<sub>2</sub>O was calibrated both for the performed for both Br<sup>-</sup>-MION-T1 and Br<sup>-</sup>-MION-T2 ~~as shown, as illustrated~~ in Figure 3. ~~The Interestingly,~~  
505 the calibration factors for both ~~of the towers do not differ from each other likely due to the towers did not show significant differences. This can be attributed to the presence of an~~ excess amount of H<sub>2</sub>O ~~which establishes an, which establishes a rapid equilibrium with Br<sup>-</sup> and H<sub>2</sub>O·Br<sup>-</sup> rapidly regardless irrespective~~ of the ionisation time.

As a reasonable binding enthalpy of SO<sub>2</sub>·Br<sup>-</sup> was predicted using quantum chemical calculations (Table 2), we continued to  
510 check whether the Br<sup>-</sup>-MION2 allows us to detect SO<sub>2</sub>. A variable amount of SO<sub>2</sub> was mixed with a fixed amount of dilution flow at a constant relative humidity (RH, 10 %) which was measured by the Br<sup>-</sup>-MION2. Clear SO<sub>2</sub>·Br<sup>-</sup> was measured and it

**Table 2.** Fragmentation enthalpies (the opposite of binding enthalpies) of analytes with the  $\text{Br}^-$ . The cluster geometry was optimised at the  $\omega\text{B97X-D/aug-cc-pVTZ-PP}$  level of theory at 298.15 K (Chai and Head-Gordon, 2008; Kendall et al., 1992). The enthalpies were calculated at the  $\text{DLPNO-CCSD(T)/def2-QZVPP}$  at 298.15 K

Cluster fragmentation pathway	Fragmentation enthalpies ( $\text{kcal mol}^{-1}$ )
$\text{I}_2 \cdot \text{Br}^- \longrightarrow \text{I}_2 + \text{Br}^-$	33.3
$\text{I}_2 \cdot \text{H}_2\text{OBr}^- \longrightarrow \text{I}_2 \cdot \text{Br}^- + \text{H}_2\text{O}$	8.0
$\text{IO} \cdot \text{Br}^- \longrightarrow \text{IO} + \text{Br}^-$	24.5
$\text{IO} \cdot \text{H}_2\text{OBr}^- \longrightarrow \text{IO} + \text{H}_2\text{O} \cdot \text{Br}^-$	21.3
$\text{IO} \cdot \text{H}_2\text{OBr}^- \longrightarrow \text{IO} \cdot \text{Br}^- + \text{H}_2\text{O}$	9.9
$\text{OIO} \cdot \text{Br}^- \longrightarrow \text{OIO} + \text{Br}^-$	23.2
$\text{OIO} \cdot \text{H}_2\text{OBr}^- \longrightarrow \text{OIO} + \text{H}_2\text{O} \cdot \text{Br}^-$	22.1
$\text{OIO} \cdot \text{H}_2\text{OBr}^- \longrightarrow \text{OIO} \cdot \text{Br}^- + \text{H}_2\text{O}$	11.9
$\text{I}_2\text{O}_3 \cdot \text{Br}^- \longrightarrow \text{IO}_3^- + \text{IBr}$	24.6
$\text{I}_2\text{O}_4 \cdot \text{Br}^- \longrightarrow \text{I}_2\text{O}_4 + \text{Br}^-$	42.6
$\text{I}_2\text{O}_4 \cdot \text{H}_2\text{OBr}^- \longrightarrow \text{I}_2\text{O}_4 + \text{H}_2\text{O} \cdot \text{Br}^-$	48.8
$\text{I}_2\text{O}_4 \cdot \text{H}_2\text{OBr}^- \longrightarrow \text{I}_2\text{O}_4 \cdot \text{Br}^- + \text{H}_2\text{O}$	10.5
$\text{HIO}_3 \cdot \text{Br}^- \longrightarrow \text{IO}_3^- + \text{HBr}$	<sup>a</sup> 29.9
$\text{HIO}_3 \cdot \text{Br}^- \longrightarrow \text{HIO}_3 + \text{Br}^-$	<sup>a</sup> 35.7
$\text{HIO}_3 \cdot \text{H}_2\text{OBr}^- \longrightarrow \text{HIO}_3 + \text{H}_2\text{O} \cdot \text{Br}^-$	33.1
$\text{HIO}_3 \cdot \text{H}_2\text{OBr}^- \longrightarrow \text{HIO}_3 \cdot \text{Br}^- + \text{H}_2\text{O}$	11.2
$\text{HIO}_3 \cdot \text{H}_2\text{OBr}^- \longrightarrow \text{IO}_3 \cdot \text{H}_2\text{O}^- + \text{HBr}$	26.7
$\text{HIO}_2 \cdot \text{Br}^- \longrightarrow \text{HIO}_2 + \text{Br}^-$	<sup>b</sup> 29.2
$\text{HIO}_2 \cdot \text{H}_2\text{OBr}^- \longrightarrow \text{HIO}_2 + \text{H}_2\text{O} \cdot \text{Br}^-$	15.5
$\text{HIO}_2 \cdot \text{H}_2\text{OBr}^- \longrightarrow \text{HIO}_2 \cdot \text{Br}^- + \text{H}_2\text{O}$	1.3
$\text{HIO}_2 \cdot \text{H}_2\text{OBr}^- \longrightarrow \text{IO}_2 \cdot \text{H}_2\text{O}^- + \text{HBr}$	27.4
$\text{HOI} \cdot \text{Br}^- \longrightarrow \text{HOI} + \text{Br}^-$	<sup>b</sup> 26.9
$\text{HOI} \cdot \text{H}_2\text{OBr}^- \longrightarrow \text{HOI} + \text{H}_2\text{O} \cdot \text{Br}^-$	22.9
$\text{HOI} \cdot \text{H}_2\text{OBr}^- \longrightarrow \text{HOI} \cdot \text{Br}^- + \text{H}_2\text{O}$	9.6
$\text{HOI} \cdot \text{H}_2\text{OBr}^- \longrightarrow \text{IO} \cdot \text{H}_2\text{O}^- + \text{HBr}$	48.4
$\text{H}_2\text{O} \cdot \text{Br}^- \longrightarrow \text{H}_2\text{O} + \text{Br}^-$	13.2
$\text{HO}_2 \cdot \text{Br}^- \longrightarrow \text{HO}_2 + \text{Br}^-$	23.1
$\text{H}_2\text{SO}_4 \cdot \text{Br}^- \longrightarrow \text{HSO}_4^- + \text{HBr}$	<sup>b</sup> 27.9
$\text{H}_2\text{SO}_4 \cdot \text{H}_2\text{OBr}^- \longrightarrow \text{H}_2\text{SO}_4 + \text{H}_2\text{O} \cdot \text{Br}^-$	36.1
$\text{H}_2\text{SO}_4 \cdot \text{H}_2\text{OBr}^- \longrightarrow \text{H}_2\text{SO}_4 \cdot \text{Br}^- + \text{H}_2\text{O}$	8.2
$\text{H}_2\text{SO}_4 \cdot \text{H}_2\text{OBr}^- \longrightarrow \text{HSO}_4 \cdot \text{H}_2\text{O}^- + \text{HBr}$	22.0
$\text{SO}_2 \cdot \text{Br}^- \longrightarrow \text{SO}_2 + \text{Br}^-$	19.4

<sup>a</sup>the fragmentation enthalpy is updated from Wang et al. (2021a) as a lower energy  $\text{HIO}_3 \cdot \text{Br}^-$  cluster geometry, which has an additional Br-I interaction, has been located in this study (see Figure A8). <sup>b</sup>Value adopted from Wang et al. (2021a).

increased linearly with the  $\text{SO}_2$  concentration in the sample flow (Figure 3). However, the calibration factor of  $\text{SO}_2$  is roughly six orders of magnitude higher than that of  $\text{H}_2\text{SO}_4$  at 10 % ~~relative humidity (RH)~~RH. This is consistent with the weaker binding of  $\text{SO}_2 \cdot \text{Br}^-$  compared with  $\text{H}_2\text{SO}_4 \cdot \text{Br}^-$ . Additionally,  $\text{SO}_2$  calibration is extremely sensitive to RH changes as can be seen in Figure 4. ~~The best detection limit achieved in this study is~~In this study, the best achieved detection limit was  $9.4 \times 10^7 \text{ cm}^{-3}$  at an RH below 0.1 %RH and theoretically. Theoretically, it is ~~feasible to further increase the sensitivity by reducing~~possible to enhance the sensitivity even further by reducing the absolute water content.

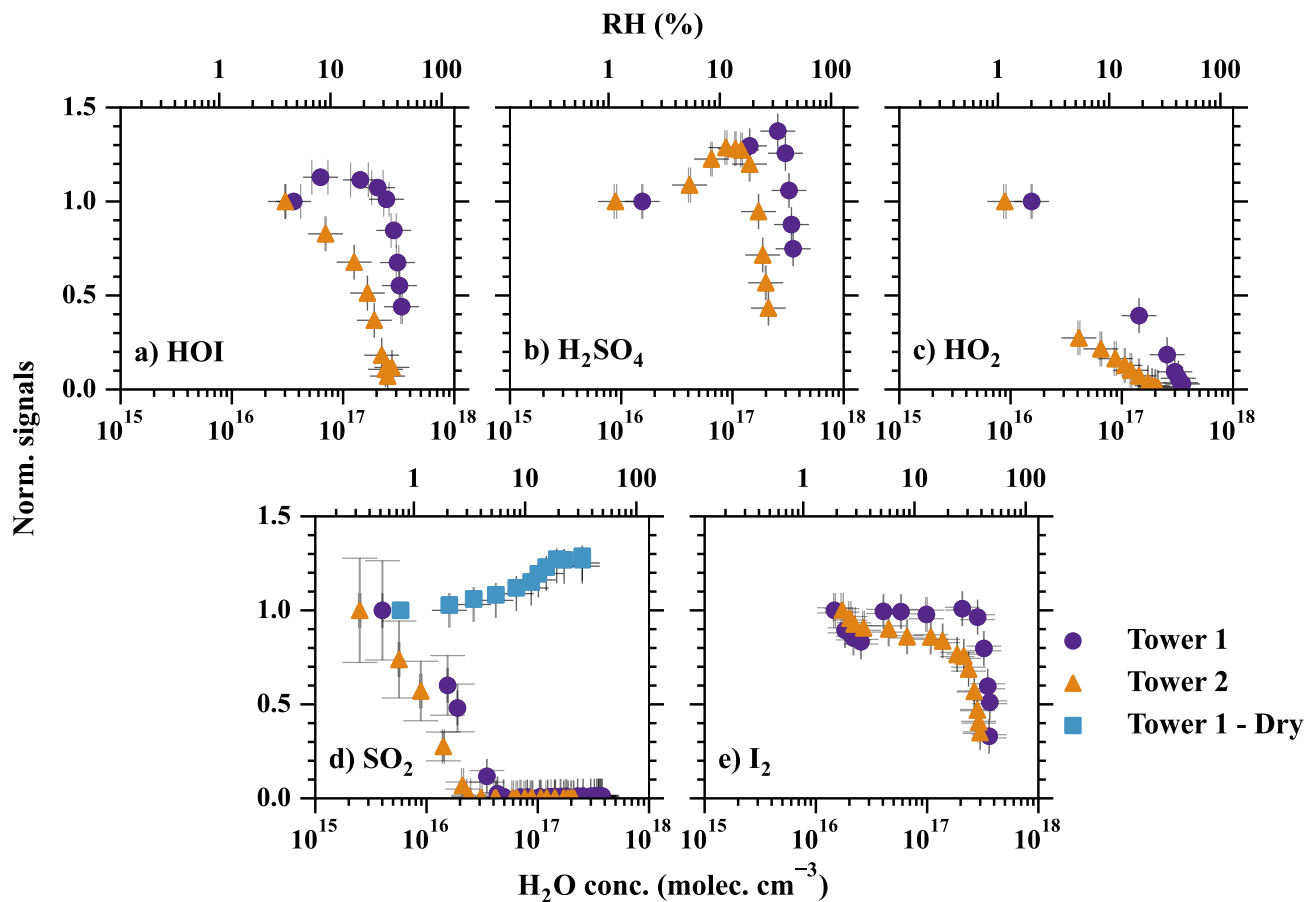


**Figure 4.** The effect of humidity on the detection efficiency of a) HOI, b)  $\text{H}_2\text{SO}_4$ , c)  $\text{HO}_2$ , d)  $\text{SO}_2$ , and e)  $\text{I}_2$ . The measured signals in each set of experiments are normalised by the signal at the lowest RH. Therefore, the normalised signals represent how the increasing RH is affecting the detection limit compared with the initial point. The ~~red and green~~purple circles and orange triangles show the detection humidity effects of tower 1 and tower 2, respectively. The ~~yellow~~blue squares refer to the experiments conducted with a dry flow added before the MION2 inlet. The RH is converted from absolute  $\text{H}_2\text{O}$  concentrations at 25 °C. Error bars represent one standard deviation.

### 3.3 Detection humidity effect

520 The measurement sensitivity of halide ~~ion-anion~~ based chemical ionisation method was regularly reported to be affected by atmospheric water content (Kercher et al., 2009; Mielke et al., 2011; Woodward-Massey et al., 2014; Lee et al., 2014). The humidity effect of atmospheric pressure Br<sup>-</sup>-MION2 could be ~~even stronger owing amplified due~~ to the higher water content ~~in the present in~~ air samples. Although ~~our earlier study~~ Wang et al. (2021a) has demonstrated that the detection of I<sub>2</sub> by Br<sup>-</sup>-MION1 was not affected within a limited humidity variation (40 - 80 % RH at -10 °C), characterisation under a wider range  
525 of humidity conditions is needed. As the detection humidity effect in this study exclusively refers to the effect of absolute humidity instead of relative humidity, absolute humidity parameters such as dew/frost point or H<sub>2</sub>O molecule concentration are commonly presented together with the relative humidity (at 25 °C, otherwise notified).

In this study, we examine the detection humidity effect of H<sub>2</sub>SO<sub>4</sub>, HOI, HO<sub>2</sub>, SO<sub>2</sub> and I<sub>2</sub> with RH from below 1 % to 60 %  
530 at 25 °C. ~~The detection humidity effect of~~ Unlike H<sub>2</sub>SO<sub>4</sub>, HO<sub>2</sub> and HOI, which require generation from a calibration source, both SO<sub>2</sub> and I<sub>2</sub> ~~is relatively easier to characterise as the calibration source is not involved~~ have their own standardised sources. This simplifies their control during the characterisation of the detection humidity effect. Therefore, a straight flow reactor is used to premix the analyte containing air sample to the Br<sup>-</sup>-MION2 (Figure A2). It is worth noting that we do not account for the wall loss of SO<sub>2</sub> and I<sub>2</sub> in the analysis. The wall loss of SO<sub>2</sub> is negligible at the time scale of the calibration processes  
535 (few seconds). Despite I<sub>2</sub> ~~being a sticky gas which both condenses to and evaporates from the wall~~ vapour can both condense on and evaporate from the walls of the flow reactor, an equilibrium can be ~~reached if given sufficient time. When equilibrium is reached, which could take~~ achieved given a sufficient amount of time. In our experiments, it took up to 24 hours ~~in our experiments to reach equilibrium. Once equilibrium is established,~~ the condensation and evaporation of I<sub>2</sub> ~~cancel balance~~ each other out ~~and thus,~~ making the estimation of I<sub>2</sub> concentration ~~is~~ straightforward.

540

On the other hand, the characterisation of the detection humidity effect of H<sub>2</sub>SO<sub>4</sub>, HOI and HO<sub>2</sub> is more challenging as the production of these species is nearly proportional to the amount of H<sub>2</sub>O passing the calibration source. Therefore, an experimental apparatus was built which enabled humidifying the air sample after the ~~calibrator~~ calibration source, thus without disturbing HO<sub>x</sub> production processes in the calibration source (Figure A3).

545

The results of the humidity characterisation are shown in Figure 4. ~~Despite~~ Although only five species were characterised and observed for their distinct humidity sensitivity ~~is observed for the mentioned five species,~~ a general conclusion can be drawn ~~for that applies to~~ essentially all of the species ~~an excess:~~ an excessive amount of water content ~~results in lower~~ leads to a decrease in detection sensitivity. The species with stronger binding with Br<sup>-</sup> exhibits ~~higher tolerance to humidity changes less~~ sensitivity to changes in humidity (e.g. H<sub>2</sub>SO<sub>4</sub> ~~and and~~ I<sub>2</sub>), while the weakly bonded ones (HOI, SO<sub>2</sub> and HO<sub>2</sub>) are strongly affected. The humidity tolerance of the measured species can be ordered as I<sub>2</sub> > HOI > HO<sub>2</sub> > SO<sub>2</sub> which is the same order as  
550

the strength of their bindings with  $\text{Br}^-$  (Table 2).

555 Interestingly, the detection humidity effect of  $\text{H}_2\text{SO}_4$  is observed to be non-linear, i.e., the detection sensitivity of  $\text{H}_2\text{SO}_4$  first increases with higher RH but eventually has a sharp drop at around 40 % RH (25 °C). The enhancement of  $\text{H}_2\text{SO}_4$  detection at below ca. 33 % RH could be contributed by two mechanisms. First, the diffusivity of  $\text{H}_2\text{SO}_4$  is lower at higher RH (Hanson and Eisele, 2000). A higher RH, therefore, reduces the wall deposition of  $\text{H}_2\text{SO}_4$  in the inlet tube, thus effectively increasing the detected  $\text{H}_2\text{SO}_4$ . This is a universal ~~systematic error which affects any factor that influences all~~  $\text{H}_2\text{SO}_4$  detection ~~technique techniques~~ with appreciable sampling line residence time. The second possibility is that at low RH regime,  $\text{H}_2\text{O}$  does enhance  
560  $\text{H}_2\text{SO}_4$  detection by offering more modes through which the excess energy of the cluster can dissipate in the formation of  $\text{H}_2\text{SO}_4 \cdot \text{Br}^-$ , thus resulting in a relatively more stable cluster (Iyer et al., 2017). Regardless of the sources of the detection humidity effect at the low water content regime, the maximum systematic error is measured to be 37 % by comparing the experiment carried out at 2 % RH (frost point of -25 °C) and the experiment carried out at 33 % (dew point of 7.6 °C) in Figure 4b. ~~As the humidity change in ambient conditions is commonly smaller than during experiments, we expect~~ Based on our findings, we anticipate that the detection humidity effect of  $\text{H}_2\text{SO}_4$  ~~is~~ would be moderate when the dew point is below ~~ca.~~ approximately 7.6 °C. However, it is important to exercise caution when conducting measurements under higher absolute humidity conditions.

Additionally, a longer ~~reaction time in the ion-molecule reaction chamber~~ ionisation time by utilising the  $\text{Br}^-$ -MION2-T2 results in a stronger detection humidity effect as shown in Figure 4. ~~Although such an~~ This phenomenon is the most significant  
570 for HOI, i.e., the detection of HOI is more humidity dependent using  $\text{Br}^-$ -MION2-T2 than  $\text{Br}^-$ -MION2-T1. Although this effect is difficult to quantify, it practically suggests that the  $\text{Br}^-$  chemical ionisation method should employ a shorter ionisation time (i.e., using the tower 1) when operating MION2 with multiple chemical ionisation methods.

In summary, we find that the detection of  $\text{Br}^-$ -MION2 is strongly affected by air water content. The atmospheric pressure  
575  $\text{Br}^-$  chemical ionisation method is suitable for laboratory experiments where water content is controlled and atmospheric observations in the cryosphere where air water content is low. Nevertheless, the humidity effect should be considered individually for different analytes and the binding enthalpy between the analyte and  $\text{Br}^-$  is likely a good indicator. As the  $\text{NO}_3^-$ -MION2 (or the  $\text{NO}_3^-$  chemical ionisation ~~, in general, in general~~) is known to have minimal detection humidity sensitivity, it is commonly operated together with the  $\text{Br}^-$ -MION2. ~~Cross-check~~ Performing a cross-check of mutually measured species ~~(e.g., , such as~~  
580  $\text{H}_2\text{SO}_4$ ,  $\text{HIO}_3$ , and oxidised organic species) ~~will give essential information on, will provide crucial insights into~~ whether and when the detection capability of  $\text{Br}^-$ -MION2 ~~detection~~ is compromised by ~~air water content~~ the water content in the air. In this ~~regard~~ context, the new design of  $\text{Br}^-$ -MION2 ~~allowing as many as, which enables~~ three chemical ionisation methods to have the same ionisation time, is essential.

### 585 3.4 Attempts to reduce the detection humidity effect

Several ways ~~Various approaches~~ were explored to ~~reduce-mitigate~~ the detection humidity effect. ~~The first and usual way of reducing the detection humidity effect is deploying~~ One commonly used method is to employ a low-pressure chemical ionisation system ~~which was regularly used for, e.g., iodide chemical ionisation systems (Lee et al., 2014) or bromide chemical ionisation~~ ionization system, which has been successfully implemented in iodide chemical ionization systems (Lee et al., 2014) and bromide chemical ionization systems (Wang et al., 2021a). However, ~~the reduction of air sample RH is at the cost of~~ reducing measurement sensitivity ~~reducing the relative humidity (RH) of the air sample comes at the expense of~~ reducing the measurement sensitivity for species detected at the collision limit, such as H<sub>2</sub>SO<sub>4</sub>, as-HIO<sub>3</sub> and I<sub>2</sub>, as the air sample ~~is unavoidably diluted~~ unavoidably undergoes dilution in this process. We estimated previously that the Br<sup>-</sup>-FIGAERO inlet had more than 10 times higher detection limit compared to the Br<sup>-</sup>-MION1 inlet (Wang et al., 2021a). For example, the Br<sup>-</sup>-FIGAERO had an HIO<sub>3</sub> detection limit of  $5.1 \times 10^6 \text{ cm}^{-3}$  which struggles to detect atmospheric ~~level~~ levels of HIO<sub>3</sub> (commonly below  $10^7 \text{ cm}^{-3}$ ) (He et al., 2021b). The lower level of detection limit provided by the Br<sup>-</sup>-MION2 inlet is therefore essential in the detection of iodine species. Another important factor is the reaction of halogen radicals with analytes. Besides halogen anions, halogen radicals can also be produced by chemical ionisation processes. While iodine radical (I·) mostly reacts with halogen species and a ~~very limited~~ minimal number of organic species, bromide radical (Br·) reacts with a wider range of organic species as it has a larger reactivity. ~~Regular~~ Conventional low-pressure systems ~~which mix analyte that involve mixing analytes~~ with reagent gases ~~(e.g., FIGAERO inlet) may introduce an additional complexity when interpreting measured,~~ such as the FIGAERO inlet, can introduce additional complexities when interpreting mass spectra. ~~Therefore, we had to seek alternatives to help~~ As a result, alternative approaches were pursued to effectively reduce the detection humidity effect.

605

The first method is the dilution method. Instead of measuring the air sample directly, a dry dilution flow was mixed with the air sample at the entrance of the Br<sup>-</sup>-MION2 inlet (see ~~supplementary~~-Figure A4). We tested this method for the SO<sub>2</sub> detection with an air sample flow of 1.8 slpm and a dilution flow of 20.7 slpm (Figure 4). The x-axis for this set of experiments represents humidity in the air sample instead of the humidity after the dilution to compare with the experiments without adding the dilution flow. We observe a significantly reduced detection humidity effect compared to the case without dilution. It is noteworthy that as the air sample ~~is was~~ diluted by a factor of ~~21.5~~ 12.5, the detection limit of the instrument is likely enhanced by the same factor. However, since the detection humidity effect for SO<sub>2</sub> is significantly higher than other species (e.g., H<sub>2</sub>SO<sub>4</sub>, HOI and I<sub>2</sub>), the dilution is still effective for SO<sub>2</sub> measurement. For example, no SO<sub>2</sub>·Br<sup>-</sup> signal would not be measured at 40 % RH (25 °C) if the air sample is not diluted but a noticeable signal would be measured if the air sample is diluted. A similar conclusion is likely applicable to other species but with a different optimal humidity cut-off.

615

The second method is additionally introducing a core-sampling device that uses the air sample as the core flow and a dry synthetic air flow as the sheath flow (~~supplementary~~-Figure A9). This takes ~~the~~ advantage of the fact that H<sub>2</sub>O diffuses into the sheath flow faster than other analytes with larger molecular weight, thus effectively reducing the RH in the core flow from which the instrument pinhole collects the most sample. ~~On the other hand,~~ Nevertheless, it is important to note that the core-

620



sampling method ~~also inevitably reduces~~, while helping to mitigate the detection humidity effect, also leads to a reduction in the  $\text{SO}_2 \cdot \text{Br}^-$  signal ~~as~~. This is because the  $\text{SO}_2$  ~~also gets diluted~~ which partially counters the ~~itself gets diluted~~, partially counteracting the benefits of the reduced detection humidity effect.

625 Various sample-to-sheath flow combinations were tested as presented in Figure 5. ~~To compare the detection coefficient to standard conditions, the~~ The measured  $\text{SO}_2 \cdot \text{Br}^-$  signal from all sets of experiments ~~is normalized~~ was normalised by the experiment with the sample-to-sheath ratio of 21:1 at 0.21 % RH (25 °C). The results ~~reveal~~ indicate that reducing the sample-to-sheath ratio effectively ~~eases~~ alleviates the  $\text{SO}_2$  detection humidity effect. ~~The results show~~ It is observed that different mixing ratios ~~only moderately affect~~ have only a moderate impact on the measured  $\text{SO}_2 \cdot \text{Br}^-$  when ~~the  $\text{H}_2\text{O}$  is smaller than concentration is below~~  $10^{16} \text{ cm}^{-3}$  (1 % RH; ~~the~~), indicating a low detection humidity effect ~~remains low~~. ~~This is likely due to the fact that the instrument pinhole primarily measures the air sample in the core flow, as it only sucks 0.8 slpm in such conditions~~. However, the core-sampling device clearly enhances the  $\text{SO}_2$  detection efficiency when the  $\text{H}_2\text{O}$  concentration is larger than  $10^{16} \text{ cm}^{-3}$ . The sample-to-sheath ratio of 1:21 enables effective detection of  $\text{SO}_2$  at around  $4.5 \times 10^{17} \text{ cm}^{-3}$  (60 % RH) of  $\text{H}_2\text{O}$  while the sample-to-sheath ratio of 21:1 is not able to detect  $\text{SO}_2$  after around  $4.3 \times 10^{16} \text{ cm}^{-3}$  of  $\text{H}_2\text{O}$  (6 % RH).

630 concentration is below  $10^{16} \text{ cm}^{-3}$  (1 % RH; ~~the~~), indicating a low detection humidity effect ~~remains low~~. ~~This is likely due to the fact that the instrument pinhole primarily measures the air sample in the core flow, as it only sucks 0.8 slpm in such conditions~~. However, the core-sampling device clearly enhances the  $\text{SO}_2$  detection efficiency when the  $\text{H}_2\text{O}$  concentration is larger than  $10^{16} \text{ cm}^{-3}$ . The sample-to-sheath ratio of 1:21 enables effective detection of  $\text{SO}_2$  at around  $4.5 \times 10^{17} \text{ cm}^{-3}$  (60 % RH) of  $\text{H}_2\text{O}$  while the sample-to-sheath ratio of 21:1 is not able to detect  $\text{SO}_2$  after around  $4.3 \times 10^{16} \text{ cm}^{-3}$  of  $\text{H}_2\text{O}$  (6 % RH).

635 Overall, the sample-to-sheath ratio of ~~21:1:21~~ is at least two orders of magnitude more effective in detecting  $\text{SO}_2$  when  $\text{H}_2\text{O}$  is greater than  ~~$10^{16}$~~   $2 \times 10^{16} \text{ cm}^{-3}$ . Therefore, the core-sampling method is an effective method for reducing the detection humidity effect of species which are weakly bonded with  $\text{Br}^-$ . ~~However, since the detection limit is nevertheless changed by~~ Despite the reduced detection humidity effect, it is important to note that the sample water content still impacts the detection limit of  $\text{SO}_2$ . Therefore, dedicated experiments ~~have to be carried out to derive~~ need to be conducted to accurately determine

640 the concentration of ~~the analyte (e.g.,  $\text{SO}_2$ )~~.

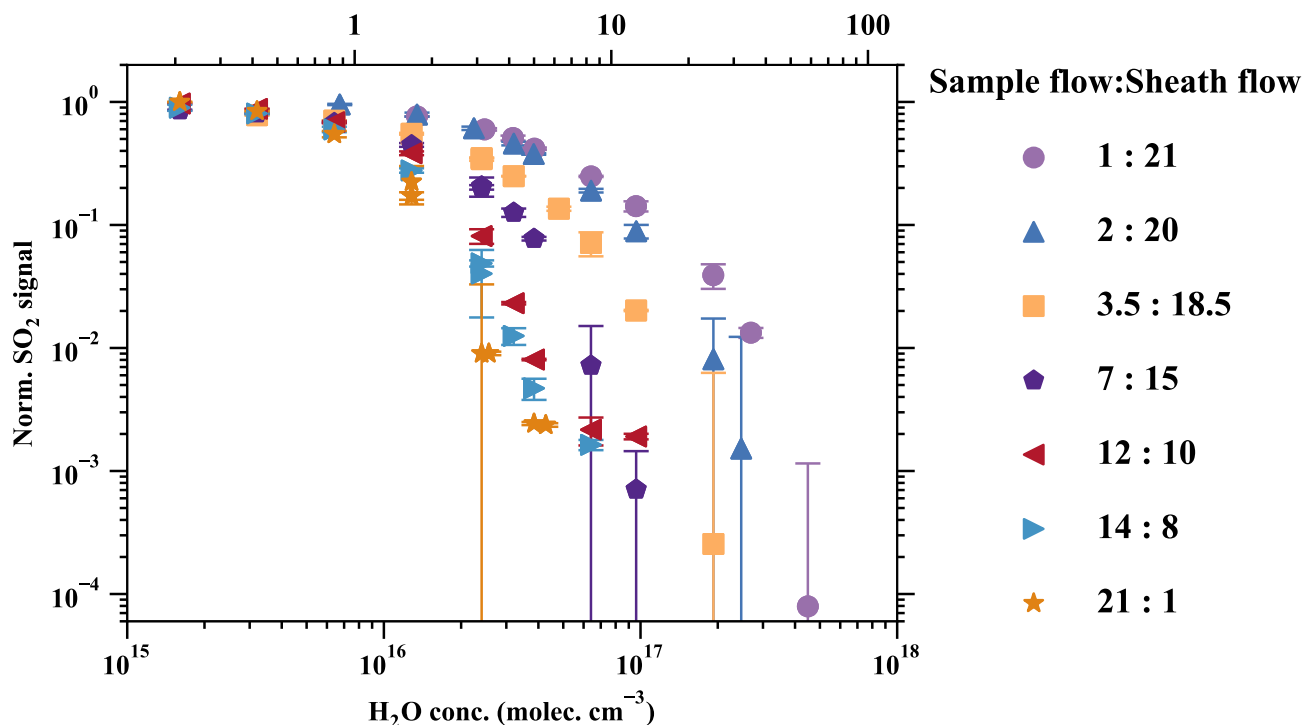


**Figure 5.** Reducing the detection humidity effect with the core sampling method (supplementary-Figure A9). This design takes the advantage of the faster diffusion of H<sub>2</sub>O than SO<sub>2</sub> from the sample flow to the sheath flow and effectively reduces the RH in the sample flow. Various sample-to-sheath ratios were tested at different H<sub>2</sub>O concentrations to find the optimal setting. All the data are normalised to the lowest RH data point in the sample-to-sheath = 21:1 experiment. Due to experimental constraints, the sample-to-sheath ratios = a) 3.5:18.5, b) 2:20 and c) 1:21 experiments started only from the second, third and fourth lowest RH points, respectively. All other experiments collected data in all humidity conditions. The error bars represent the standard deviation of the normalised SO<sub>2</sub> signals.

### 3.5 Limit of detection

The limit of detection (LOD) is an essential parameter for a chemical ionisation inlet system. For the convenience of inter-comparison, we define the LOD in this study as:

$$645 \quad \text{LOD} = \mu + 3 \times \sigma \quad (3)$$

where  $\mu$  is the mean value of one-hour mass spectrometric data with a one-minute time resolution and  $\sigma$  is the standard variation of the same data. Both  $\mu$  and  $\sigma$  include the experimentally derived calibration coefficient. The species without direct calibration utilise the calibration coefficient of H<sub>2</sub>SO<sub>4</sub>, thus the LODs for these species generally represent the lower limit. The

650 ~~LODs are measured by passing LOD is determined by introducing~~ pure nitrogen or synthetic air ~~to into~~ the chemical ionisation inlet ~~in which case, where~~ none of the species listed in Table 1 ~~is expected. It should be noted~~ are expected to be present. It is important to emphasise that this LOD definition is ~~suitable for disentangling specifically suitable for distinguishing~~ trace gas

concentrations from background levels in long-term observations. ~~Values above the LOD can commonly be distinguished from the time series. If one does a careful analysis of the measured mass spectra, a lower value may be recognised.~~

655 The reported LODs can be affected by many factors. Some of these factors are 1) the purity of the reagent source (e.g., ~~nitric acid solution and dibromomethane solution~~  $\text{HNO}_3$  or  $\text{CH}_2\text{Br}_2$  solution), 2) the purity of the sample air used at the LOD determination experiment, 3) the signal-to-noise (electronic background noise) ratio of the instrument, 4) the ~~softness of fragmentation level (controlled by~~ the tuning of the ~~instrument) of the~~ mass spectrometer, ~~and~~ 5) the humidity of the sample air used at the LOD determination experiment (for  $\text{Br}^-$  chemical ionisation ~~)method~~ ~~and 6) different ways of estimating LODs.~~

660

~~Due to the complex nature of the LOD determination, the MION2 inlet was coupled with two independent mass spectrometers (APi1 and APi2, respectively, see Table 1) to test its robustness. The LOD determination experiments were carried out with APi1 and APi2 in two independent laboratory environments with independent reagent sources and sample air. These two instruments were also individually tuned, thus having different signal-to-noise ratios and fragmentation levels. The results of the LOD determination experiments are tabulated in Table 1. Both of the MION2-T1-APi1 and MION2-T1-APi2 achieved LODs at the level of  $10^5 \text{ cm}^{-3}$  for species that are detected at the collision limit (e.g., , and). In general, the MION2-T1-APi2 has a slightly lower LOD compared with MION2-T1-APi1. This could result from the fact that the APi1 has not been serviced for more than four years by the point of the experiments and the multi-channel plate could have degraded.~~

670 It is worth noting that it may appear that the ~~and~~ LODs of MION2-T1 ( $1 \times 10^5 \text{ cm}^{-3}$  and  $3.3 \times 10^5 \text{ cm}^{-3}$ ) are similar to that reported for MION1-T1 ( $2 \times 10^5 \text{ cm}^{-3}$  and  $3.8 \times 10^5 \text{ cm}^{-3}$ ) in our earlier study (Wang et al., 2021a). This is because the mass spectrometer used in Wang et al. (2021a) (noted as APi3) had a higher signal-to-noise ratio compared with the APi1. Therefore, getting similar LODs from the MION2-T1-APi1 and MION1-T1-APi3 already suggests that the MION2 inlet has improved its performance. ~~In order to avoid this systematic error,~~ ~~Therefore, comparing the LODs derived in this study with earlier studies may not be meaningful.~~ Hence, we additionally compared the  $\text{H}_2\text{SO}_4$  LOD of the MION2 inlet with ~~that of the the widely-used~~ Eisele-type inlet, both attached to the ~~APi1 same mass spectrometer~~ (Table 1). The direct comparison suggests that the ~~MION2-T1-Br<sup>-</sup>-MION2-T1~~ LOD is roughly 30 % higher than the LOD of the ~~widely-used~~ Eisele inlet, thus a comparable performance. When we increased the ionisation time from 35 ms (~~MION2-T1-Br<sup>-</sup>-MION2-T1~~) to 300 ms (~~MION2-T2-Br<sup>-</sup>-MION2-T2~~), the LOD of ~~MION2-Br<sup>-</sup>-MION2~~ for  $\text{H}_2\text{SO}_4$  is further reduced by a factor of three, thus ~~MION2-T2-Br<sup>-</sup>-MION2-T2~~ performs better than the Eisele inlet. This suggests that the MION2 inlet ~~achieves comparable~~ ~~(MION2-T1 can achieve comparable~~ ( $\text{Br}^-$ -~~MION2-T1~~) or even better (~~MION2-T2) LODs-Br<sup>-</sup>-MION2-T2) LOD~~ than the Eisele inlet. ~~Additional tuning of the ionisation time may further increase the advantage for chemical ionisation methods that are less affected by air-water content (e.g., -CIMS).~~

685 Additionally, the Eisele-type inlet was regularly shown to have ~~LODs a LOD~~ as low as  $10^4 \text{ cm}^{-3}$  (Jokinen et al., 2012), a well-performing mass spectrometer ~~will likely may~~ further reduce the ~~LODs LOD~~ of MION2. Nevertheless, the ~~achieved LODs are low enough attained levels of LOD are sufficiently low~~ for atmospheric measurements ~~as the discussed molecules commonly need to be.~~ ~~The molecules in question typically require concentrations~~ above  $10^6 \text{ cm}^{-3}$  to ~~have a significant impact~~

exert a significant influence on atmospheric chemistry and aerosol formation.

### 3.6 Voltage scanning and cluster formation enthalpy

690 Collision induced cluster fragmentation is an unavoidable issue which affects the detection of analytes that are weakly bonded with the reagent ion. Since if a charged cluster is loosely bonded, collisions between charged clusters and air molecules in the atmospheric pressure interface may break a large portion of the charged clusters apart prior to reaching the detector (Pasananti et al., 2019). Therefore, charged cluster binding strength is an important factor determining whether an ~~analyte-charger~~ analyte-reagent ion cluster can be measured by the mass spectrometer (Iyer et al., 2016; Lopez-Hilfiker et al., 2016; Wang et al., 695 2021a). Lopez-Hilfiker et al. (2016) has shown that the level of collision induced cluster fragmentation is associated with the voltage differences between the first and second quadrupoles in the atmospheric pressure interface of the mass spectrometer. The voltage difference was shown to be indicative of the fragmentation level of the CIMS and it positively correlates with the cluster formation enthalpy (Iyer et al., 2016).

700 In this study, we carried out voltage scan experiments with the same procedures as described in Lopez-Hilfiker et al. (2016). Briefly, we kept the voltage differences inside two individual quadruples constant while changing the voltage difference between these two quadruples to modulate energies in the collision processes and the results are shown in Figure 6. Generally, a higher voltage difference indicates a higher fragmentation level which in turn results in a lower remaining fraction of charged clusters. Charged clusters that are less sensitive to voltage changes, especially in the low voltage difference regime (~~e.g.,  $\Delta V$~~   $< 10$  V), are more stable.

A series of iodine oxides and oxoacids is evaluated together with other inorganic species such as H<sub>2</sub>O, HO<sub>2</sub>, SO<sub>2</sub> and H<sub>2</sub>SO<sub>4</sub> (Figure 6). Based on the results, we categorise the analytes into three categories: 1) analytes which are strongly bonded with Br<sup>-</sup>, 2) analytes which are moderately bonded with Br<sup>-</sup> and 3) analytes which are weakly bonded with Br<sup>-</sup>. The species 710 H<sub>2</sub>SO<sub>4</sub>, HIO<sub>3</sub>, HIO<sub>2</sub>, and I<sub>2</sub>O<sub>4</sub> ~~clearly fall can be classified~~ into the first category ~~as since~~ the initial change ~~of in~~ voltage difference does not ~~affect the normalized signalsignificantly, i. e., they have a significant impact on the normalised signal. This~~ indicates that these species are detected at the collision limit. It is also apparent that H<sub>2</sub>O, HO<sub>2</sub> and SO<sub>2</sub> belong to the third category since a small increase in the voltage difference leads to substantially reduced normalised ratios. Finally, IO, OIO, I<sub>2</sub>O<sub>3</sub> and HOI are moderately bonded with Br<sup>-</sup>. These moderately bonded charged clusters can reach a close to collision limit 715 detection if the instrument is softly tuned (the voltage difference is small) but their detection sensitivity can change dramatically if the instrument fragmentation level is high. Lopez-Hilfiker et al. (2016) defined a parameter  $\Delta V_{50}$  ( $dV_{50}$ , i.e., the  $dV$  value at half the maximum of signal remaining) to describe the analyte and reagent ion binding strength. In this study, the  $dV_{50}$  is defined by the following equation:

$$\text{NSR} = \frac{\text{SR}}{1 + e^{-k \times (dV - dV_{50})}} + \text{SR}_{\text{max,pred}} \quad (4)$$

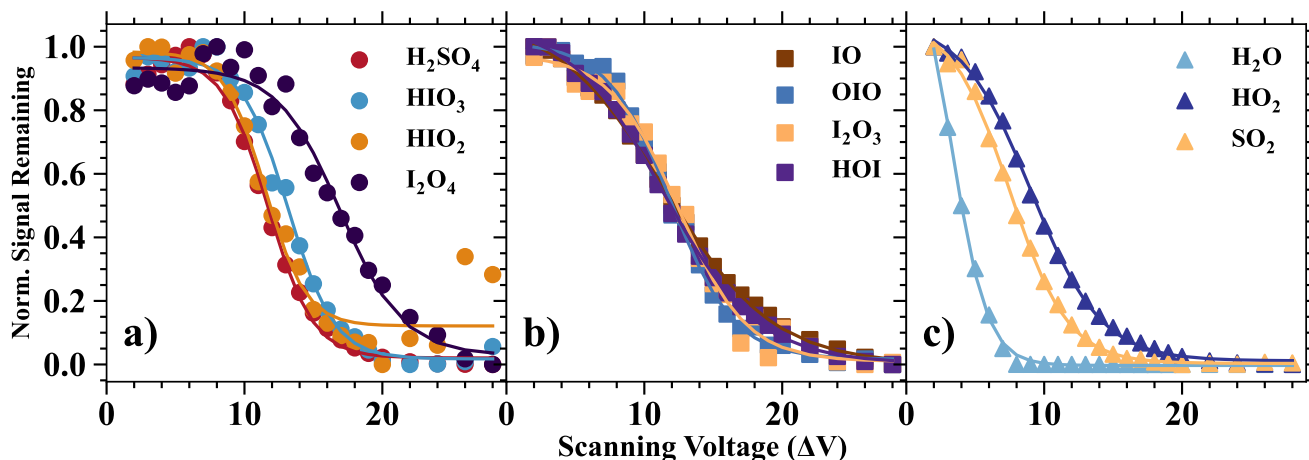


**Figure 6.** Normalised signal remaining vs. the scanning voltage ( $\Delta V$ ). The normalised signal remaining of each species is normalised by the maximum and minimum values of its values with different  $\Delta V$  (or  $dV$ ). The  $\Delta V$  describes the voltage difference between the skimmer and the second quadrupole and can be considered an indicator of the softness of the instrument tuning (Lopez-Hilfiker et al., 2016). A higher  $\Delta V$  commonly indicates a more fragmenting setting.

720 where NSR is the normalised signal remaining, SR is the signal remaining,  $dV_{50}$  is the desired fitted value as represented in Figure 7 and  $SR_{\max, \text{pred}}$  is the fitted value that represents the maximum SR when a compound does not undergo fragmentation while passing through the ion optics.

725 Additionally, formation free enthalpies of various charged clusters are calculated using quantum chemical calculations (see Methods) and are compared with the voltages at which 50% of the charged clusters dissociate ( $\Delta V_{50}$ )  $dV_{50}$  as shown in Figure 7. These The two sets of parameters are, consisting of theoretical predictions and measurements of the binding strength and they show a consistent picture, as shown previously and in this study (Lopez-Hilfiker et al., 2016; Iyer et al., 2016). As a, provide a consistent understanding as demonstrated in previous studies (Lopez-Hilfiker et al., 2016; Iyer et al., 2016). In summary, strongly bonded charged clusters have larger fragmentation free exhibit larger fragmentation-free enthalpies, larger  $\Delta V_{50}$  values and a lower calibration factor (e.g.,  $dV_{50}$  values, and lower calibration factors. Examples of such species include  $H_2SO_4 \cdot Br^-$ , and  $I_2 \cdot Br^-$ ). The. On the other hand, weakly bonded charged clusters have the opposite properties (e.g., exhibit opposite properties, including species like  $HO_2 \cdot Br^-$ ,  $H_2O \cdot Br^-$  and  $SO_2 \cdot Br^-$ ).

730

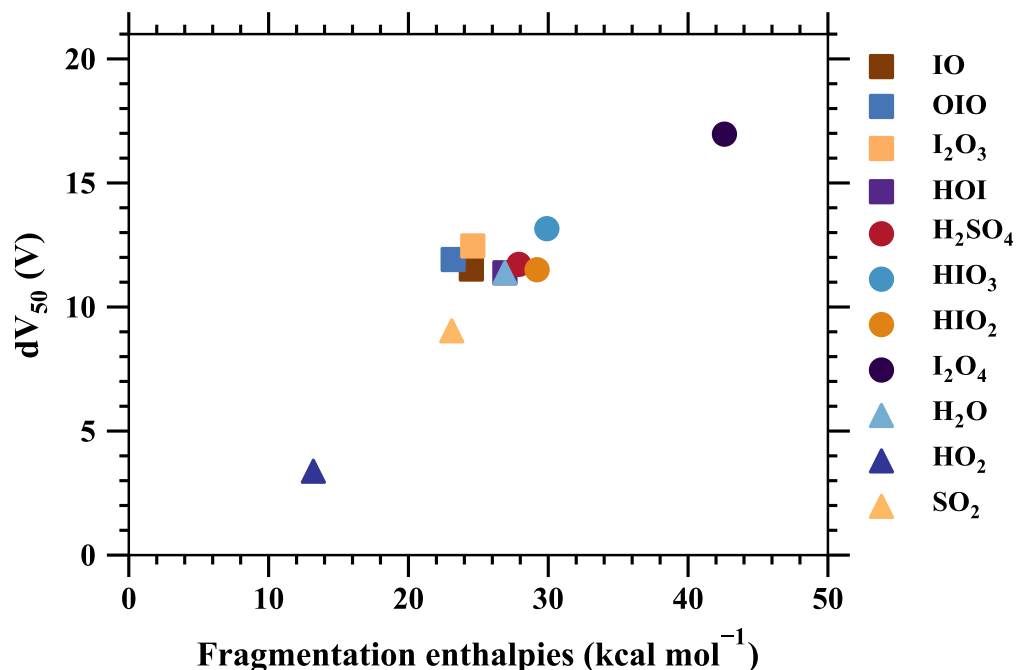


**Figure 7.** The voltage at which 50 % of analyte-bromide adducts have dissociated ( $\Delta 50dV_{50}$ ) vs. the fragmentation free enthalpies of the adducts (Table 2).

### 3.7 Validation of the measurement of iodine-containing species

735 Oxidised iodine vapours have been shown to influence atmospheric oxidation capacity (Sherwen et al., 2016; Wang et al., 2021b) (Saiz-Lopez et al., 2014; Sherwen et al., 2016; Wang et al., 2021b) and particle formation processes (Hoffmann et al., 2001; O'Dowd et al., 2002). Recent publications have suggested-proposed iodine oxoacids as the critical driver for iodine particle formation processes (Sipilä et al., 2016; Baccarini et al., 2020; He et al., 2021b, a; Zhang et al., 2022; Liu et al., 2023). However, active debate remains concerning the presence of gaseous HIO<sub>3</sub> and whether HIO<sub>3</sub> plays an important role in atmospheric aerosol nucleation. For example, a recent laboratory study shed doubts on the existence of gaseous HIO<sub>3</sub> as the authors only managed to measure HIO<sub>3</sub> in the particle phase with a photoionisation mass spectrometer but not in the gas phase. They concluded that the particle phase HIO<sub>3</sub> was formed from higher iodine oxides  $I_2O_3$  instead of from gaseous HIO<sub>3</sub> (Gómez Martín et al., 2020). Additionally, they hypothesised-Furthermore, they proposed a hypothesis that the IO<sub>3</sub><sup>-</sup> signal, which was previously interpreted as part of the previously attributed to gaseous HIO<sub>3</sub> measured by the measurements using

745 NO<sub>3</sub><sup>-</sup>-CIMS (Sipilä et al., 2016), could also originate from I<sub>2</sub>O<sub>y</sub> (where y = 2-4) species. Their evidence is primarily the exothermicity of the I<sub>2</sub>O<sub>2-3</sub> reactions with NO<sub>3</sub><sup>-</sup> which forms IO<sub>3</sub><sup>-</sup> as part of the products. However, it should be noted that exothermic reactions do not guarantee that the reactions occur at significant rates. For example, reactions such as



involves breaking ~~several multiple~~ strong I-O and N-O bonds ~~that, which~~ are likely associated with high kinetic barriers ~~and~~  
750 ~~one could expect. As a result, it can be anticipated~~ that this reaction does not occur as ~~fast as the rapidly as the reaction~~  $\text{HIO}_3$   
 $+ \text{NO}_3^- \rightarrow \text{IO}_3^- + \text{HNO}_3$  ~~reaction, in which case only one, where only a single~~ proton transfer reaction ~~occurs~~ ~~takes place.~~

~~It is worthwhile to note that both our earlier studies (He et al., 2021b; Finkenzeller et al., 2022) and (Gómez Martín et al., 2020, 2022)~~  
~~concluded that is the primary form of . Fortunately, gaseous is well measured by both the and chemical ionisation methods.~~  
755 ~~Finkenzeller et al. (2022) calculated the cluster formation enthalpy of as  $-45.6 \text{ kcal mol}^{-1}$ , which indicates that the cluster is~~  
~~extremely stable. Gómez Martín et al. (2020) found that the  $+ \rightarrow$  products + reaction is endothermic thus less likely to occur.~~  
~~The same also applies to the chemical ionisation method. As already discussed in the last section, voltage scan experiments~~  
~~indicate that the cluster is in fact the most stable cluster among the examined clusters (see Figure 7). Therefore, is detected at~~  
~~the collision limit with the chemical ionisation method and it does not fragment into species such as .~~

760 In a more recent study, Gómez Martín et al. (2022) alternatively used the nitrate chemical ionisation method and detected  
gaseous  $\text{HIO}_3$ , ~~thus confirming consistent with~~ our earlier studies (Sipilä et al., 2016; He et al., 2021b, a) of (Sipilä et al., 2016; He et al., 2022)  
~~regarding~~ the existence of gaseous  $\text{HIO}_3$ . However, the authors ~~additionally also~~ suggested that the measured  $\text{HIO}_3 \cdot \text{NO}_3^-$  ion,  
~~which was previously~~ interpreted as  $\text{HIO}_3$  ~~could also be formed from, could potentially be formed through~~ reactions such as  
~~below: the following:~~



due to the reaction being exothermic. Besides the same reasons noted above, this hypothesis is challenged by the fact that the  
reaction



is a favoured pathway compared to the reaction 6 as shown in Figure 8. We further estimate that the MESMER derived overall  
770 rate coefficients at 298 K, 1 atm for reactions 6 and 7 ~~and they~~ are  $2.3 \times 10^{-12} \text{ cm}^3 \text{ molec}^{-1} \text{ s}^{-1}$ , and  $1.26 \times 10^{-9} \text{ cm}^3 \text{ molec}^{-1}$   
 $\text{s}^{-1}$ , respectively. Therefore, the yield of the reaction 7 is close to unity and cannot affect the  $\text{HIO}_3$  detection.

~~It is essential to highlight that our previous studies (He et al., 2021b; Finkenzeller et al., 2022) as well as the studies by~~  
~~Gómez Martín et al. (2020, 2022) have consistently concluded that  $\text{I}_2\text{O}_4$  is the predominant form of  $\text{I}_2\text{O}_y$ . Fortunately, the~~  
775 ~~gaseous  $\text{I}_2\text{O}_4$  species can be effectively measured using both the  $\text{NO}_3^-$  and  $\text{Br}^-$  chemical ionisation methods. Finkenzeller et al. (2022)~~  
~~calculated the cluster formation enthalpy of  $\text{I}_2\text{O}_4 \cdot \text{NO}_3^-$  as  $-45.6 \text{ kcal mol}^{-1}$ , which indicates that the  $\text{I}_2\text{O}_4 \cdot \text{NO}_3^-$  cluster is~~  
~~extremely stable. Gómez Martín et al. (2020) found that the  $\text{I}_2\text{O}_4 + \text{NO}_3^- \rightarrow$  products +  $\text{IO}_3^-$  reaction is endothermic thus less~~  
~~likely to occur. The same principle applies to the  $\text{Br}^-$  chemical ionisation method as well. As mentioned earlier in the previous~~  
~~section, voltage scan experiments have shown that the  $\text{I}_2\text{O}_4 \cdot \text{Br}^-$  cluster is the most stable among the clusters investigated (refer~~  
780 ~~to Figure 7). Consequently,  $\text{I}_2\text{O}_4$  is detected at the collision limit using the  $\text{Br}^-$  chemical ionisation method, and it does not~~  
~~fragment into species such as  $\text{IO}_3^-$ . Given that the measured concentration of  $\text{I}_2\text{O}_4$  is more than one order of magnitude lower~~

than that of  $\text{HIO}_3$  according to previous studies (Wang et al., 2021a; He et al., 2021b; Finkenzeller et al., 2022), it is unlikely that  $\text{I}_2\text{O}_y$  species have a significant impact on the detection of  $\text{HIO}_3$ .

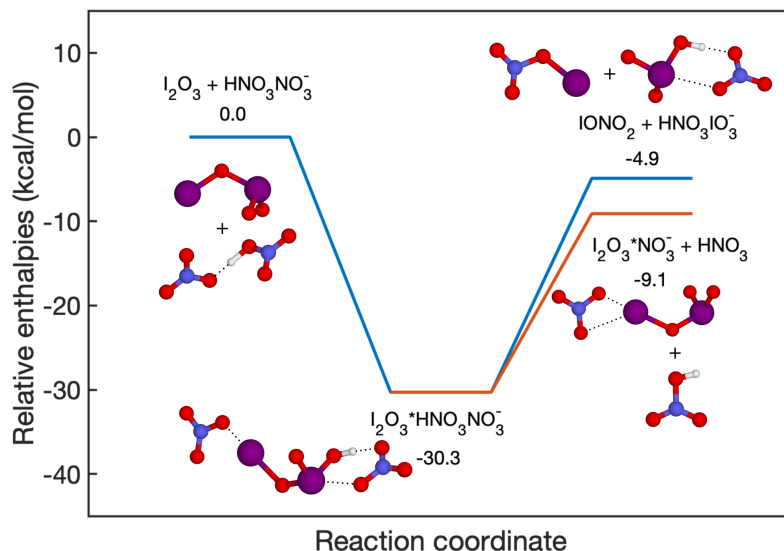


**Figure 8.** Fragmentation pathways of  $\text{I}_2\text{O}_3 \cdot \text{HNO}_3\text{NO}_3^-$ . The enthalpies are calculated at the DLPNO-CCSD(T)/def2-QZVPP//wb97X-D/aug-cc-pVTZ-PP level of theory.

785 Most importantly, higher iodine oxides and iodine oxoacids are formed through complex and distinct chain reactions. Laboratory experiments with elevated iodine concentrations could inevitably disturb the ratio of iodine oxides to iodine oxoacids. The concentration of iodine monoxide (IO) is commonly considered a good indicator of the intensity of atmospheric iodine activities and was shown to influence the ratio of [iodine oxides and iodine oxoacids](#) (Finkenzeller et al., 2022). We [took advantage of capitalised on](#) this phenomenon and [carried out conducted](#) chemical perturbation experiments by vary-

790 [ing the concentration of ozone \(O<sub>3</sub> while keeping concentration and-\)](#), while keeping the concentration of iodine (I<sub>2</sub>) and the light intensity constant in a laminar flow reactor. The experiments were [repeated replicated](#) for both the Br<sup>-</sup>-MION2-T1 and NO<sub>3</sub><sup>-</sup>-MION2-T1 [shown, as illustrated](#) in Figure 9. The measured IO<sub>3</sub><sup>-</sup> signal is compared with HIO<sub>3</sub>·NO<sub>3</sub><sup>-</sup> from the NO<sub>3</sub><sup>-</sup>-MION2-T1 and to HIO<sub>3</sub>·Br<sup>-</sup>, I<sub>2</sub>O<sub>3</sub>·Br<sup>-</sup> and I<sub>2</sub>O<sub>4</sub>·Br<sup>-</sup> from the Br<sup>-</sup>-MION2-T1 to find out the origin of IO<sub>3</sub><sup>-</sup>. [Interestingly, the gaseous signals](#) It is worth noting that the gaseous signals of HIO<sub>3</sub> (HIO<sub>3</sub>·NO<sub>3</sub><sup>-</sup> and HIO<sub>3</sub>·Br<sup>-</sup>) [are perfectly linear with](#)

795 [exhibit a perfectly linear relationship with the signals of IO<sub>3</sub><sup>-</sup>](#). However, the [signals, while the signals of I<sub>2</sub>O<sub>3</sub>·Br<sup>-</sup> and I<sub>2</sub>O<sub>4</sub>·Br<sup>-</sup> show demonstrate a](#) non-linear dependence on IO<sub>3</sub><sup>-</sup>. This suggests that the primary source of IO<sub>3</sub><sup>-</sup> is gaseous HIO<sub>3</sub>, since if I<sub>2</sub>O<sub>y</sub> does contribute to IO<sub>3</sub><sup>-</sup>, a non-linear correlation between HIO<sub>3</sub>·NO<sub>3</sub><sup>-</sup> and HIO<sub>3</sub>·Br<sup>-</sup> with IO<sub>3</sub><sup>-</sup> would be ex-



pected.

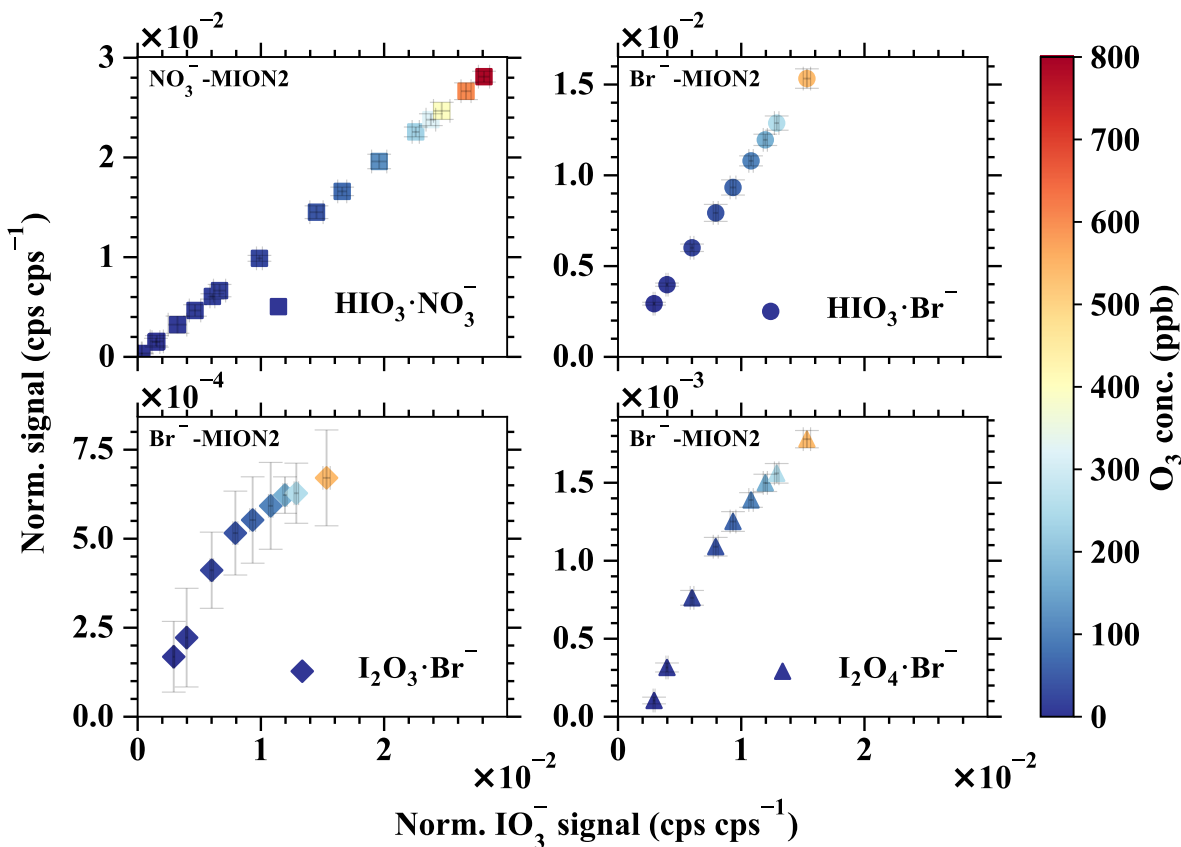


**Figure 9.** The normalised  $\text{IO}_3^-$  signal vs. the normalised signals of a)  $\text{HIO}_3 \cdot \text{NO}_3^-$ , b)  $\text{HIO}_3 \cdot \text{Br}^-$ , c)  $\text{I}_2\text{O}_3 \cdot \text{Br}^-$ , and d)  $\text{I}_2\text{O}_4 \cdot \text{Br}^-$ . The iodine injection and light intensity were kept constant but the  $\text{O}_3$  concentration was varied to modulate the ratio of iodine oxides to oxoacids. Error bars show one standard deviation. Notice the different y-axis scales.

800 **In summary** Therefore, we conclude that the  $\text{I}_2\text{O}_y$  is unlikely to significantly contribute to the  $\text{IO}_3^-$  signal at a significant level in atmospheric relevant under atmospheric conditions. Experiments carried out with ambient level precursors consistently show conducted with ambient level precursors consistently demonstrate that gaseous  $\text{I}_2\text{O}_4$  is significantly considerably less abundant compared with to  $\text{HIO}_3$  (He et al., 2021b, a; Finkenzeller et al., 2022). Model simulation simulations of iodine chemistry at the Maïdo observatory has further shown that the sum further indicate that the combined concentration of  $\text{I}_2\text{O}_3$  and  $\text{I}_2\text{O}_4$  is  
 805 only at around 1 % of  $\text{HIO}_3$  thus, making it unlikely to affect  $\text{HIO}_3$  measurements and iodine particle formation processes the formation of iodine particles in boundary layer conditions (Finkenzeller et al., 2022).

## 4 Summary

In this study, we present an upgraded version of the multi-scheme chemical ionisation inlet ~~version 2~~ (known as MION2). It is capable of simultaneously operating in atmospheric ion measurement mode and employing multiple chemical ionisation methods. ~~While the~~ ~~Although the fundamental~~ concept of this inlet ~~is identical to the~~ ~~remains the same as~~ MION1 (Rissanen et al., 2019), ~~this new version improves its performance in~~ ~~the new version significantly improves performance by effectively~~ focusing reagent ions ~~(thus having lower LODs), enhances its~~, resulting in lower limits of detection (LODs). Moreover, it enhances operational stability and ~~additionally allows to operate~~ ~~enables the concurrent use of~~ multiple chemical ionisation methods with the same ionisation time.

815

We further developed a Python open-source flow reactor kinetic model (MARFORCE, see Shen and He (2023)) to simulate convection-diffusion-reaction equations in cylindrical flow reactors ~~in order~~ to calibrate gaseous species such as H<sub>2</sub>SO<sub>4</sub>, HOI, and HO<sub>2</sub>. The model is also compatible with the widely-used Master Chemical Mechanism, thus allowing future implementation of other chemical mechanisms.

820

The MION2 inlet was further characterised for the detection of various inorganic species using the ~~MION2 inlet with the~~ Br<sup>-</sup> and NO<sub>3</sub><sup>-</sup> chemical ionisation methods ~~was further characterised~~ at two different ionisation times. H<sub>2</sub>SO<sub>4</sub>, HOI, and HO<sub>2</sub> were calibrated by ~~utilising the photo-chemical~~ ~~employing the MARFORCE model, which quantifies their photochemical~~ production in a flow reactor ~~and quantification by the MARFORCE model. We further estimate that the LODs are around~~. ~~Based on our estimations, the limits of detection (LODs) are approximately~~ 10<sup>5</sup> molec. cm<sup>-3</sup> (~~1-min 1-minute~~ data averaging) for ~~e.g., species like~~ H<sub>2</sub>SO<sub>4</sub> and HIO<sub>3</sub> when the ionisation time is ~~at set to~~ 35 ms. ~~When~~ ~~By~~ using a longer ionisation time (300 ms), the LOD for H<sub>2</sub>SO<sub>4</sub> is further reduced to 2.9 × 10<sup>4</sup> molec. cm<sup>-3</sup> (~~ea. approximately~~ 1 ppqv). A direct comparison ~~shows demonstrates~~ that the MION2 inlet ~~has exhibits~~ comparable or even better LODs compared to the widely-used Eisele inlet (Jokinen et al., 2012). ~~Therefore, the~~ ~~Hence, this~~ upgraded version of the inlet ~~provides extremely high sensitivity toward~~ ~~measuring offers exceptional sensitivity for the measurement of~~ trace gases relevant to atmospheric particle formation.

830

~~Additionally, we characterised the detection~~ ~~Furthermore, we conducted an assessment of the detection capabilities~~ of SO<sub>2</sub> and I<sub>2</sub> ~~as they are important since they serve as crucial~~ precursors for H<sub>2</sub>SO<sub>4</sub> and HIO<sub>3</sub> ~~respectively~~. We found that the Br<sup>-</sup>-MION2 inlet is capable of detecting SO<sub>2</sub> by diluting a gas cylinder ~~of a known amount containing a known quantity~~ of SO<sub>2</sub>. ~~Besides our previous methods to calibrate~~ ~~In addition to our previously established methods for calibrating~~ gaseous I<sub>2</sub> (Wang et al., 2021a; Tham et al., 2021), we successfully ~~adapted employed~~ a derivatization approach in ~~combination conjunction~~ with high-performance liquid chromatography ~~method which quantified to quantify the~~ iodine permeation rate ~~of merely~~, ~~which was found to be as low as~~ 17.3 ng min<sup>-1</sup>. The I<sub>2</sub> calibration ~~of using the~~ Br<sup>-</sup>-MION2 ~~further shows inlet further confirms~~ that I<sub>2</sub> is detected at the collision limit, similar to H<sub>2</sub>SO<sub>4</sub> ~~and consistent with our earlier estimation~~, ~~and aligns with our previous~~

835

840 estimations (Wang et al., 2021a).

As the  $\text{Br}^-$ -MION2 measures  $\text{H}_2\text{O}$  in the form of  $\text{H}_2\text{O}\cdot\text{Br}^-$ , we quantified the  $\text{H}_2\text{O}$  detection with a dew point mirror instrument by running them side by side. As a large portion of  $\text{Br}^-$  is converted to  $\text{H}_2\text{O}\cdot\text{Br}^-$  in the ion-molecule reaction chamber, we predicted the fragmentation pathways of analyte- $\text{H}_2\text{O}\cdot\text{Br}^-$  clusters using quantum chemical calculations. We  
845 show that  $\text{H}_2\text{O}$  evaporates from the analyte- $\text{H}_2\text{O}\cdot\text{Br}^-$  clusters when passing the ion optics of our mass spectrometer due to the weak attachment of  $\text{H}_2\text{O}$  to the charged clusters. However, the chemical signature of the analyte is commonly preserved as the analyte- $\text{Br}^-$  cluster or deprotonated analyte anion. ~~Additionally, the~~

~~The~~ detection using the  $\text{Br}^-$  chemical ionisation method at atmospheric pressure is ~~affected by excessive air water content.~~  
850 ~~For analytes which susceptible to the presence of excessive moisture in the air. Analytes that~~ are detected at the collision limit (e.g., such as  $\text{H}_2\text{SO}_4$ ,  $\text{HIO}_3$  and  $\text{I}_2$ ), ~~we find a sharp decrease,~~ exhibit a significant decline in measurement sensitivity ~~after when~~ the dew point ~~is above exceeds~~ 0.5 - 10.5 °C (20 - 40 % RH). ~~The Furthermore, the~~ detection of weakly bonded ~~analytes (e.g., analytes, such as  $\text{HO}_2$  and  $\text{SO}_2$ ) show intensified water influence even with a dew point,~~ is more profoundly affected by water content, even when the dew point is below 0 °C. For ~~example, LOD of instance, the limit of detection (LOD)~~  
855 ~~for  $\text{HO}_2$  is roughly approximately~~ one order of magnitude higher than that of  $\text{H}_2\text{SO}_4$  at 2.7 % RH ~~and the LOD of,~~ while the LOD for  $\text{SO}_2$  is roughly approximately three orders of magnitude higher than that of  $\text{H}_2\text{SO}_4$  at below 0.1 % RH.

In order to ~~reduce the detection humidity effect, a~~ mitigate the impact of humidity on detection, two methods, namely the dilution method and ~~a the~~ core-sampling method, were tested in this study. We found that ~~these methods do reduce the detection~~  
860 ~~humidity effect. Both of these methods enable both methods effectively reduce the influence of humidity on detection. By~~ employing these methods, it becomes possible to detect ambient level levels of  $\text{SO}_2$  (below 1 part per billion ~~in volume~~) with by volume even at RH levels of up to 50 %RH ~~which is otherwise not possible. It,~~ which would otherwise be challenging. ~~However, it~~ should be noted that the utilisation use of these methods ~~unavoidably dilutes the air sample thus inevitably results~~ in sample dilution, thereby affecting the detection of species ~~which are less severely that are less~~ affected by air water con-  
865 tent (e.g., such as  $\text{H}_2\text{SO}_4$ ,  $\text{HOI}$  and  $\text{I}_2$ ). Therefore, these methods should be ~~deployed only employed~~ employed selectively, when there is a ~~clear aims~~ specific objective, such as detecting extremely low levels of  $\text{SO}_2$  or when the sample's dew point is higher than 10 °C (40 % RH). This ~~suggests implies~~ that atmospheric pressure  $\text{Br}^-$  chemical ionisation is suitable for laboratory experiments with controlled ~~relative humidity and RH and for~~ ambient measurements in relatively cold environments. When interpreting data ~~from obtained through the~~ atmospheric pressure  $\text{Br}^-$  chemical ionisation method, ~~the impact of water should~~  
870 ~~be carefully treated using it is crucial to carefully account for the influence of water by employing~~ analytical characterisation or ~~fragmentation enthalpy prediction. As predicting fragmentation enthalpy. Despite these considerations,~~ the MION2 ~~allows to operate water insensitive inlet, which allows for the concurrent operation of the water-insensitive~~  $\text{NO}_3^-$  chemical ionisation method and ~~water sensitive but more capable the water-sensitive yet more versatile~~  $\text{Br}^-$  chemical ionisation method ~~together,~~ it will nevertheless reveal greater details of the atmosphere compared to, provides a more comprehensive understanding of

875 atmospheric conditions compared to using either of these methods ~~alone~~in isolation.

Finally, we validated the measurement of gaseous  $\text{HIO}_3$  using both the  $\text{NO}_3^-$  and  $\text{Br}^-$  chemical ionisation methods ~~are validated~~. The signal of  $\text{HIO}_3$  ~~commonly~~typically consists of  $\text{IO}_3^-$  and either  $\text{HIO}_3 \cdot \text{NO}_3^-$  or  $\text{HIO}_3 \cdot \text{Br}^-$ , depending on the chemical ionisation method ~~utilised~~. ~~We have experimentally and theoretically validated that all of the~~ employed. Through  
880 experimental and theoretical validation, we confirmed that all three ions primarily originate from genuine gaseous  $\text{HIO}_3$  and that iodine oxides do not contribute to ~~these ions at the formation of these ions under~~ atmospherically relevant conditions.

*Code availability.* The MARFORCE model is shared through GitHub repository (<https://github.com/momo-catcat/MARFORCE-flowtube>). Other data analysis codes can be requested from the corresponding authors.

*Data availability.* Data is available upon request from the corresponding authors.

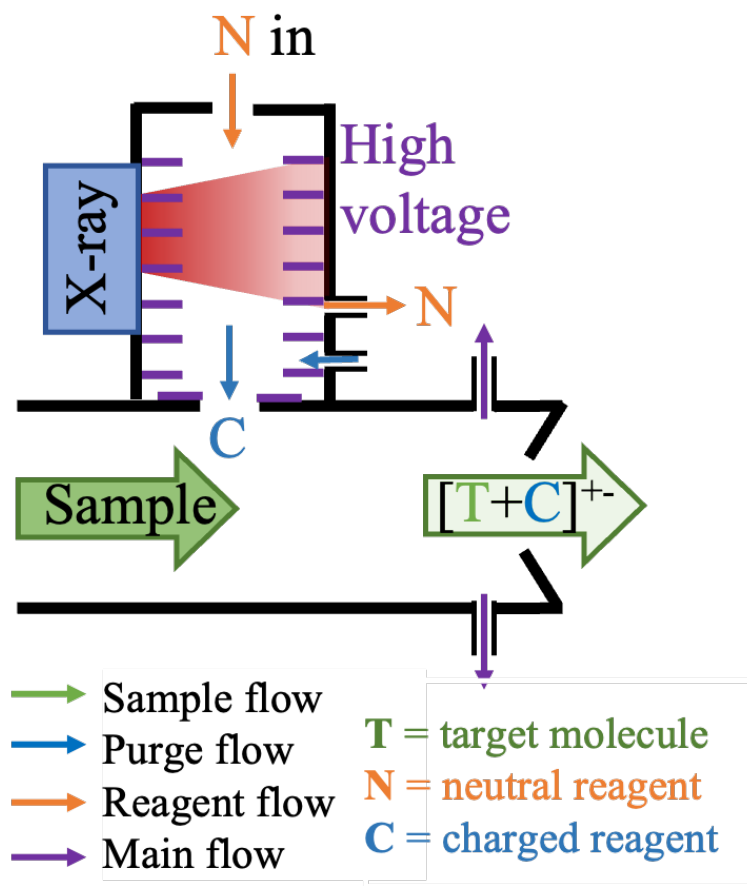
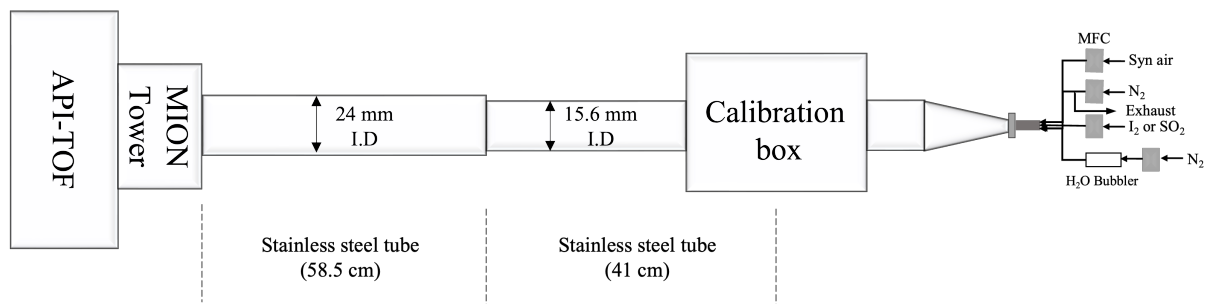
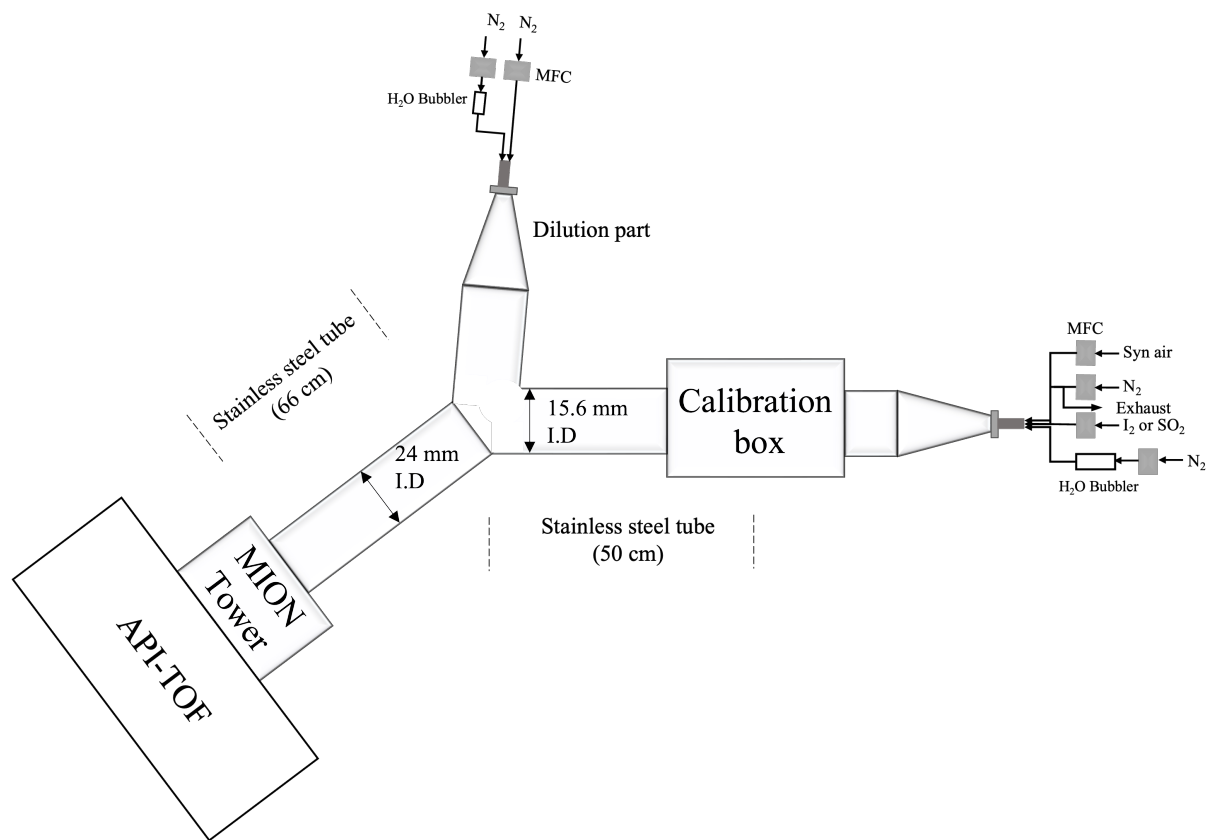


Figure A1. Schematic of the single-source ionisation scheme of the MION2 inlet.



**Figure A2.** Schematic of a typical calibration experiment connecting the MION2 inlet (I.D. 24 mm) with the calibration source (I.D. 15.6 mm).



**Figure A3.** Schematic of the setup for examining the detection humidity effect of  $\text{H}_2\text{SO}_4$ ,  $\text{HOI}$  and  $\text{HO}_2$ .

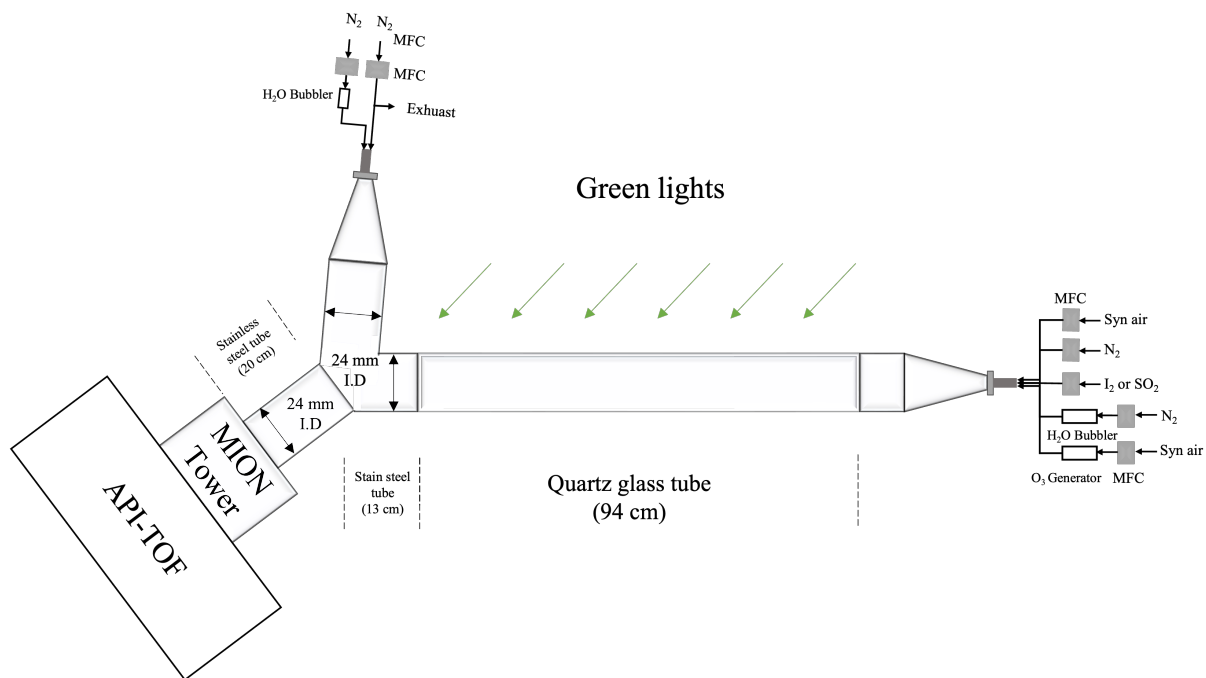


**Figure A4.** Schematic of the experimental setup for iodine chemistry experiments to produce higher concentrations of iodine oxides and oxoacids.



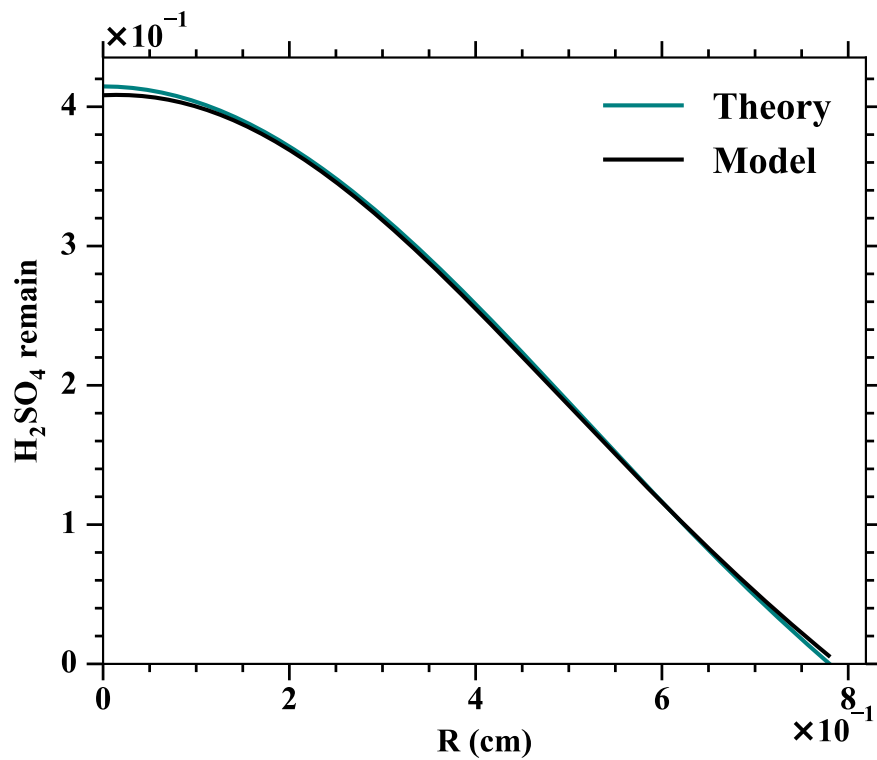


**Figure A5.** Comparison of the H<sub>2</sub>SO<sub>4</sub> profiles at the outlet of a flow reactor. Theoretical values are predicted using Alonso et al. (2016) and the model results indicate the MARFORCE simulation. In both the theoretical prediction and the MARFORCE model, the tube length is assumed to be two meters, the inlet flow is set to 10 slpm and the diffusivity of H<sub>2</sub>SO<sub>4</sub> is set to 0.088 cm<sup>2</sup>s<sup>-1</sup>.

geometry optimised at the  $\omega$ B97X-D/aug-cc-pVTZ-PP level of theory at 298.15 K. Color coding: Iodine = purple, oxygen = red, hydrogen = white, bromine = brown.

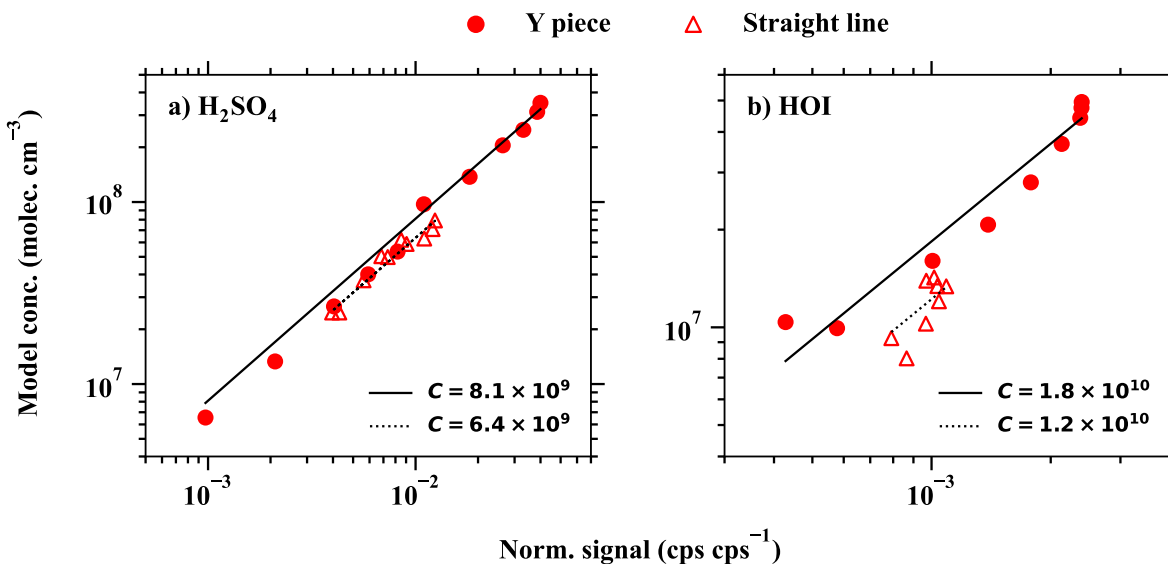


**Figure A6.** Comparing calibration experiments of a)  $\text{H}_2\text{SO}_4$  and HOI with a straight tube (Figure A2) or additionally with a dilution flow (Figure A3). The difference in the calibration coefficients between the two experimental setups is the result of the less accurate representation of fluid dynamics when the dilution flow is added (Figure A3).

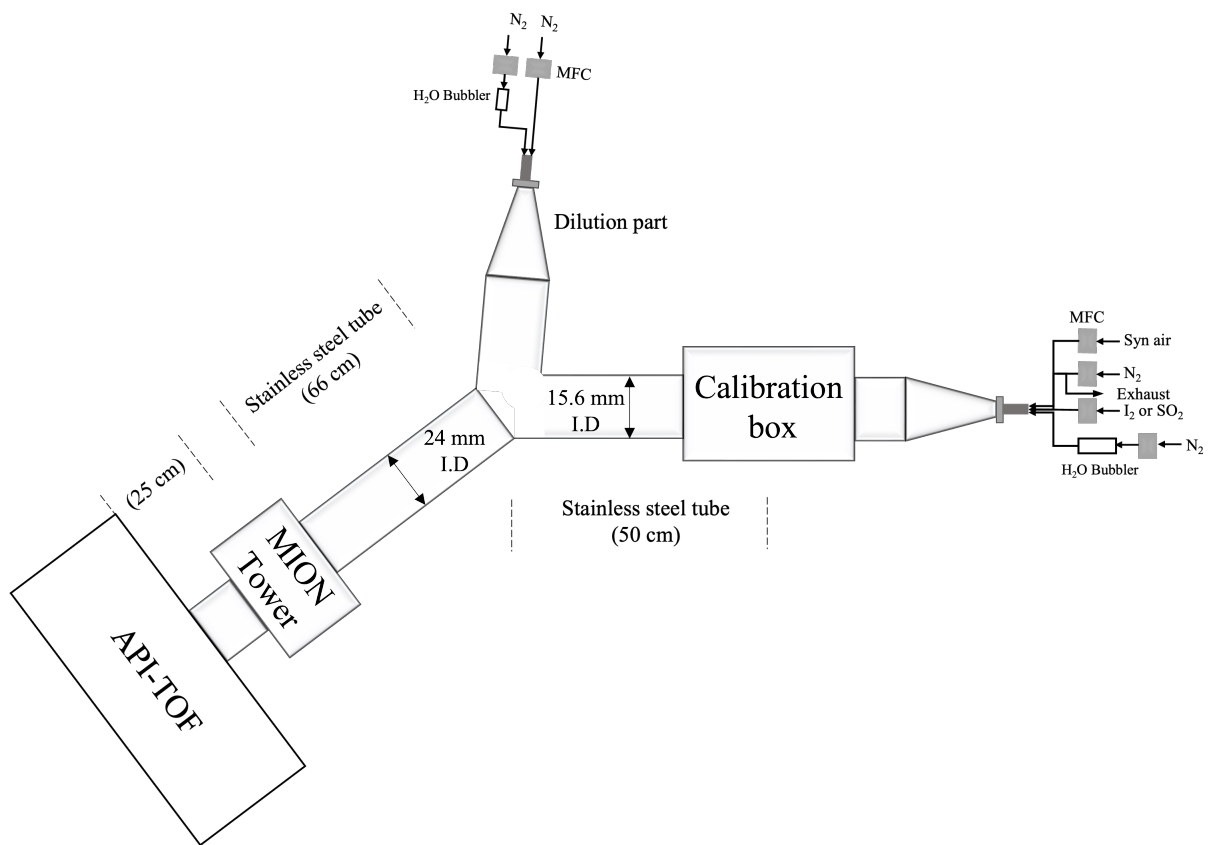


**Figure A7.** Schematic of the setup for H<sub>2</sub>SO<sub>4</sub>, HOI and HO<sub>2</sub> calibration experiment with the tower 2. The difference between this setup and the one shown in Figure A3 is that the position of the MION2 tower is changed from tower 1 to tower 2.

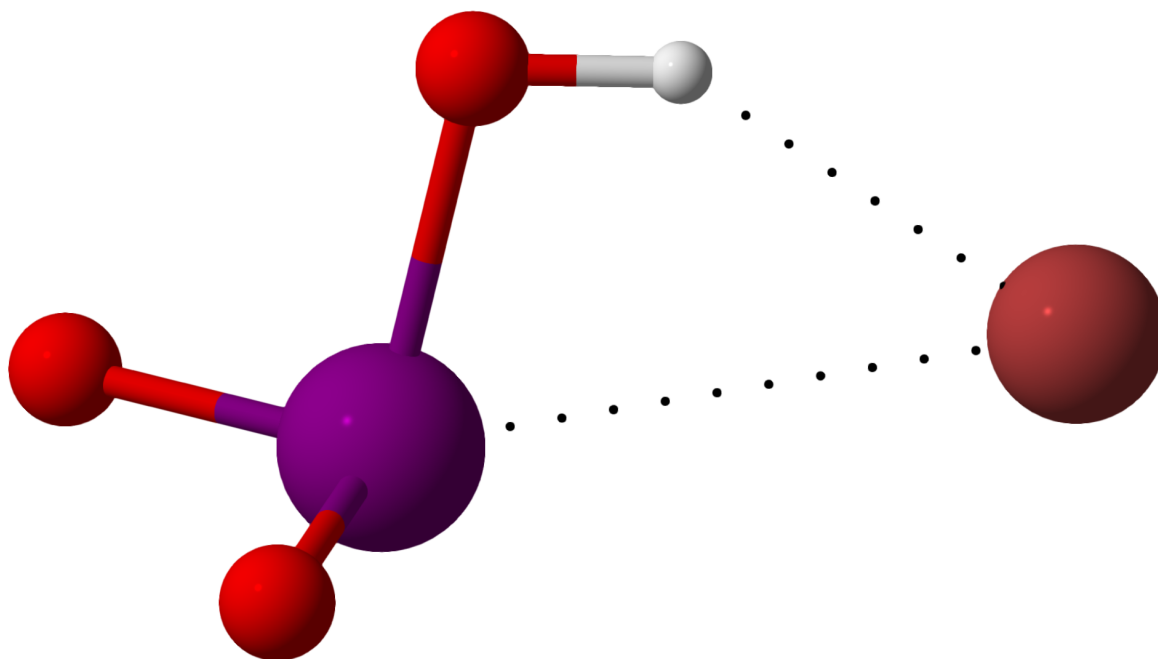


**Figure A8.** The configuration of HIO<sub>3</sub> · Br<sup>-</sup> geometry optimised at the core-sampling device (Karsa Ltd. B97X-D/aug-cc-pVTZ-PP level of theory at 298.15 K. ) which is used for adjusting the sheath and sample flows Color coding: Iodine = purple, oxygen = red, hydrogen = white, bromine = brown.

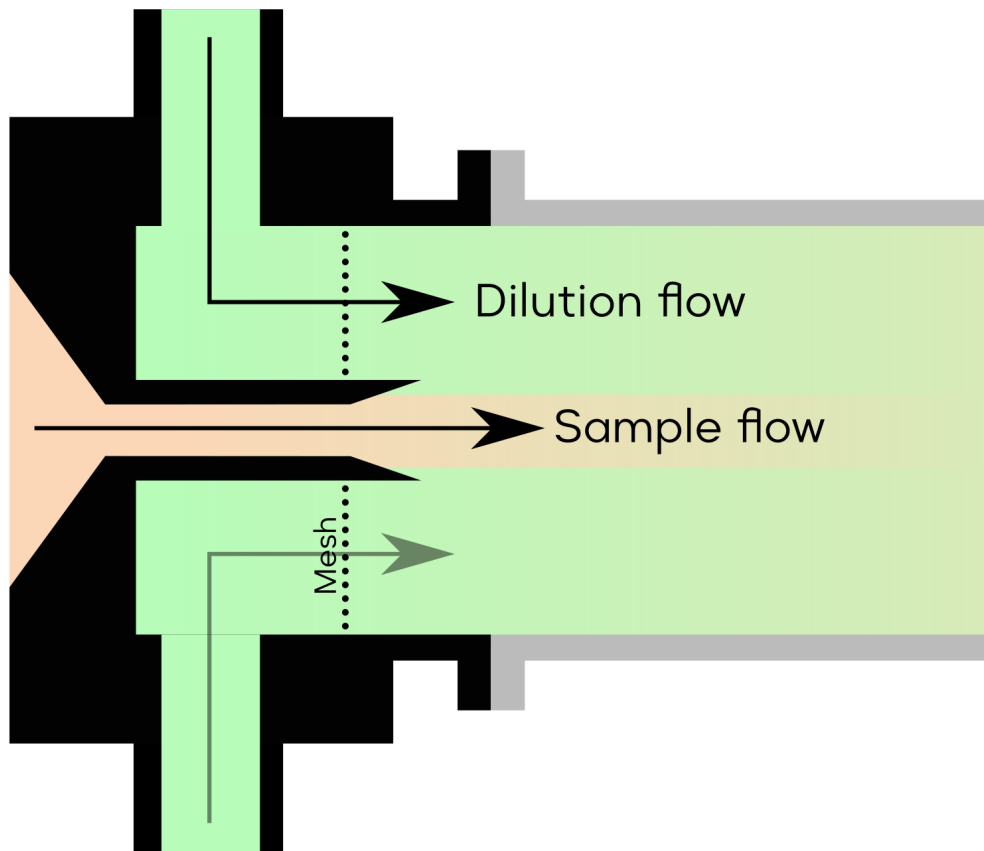


**Figure A9.** The configuration of the core-sampling device (Karsa Ltd.) which is used for adjusting the sheath and sample flows. This core-sampling piece features three ports for the dilution flows which pass through a mesh and further mixed with the sample flow.

**Table A1.** Chemical reactions and the reaction rate coefficients used for H<sub>2</sub>SO<sub>4</sub> and HOI calibration experiments

Chemical reactions	Reaction rate coefficients
H <sub>2</sub> SO <sub>4</sub> calibration:	
1. OH + SO <sub>2</sub> = HSO <sub>3</sub>	<sup>a</sup> $1.32 \times 10^{-12} \times (Temp/300)^{-0.7}$
2. OH + HO <sub>2</sub> = H <sub>2</sub> O + O <sub>2</sub>	<sup>b</sup> $4.8 \times 10^{-11} \times \exp(250/Temp)$
3. HO <sub>2</sub> + HO <sub>2</sub> = H <sub>2</sub> O <sub>2</sub>	<sup>b</sup> $(2.2 \times 10^{-13} \times \exp(600/Temp) + 1.9 \times 10^{-33} \times M \times \exp(980/Temp)) \times KMT06$
4. OH + OH = H <sub>2</sub> O <sub>2</sub>	<sup>c</sup> $2 \times 6.9 \times 10^{-31} \times (Temp/300)^{-0.8} \times p/(1.38 \times 10^{-23})/Temp/10^6$
4. OH + OH = H <sub>2</sub> O	<sup>b</sup> $6.2 \times 10^{-14} \times (Temp/298)^{2.6} \times \exp(945/Temp)$
6. HSO <sub>3</sub> + O <sub>2</sub> = HO <sub>2</sub> + SO <sub>3</sub>	<sup>b</sup> $1.3 \times 10^{-12} \times \exp(-330/Temp)$
7. SO <sub>3</sub> + 2H <sub>2</sub> O = H <sub>2</sub> SO <sub>4</sub>	<sup>b</sup> $3.9 \times 10^{-41} \times \exp(6830.6/Temp)$
HOI calibration:	
1. IO + IO = I + I	<sup>d</sup> $0.11 \times 5.4 \times 10^{-11} \times \exp(180/Temp)$
2. IO + IO = OIO + I	<sup>d</sup> $0.38 \times 5.4 \times 10^{-11} \times \exp(180/Temp)$
3. IO + IO = I <sub>2</sub> O <sub>2</sub>	<sup>d</sup> $0.45 \times 5.4 \times 10^{-11} \times \exp(180/Temp)$
4. I <sub>2</sub> + OH = HOI + I	<sup>e</sup> $2.1 \times 10^{-10}$
5. IO + OIO = I <sub>2</sub> O <sub>3</sub>	<sup>f</sup> $w1a \times \exp(w2a \times Temp)$
6. OIO + OIO = I <sub>2</sub> O <sub>4</sub>	<sup>f</sup> $w1b \times \exp(w2b \times Temp)$
7. IO + OH = HO <sub>2</sub> + I	<del><sup>g</sup><math>1.0 \times 10^{-10}</math></del> <sup>g</sup> $1.0 \times 10^{-10}$
8. HI + OH = H <sub>2</sub> O + I	<sup>b</sup> $1.6 \times 10^{-11} \times \exp(440/Temp)$
9. HOI + OH = H <sub>2</sub> O + IO	<del><sup>h</sup><math>2.0 \times 10^{-13}</math></del> <sup>h</sup> $2.0 \times 10^{-13}$
10. I + HO <sub>2</sub> = HI + O <sub>2</sub>	<sup>i</sup> $1.47 \times 10^{-11} \times \exp(-1090/Temp)$
11. IO + HO <sub>2</sub> = HOI + O <sub>2</sub>	<sup>b</sup> $1.4 \times 10^{-11} \times \exp(540/Temp)$
12. OH + OH = H <sub>2</sub> O <sub>2</sub>	<sup>c</sup> $2 \times 6.9 \times 10^{-31} \times (Temp/300)^{-0.8} \times p/(1.38 \times 10^{-23})/Temp/10^6$
13. OH + OH = H <sub>2</sub> O	<sup>b</sup> $6.2 \times 10^{-14} \times (Temp/298)^{2.6} \times \exp(945/Temp)$
14. OH + HO <sub>2</sub> = H <sub>2</sub> O + O <sub>2</sub>	<sup>b</sup> $4.8 \times 10^{-11} \times \exp(250/Temp)$
15. HO <sub>2</sub> + HO <sub>2</sub> = H <sub>2</sub> O <sub>2</sub>	<sup>b</sup> $2.2 \times 10^{-13} \times KMT06 \times \exp(600/Temp) + 1.9 \times 10^{-33} \times M \times KMT06 \times \exp(980/Temp)$

<sup>a</sup>Wine et al. (1984); <sup>b</sup>Atkinson et al. (2004); <sup>c</sup>Zellner et al. (1988); <sup>d</sup>Bloss et al. (2001); <sup>e</sup>Gilles et al. (1999); <sup>f</sup>Saiz-Lopez et al. (2014);

<sup>g</sup>Bösch (2003); <sup>h</sup>Chameides and Davis (1980); <sup>i</sup>Jenkin et al. (1990).

KMT06 =  $1 + (1.4 \times 10^{-21} \times \exp(2200/Temp) \times [H_2O])$ , [H<sub>2</sub>O] is the absolute water concentration. *M* is the total number of molecules in the atmosphere. *p* is the pressure.

$$w1a = 4.7 \times 10^{-10} - 1.4 \times 10^{-5} \times \exp(-0.75 \times p/1.62265) + 5.51868 \times 10^{-10} \times \exp(-0.75 \times p/199.328);$$

$$w2a = -0.00331 - 0.00514 \times \exp(-0.75 \times p/325.68711) - 0.00444 \times \exp(-0.75 \times p/40.81609);$$

$$w1b = 1.166 \times 10^{-9} - 7.796 \times 10^{-10} \times \exp(-0.75 \times p/22.093) + 1.038 \times 10^{-9} \times \exp(-0.75 \times p/568.154);$$

$$w2b = -0.00813 - 0.00382 \times \exp(-0.75 \times p/45.57591) - 0.00643 \times \exp(-0.75 \times p/417.95061).$$

*Author contributions.* X.-C.H. and J.S. designed and carried out the experiments. J.S. and X.-C.H. wrote the MARFORCE model. J.Z. wrote the documentation of the MARFORCE model. S.I. carried out quantum chemical calculations. N.M.M., M.Koi. and M.M.K. analysed molecular iodine samples. J.K., P.J., M.S. and J.M. provided technical support. X.-C.H. wrote the manuscript with contributions from J.S., N.M.M., P.J. and S.I. Finally, J.K., J.S., M.R., S.I., D.R.W. and M.Kul. commented on and edited the manuscript.

890 *Competing interests.* Paxton Juuti and Jyri Mikkilä work for Karsa, Ltd. Finland. Juha Kangasluoma works partially for Karsa, Ltd. Finland

*Acknowledgements.* We thank the ACCC Flagship funded by the Academy of Finland grant number 337549, the Academy professorship funded by the Academy of Finland (grant no. 302958), Academy of Finland projects no. 331207, 346370, 325656, 316114, 314798, 325647, 341349 and 349659. This project has received funding from the European Research Council under the European Union's Horizon 2020 research and innovation programme under Grant Contract No. 742206 and 101002728. The Arena for the gap analysis of the existing  
895 Arctic Science Co-Operations (AASCO) funded by Prince Albert Foundation Contract No 2859. M.Kul. thanks the Jane and Aatos Erkkö Foundation for providing funding. M.Kul. and X.-C.H thank the Jenny and Antti Wihuri Foundation for funding this research. We also thank Miska Olin, Gustaf Lönn and Heikki Junninen for their helpful discussions and contributions to the MARFORCE model. Simon Patrick O'Meara and Gordon McFiggans are acknowledged for their contributions to the MCM interpreter in the MARFORCE model.

## References

- 900 Agarwal, B., González-Méndez, R., Lanza, M., Sulzer, P., Märk, T. D., Thomas, N., and Mayhew, C. A.: Sensitivity and Selectivity of Switchable Reagent Ion Soft Chemical Ionization Mass Spectrometry for the Detection of Picric Acid, *The Journal of Physical Chemistry A*, 118, 8229–8236, <https://doi.org/10.1021/jp5010192>, 2014.
- Alonso, M., Carsí, M., and Huang, C.-H.: Using the fully developed concentration profile to determine particle penetration in a laminar flow tube, *Journal of Aerosol Science*, 97, 34–37, <https://doi.org/10.1016/j.jaerosci.2016.04.002>, 2016.
- 905 Atkinson, R., Baulch, D. L., Cox, R. A., Crowley, J. N., Hampson, R. F., Hynes, R. G., Jenkin, M. E., Rossi, M. J., and Troe, J.: Evaluated kinetic and photochemical data for atmospheric chemistry: Volume I - gas phase reactions of O<sub>x</sub>, HO<sub>x</sub>, NO<sub>x</sub> and SO<sub>x</sub> species, *Atmospheric Chemistry and Physics*, 4, 1461–1738, <https://doi.org/10.5194/acp-4-1461-2004>, 2004.
- Baccarini, A., Karlsson, L., Dommen, J., Duplessis, P., Vüllers, J., Brooks, I. M., Saiz-Lopez, A., Salter, M., Tjernström, M., Baltensperger, U., Zieger, P., and Schmale, J.: Frequent new particle formation over the high Arctic pack ice by enhanced iodine emissions, *Nature*
- 910 *Communications*, 11, 4924, <https://doi.org/10.1038/s41467-020-18551-0>, 2020.
- Berndt, T., Richters, S., Jokinen, T., Hyttinen, N., Kurtén, T., Otkjær, R. V., Kjaergaard, H. G., Stratmann, F., Herrmann, H., Sipilä, M., Kulmala, M., and Ehn, M.: Hydroxyl radical-induced formation of highly oxidized organic compounds, *Nature Communications*, 7, 13 677, <https://doi.org/10.1038/ncomms13677>, 2016.
- Bloss, W. J., Rowley, D. M., Cox, R. A., and Jones, R. L.: Kinetics and Products of the IO Self-Reaction, *The Journal of Physical Chemistry*
- 915 *A*, 105, 7840–7854, <https://doi.org/10.1021/jp0044936>, 2001.
- Breitenlechner, M., Fischer, L., Hainer, M., Heinritzi, M., Curtius, J., and Hansel, A.: PTR3: An Instrument for Studying the Lifecycle of Reactive Organic Carbon in the Atmosphere, *Analytical Chemistry*, 89, 5824–5831, <https://doi.org/10.1021/acs.analchem.6b05110>, 2017.
- Brophy, P. and Farmer, D. K.: A switchable reagent ion high resolution time-of-flight chemical ionization mass spectrometer for real-time measurement of gas phase oxidized species: characterization from the 2013 southern oxidant and aerosol study, *Atmospheric Measurement*
- 920 *Techniques*, 8, 2945–2959, <https://doi.org/10.5194/amt-8-2945-2015>, 2015.
- Bösch, H.: Upper limits of stratospheric IO and OIO inferred from center-to-limb-darkening-corrected balloon-borne solar occultation visible spectra: Implications for total gaseous iodine and stratospheric ozone, *Journal of Geophysical Research*, 108, 4455, <https://doi.org/10.1029/2002JD003078>, 2003.
- Caldwell, G. W., Masucci, J. A., and Ikonomou, M. G.: Negative ion chemical ionization mass spectrometry—binding of molecules to
- 925 bromide and iodide anions, *Organic Mass Spectrometry*, 24, 8–14, <https://doi.org/10.1002/oms.1210240103>, 1989.
- Chai, J.-D. and Head-Gordon, M.: Long-range corrected hybrid density functionals with damped atom–atom dispersion corrections, *Physical Chemistry Chemical Physics*, 10, 6615, <https://doi.org/10.1039/b810189b>, 2008.
- Chameides, W. L. and Davis, D. D.: Iodine: Its possible role in tropospheric photochemistry, *Journal of Geophysical Research: Oceans*, 85, 7383–7398, <https://doi.org/10.1029/JC085iC12p07383>, 1980.
- 930 Creasey, D. J., Heard, D. E., and Lee, J. D.: Absorption cross-section measurements of water vapour and oxygen at 185 nm. Implications for the calibration of field instruments to measure OH, HO<sub>2</sub> and RO<sub>2</sub> radicals, *Geophysical Research Letters*, 27, 1651–1654, <https://doi.org/10.1029/1999GL011014>, 2000.
- Ehn, M., Thornton, J. A., Kleist, E., Sipilä, M., Junninen, H., Pullinen, I., Springer, M., Rubach, F., Tillmann, R., Lee, B., Lopez-Hilfiker, F., Andres, S., Acir, I.-H., Rissanen, M., Jokinen, T., Schobesberger, S., Kangasluoma, J., Kontkanen, J., Nieminen, T., Kurtén, T., Nielsen,
- 935 L. B., Jørgensen, S., Kjaergaard, H. G., Canagaratna, M., Maso, M. D., Berndt, T., Petäjä, T., Wahner, A., Kerminen, V.-M., Kulmala,



- M., Worsnop, D. R., Wildt, J., and Mentel, T. F.: A large source of low-volatility secondary organic aerosol, *Nature*, 506, 476–479, <https://doi.org/10.1038/nature13032>, 2014.
- Eisele, F. L. and Tanner, D. J.: Measurement of the gas phase concentration of H<sub>2</sub>SO<sub>4</sub> and methane sulfonic acid and estimates of H<sub>2</sub>SO<sub>4</sub> production and loss in the atmosphere, *Journal of Geophysical Research: Atmospheres*, 98, 9001–9010, <https://doi.org/10.1029/93JD00031>, 940 1993.
- Feller, D.: The role of databases in support of computational chemistry calculations, *Journal of Computational Chemistry*, 17, 1571–1586, [https://doi.org/10.1002/\(SICI\)1096-987X\(199610\)17:13<1571::AID-JCC9>3.0.CO;2-P](https://doi.org/10.1002/(SICI)1096-987X(199610)17:13<1571::AID-JCC9>3.0.CO;2-P), 1996.
- Finkenzeller, H., Iyer, S., He, X.-C., Simon, M., Koenig, T. K., Lee, C. F., Valiev, R., Hofbauer, V., Amorim, A., Baalbaki, R., Baccarini, A., Beck, L., Bell, D. M., Caudillo, L., Chen, D., Chiu, R., Chu, B., Dada, L., Duplissy, J., Heinritzi, M., Kempainen, D., Kim, C., Krechmer, 945 J., Kürten, A., Kvashnin, A., Lamkaddam, H., Lee, C. P., Lehtipalo, K., Li, Z., Makhmutov, V., Manninen, H. E., Marie, G., Marten, R., Mauldin, R. L., Mentler, B., Müller, T., Petäjä, T., Philippov, M., Ranjithkumar, A., Rörup, B., Shen, J., Stolzenburg, D., Tauber, C., Tham, Y. J., Tomé, A., Vazquez-Pufleau, M., Wagner, A. C., Wang, D. S., Wang, M., Wang, Y., Weber, S. K., Nie, W., Wu, Y., Xiao, M., Ye, Q., Zauner-Wieczorek, M., Hansel, A., Baltensperger, U., Brioude, J., Curtius, J., Donahue, N. M., Haddad, I. E., Flagan, R. C., Kulmala, M., Kirkby, J., Sipilä, M., Worsnop, D. R., Kurten, T., Rissanen, M., and Volkamer, R.: The gas-phase formation mechanism of iodic acid as 950 an atmospheric aerosol source, *Nature Chemistry*, <https://doi.org/10.1038/s41557-022-01067-z>, 2022.
- Frisch, M. J., Trucks, G. W., Schlegel, H. B., Scuseria, G. E., Robb, M. A., Cheeseman, J. R., Scalmani, G., Barone, V., Petersson, G. A., Nakatsuji, H., Li, X., Caricato, M., Marenich, A. V., Bloino, J., Janesko, B. G., Gomperts, R., Mennucci, B., Hratchian, H. P., Ortiz, J. V., Izmaylov, A. F., Sonnenberg, J. L., Williams, Ding, F., Lipparini, F., Egidi, F., Goings, J., Peng, B., Petrone, A., Henderson, T., Ranasinghe, D., Zakrzewski, V. G., Gao, J., Rega, N., Zheng, G., Liang, W., Hada, M., Ehara, M., Toyota, K., Fukuda, R., Hasegawa, 955 J., Ishida, M., Nakajima, T., Honda, Y., Kitao, O., Nakai, H., Vreven, T., Throssell, K., Montgomery Jr., J. A., Peralta, J. E., Ogliaro, F., Bearpark, M. J., Heyd, J. J., Brothers, E. N., Kudin, K. N., Staroverov, V. N., Keith, T. A., Kobayashi, R., Normand, J., Raghavachari, K., Rendell, A. P., Burant, J. C., Iyengar, S. S., Tomasi, J., Cossi, M., Millam, J. M., Klene, M., Adamo, C., Cammi, R., Ochterski, J. W., Martin, R. L., Morokuma, K., Farkas, O., Foresman, J. B., and Fox, D. J.: *Gaussian 16 Rev. C.01*, 2016.
- Fuller, E. N., Schettler, P. D., and Giddings, J. C.: NEW METHOD FOR PREDICTION OF BINARY GAS-PHASE DIFFUSION COEFFICIENTS, *Industrial & Engineering Chemistry*, 58, 18–27, <https://doi.org/10.1021/ie50677a007>, 960 1966.
- Gilles, M. K., Burkholder, J. B., and Ravishankara, A. R.: Rate coefficients for the reaction of OH with Cl<sub>2</sub>, Br<sub>2</sub>, and I<sub>2</sub> from 235 to 354 K, *International Journal of Chemical Kinetics*, 31, 417–424, [https://doi.org/10.1002/\(SICI\)1097-4601\(1999\)31:6<417::AID-KIN3>3.0.CO;2-A](https://doi.org/10.1002/(SICI)1097-4601(1999)31:6<417::AID-KIN3>3.0.CO;2-A), 1999.
- Gormley, P. and Kennedy, M.: Diffusion from a stream flowing through a cylindrical tube, in: *Proceedings of the Royal Irish Academy. Section A: Mathematical and Physical Sciences*, vol. 52, pp. 163–169, JSTOR, 1948.
- Gálvez, O., Gómez Martín, J. C., Gómez, P. C., Saiz-Lopez, A., and Pacios, L. F.: A theoretical study on the formation of iodine oxide aggregates and monohydrates, *Physical Chemistry Chemical Physics*, 15, 15 572, <https://doi.org/10.1039/c3cp51219c>, 2013.
- Gómez Martín, J. C., Lewis, T. R., Blitz, M. A., Plane, J. M. C., Kumar, M., Francisco, J. S., and Saiz-Lopez, A.: A gas-to-particle conversion mechanism helps to explain atmospheric particle formation through clustering of iodine oxides, *Nature Communications*, 11, 4521, 970 <https://doi.org/10.1038/s41467-020-18252-8>, 2020.
- Gómez Martín, J. C., Lewis, T. R., James, A. D., Saiz-Lopez, A., and Plane, J. M. C.: Insights into the Chemistry of Iodine New Particle Formation: The Role of Iodine Oxides and the Source of Iodic Acid, *Journal of the American Chemical Society*, p. jacs.1c12957, <https://doi.org/10.1021/jacs.1c12957>, 2022.

- Hansel, A., Jordan, A., Holzinger, R., Prazeller, P., Vogel, W., and Lindinger, W.: Proton transfer reaction mass spectrometry: on-line trace gas analysis at the ppb level, *International Journal of Mass Spectrometry and Ion Processes*, 149-150, 609–619, [https://doi.org/10.1016/0168-1176\(95\)04294-U](https://doi.org/10.1016/0168-1176(95)04294-U), 1995.
- Hanson, D. R. and Eisele, F.: Diffusion of H<sub>2</sub>SO<sub>4</sub> in Humidified Nitrogen: Hydrated H<sub>2</sub>SO<sub>4</sub>, *The Journal of Physical Chemistry A*, 104, 1715–1719, <https://doi.org/10.1021/jp993622j>, 2000.
- He, X.-C.: From the measurement of halogenated species to iodine particle formation, Ph.D. thesis, University of Helsinki, Helsinki, <https://helda.helsinki.fi/handle/10138/229173>, 2017.
- He, X.-C., Iyer, S., Sipilä, M., Ylisirniö, A., Peltola, M., Kontkanen, J., Baalbaki, R., Simon, M., Kürten, A., Tham, Y. J., Pesonen, J., Ahonen, L. R., Amanatidis, S., Amorim, A., Baccharini, A., Beck, L., Bianchi, F., Brilke, S., Chen, D., Chiu, R., Curtius, J., Dada, L., Dias, A., Dommen, J., Donahue, N. M., Duplissy, J., El Haddad, I., Finkenzeller, H., Fischer, L., Heinritzi, M., Hofbauer, V., Kangasluoma, J., Kim, C., Koenig, T. K., Kubečka, J., Kvashnin, A., Lamkaddam, H., Lee, C. P., Leiminger, M., Li, Z., Makhmutov, V., Xiao, M., Marten, R., Nie, W., Onnela, A., Partoll, E., Petäjä, T., Salo, V.-T., Schuchmann, S., Steiner, G., Stolzenburg, D., Stozhkov, Y., Tauber, C., Tomé, A., Väisänen, O., Vazquez-Pufleau, M., Volkamer, R., Wagner, A. C., Wang, M., Wang, Y., Wimmer, D., Winkler, P. M., Worsnop, D. R., Wu, Y., Yan, C., Ye, Q., Lehtinen, K., Nieminen, T., Manninen, H. E., Rissanen, M., Schobesberger, S., Lehtipalo, K., Baltensperger, U., Hansel, A., Kerminen, V.-M., Flagan, R. C., Kirkby, J., Kurtén, T., and Kulmala, M.: Determination of the collision rate coefficient between charged iodine acid clusters and iodine acid using the appearance time method, *Aerosol Science and Technology*, 55, 231–242, <https://doi.org/10.1080/02786826.2020.1839013>, 2021a.
- He, X.-C., Tham, Y. J., Dada, L., Wang, M., Finkenzeller, H., Stolzenburg, D., Iyer, S., Simon, M., Kürten, A., Shen, J., Rörup, B., Rissanen, M., Schobesberger, S., Baalbaki, R., Wang, D. S., Koenig, T. K., Jokinen, T., Sarnela, N., Beck, L. J., Almeida, J., Amanatidis, S., Amorim, A., Ataei, F., Baccharini, A., Bertozzi, B., Bianchi, F., Brilke, S., Caudillo, L., Chen, D., Chiu, R., Chu, B., Dias, A., Ding, A., Dommen, J., Duplissy, J., El Haddad, I., Gonzalez Carracedo, L., Granzin, M., Hansel, A., Heinritzi, M., Hofbauer, V., Junninen, H., Kangasluoma, J., Kemppainen, D., Kim, C., Kong, W., Krechmer, J. E., Kvashin, A., Laitinen, T., Lamkaddam, H., Lee, C. P., Lehtipalo, K., Leiminger, M., Li, Z., Makhmutov, V., Manninen, H. E., Marie, G., Marten, R., Mathot, S., Mauldin, R. L., Mentler, B., Möhler, O., Müller, T., Nie, W., Onnela, A., Petäjä, T., Pfeifer, J., Philippov, M., Ranjithkumar, A., Saiz-Lopez, A., Salma, I., Scholz, W., Schuchmann, S., Schulze, B., Steiner, G., Stozhkov, Y., Tauber, C., Tomé, A., Thakur, R. C., Väisänen, O., Vazquez-Pufleau, M., Wagner, A. C., Wang, Y., Weber, S. K., Winkler, P. M., Wu, Y., Xiao, M., Yan, C., Ye, Q., Ylisirniö, A., Zauner-Wieczorek, M., Zha, Q., Zhou, P., Flagan, R. C., Curtius, J., Baltensperger, U., Kulmala, M., Kerminen, V.-M., Kurtén, T., Donahue, N. M., Volkamer, R., Kirkby, J., Worsnop, D. R., and Sipilä, M.: Role of iodine oxoacids in atmospheric aerosol nucleation, *Science*, 371, 589–595, <https://doi.org/10.1126/science.abe0298>, 2021b.
- Hearn, J. D. and Smith, G. D.: A Chemical Ionization Mass Spectrometry Method for the Online Analysis of Organic Aerosols, *Analytical Chemistry*, 76, 2820–2826, <https://doi.org/10.1021/ac049948s>, 2004.
- Hoffmann, T., O’Dowd, C. D., and Seinfeld, J. H.: Iodine oxide homogeneous nucleation: An explanation for coastal new particle production, *Geophysical Research Letters*, 28, 1949–1952, <https://doi.org/10.1029/2000GL012399>, 2001.
- Huey, L. G.: Measurement of trace atmospheric species by chemical ionization mass spectrometry: Speciation of reactive nitrogen and future directions, *Mass Spectrometry Reviews*, 26, 166–184, <https://doi.org/10.1002/mas.20118>, 2007.
- Iyer, S., Lopez-Hilfiker, F., Lee, B. H., Thornton, J. A., and Kurtén, T.: Modeling the Detection of Organic and Inorganic Compounds Using Iodide-Based Chemical Ionization, *The Journal of Physical Chemistry A*, 120, 576–587, <https://doi.org/10.1021/acs.jpca.5b09837>, 2016.

- 1010 Iyer, S., He, X., Hyttinen, N., Kurtén, T., and Rissanen, M. P.: Computational and Experimental Investigation of the Detection of HO<sub>2</sub> Radical and the Products of Its Reaction with Cyclohexene Ozonolysis Derived RO<sub>2</sub> Radicals by an Iodide-Based Chemical Ionization Mass Spectrometer, *The Journal of Physical Chemistry A*, 121, 6778–6789, <https://doi.org/10.1021/acs.jpca.7b01588>, 2017.
- Jenkin, M. E., Cox, R. A., Mellouki, A., Le Bras, G., and Poulet, G.: Kinetics of the reaction of iodine atoms with hydroperoxy radicals, *The Journal of Physical Chemistry*, 94, 2927–2934, <https://doi.org/10.1021/j100370a036>, 1990.
- 1015 Jenkin, M. E., Saunders, S. M., and Pilling, M. J.: The tropospheric degradation of volatile organic compounds: a protocol for mechanism development, *Atmospheric Environment*, 31, 81–104, [https://doi.org/10.1016/S1352-2310\(96\)00105-7](https://doi.org/10.1016/S1352-2310(96)00105-7), 1997.
- Jokinen, T., Sipilä, M., Junninen, H., Ehn, M., Lönn, G., Hakala, J., Petäjä, T., Mauldin, R. L., Kulmala, M., and Worsnop, D. R.: Atmospheric sulphuric acid and neutral cluster measurements using CI-API-TOF, *Atmospheric Chemistry and Physics*, 12, 4117–4125, <https://doi.org/10.5194/acp-12-4117-2012>, 2012.
- 1020 Jordan, A., Haidacher, S., Hanel, G., Hartungen, E., Herbig, J., Märk, L., Schottkowsky, R., Seehauser, H., Sulzer, P., and Märk, T.: An online ultra-high sensitivity Proton-transfer-reaction mass-spectrometer combined with switchable reagent ion capability (PTR+SRI-MS), *International Journal of Mass Spectrometry*, 286, 32–38, <https://doi.org/10.1016/j.ijms.2009.06.006>, 2009.
- Junninen, H., Ehn, M., Petäjä, T., Luosujärvi, L., Kotiaho, T., Kostianen, R., Rohner, U., Gonin, M., Fuhrer, K., Kulmala, M., and Worsnop, D. R.: A high-resolution mass spectrometer to measure atmospheric ion composition, *Atmospheric Measurement Techniques*, 3, 1039–1053, <https://doi.org/10.5194/amt-3-1039-2010>, 2010.
- 1025 Kendall, R. A., Dunning, T. H., and Harrison, R. J.: Electron affinities of the first-row atoms revisited. Systematic basis sets and wave functions, *The Journal of Chemical Physics*, 96, 6796–6806, <https://doi.org/10.1063/1.462569>, 1992.
- Kercher, J. P., Riedel, T. P., and Thornton, J. A.: Chlorine activation by N<sub>2</sub>O<sub>5</sub>: simultaneous, in situ detection of ClNO<sub>2</sub> and N<sub>2</sub>O<sub>5</sub> by chemical ionization mass spectrometry, *Atmos. Meas. Tech.*, 2, 193–204, <https://doi.org/10.5194/amt-2-193-2009>, 2009.
- 1030 Kirkby, J., Curtius, J., Almeida, J., Dunne, E., Duplissy, J., Ehrhart, S., Franchin, A., Gagné, S., Ickes, L., Kürten, A., Kupc, A., Metzger, A., Riccobono, F., Rondo, L., Schobesberger, S., Tsagkogeorgas, G., Wimmer, D., Amorim, A., Bianchi, F., Breitenlechner, M., David, A., Dommen, J., Downard, A., Ehn, M., Flagan, R. C., Haider, S., Hansel, A., Hauser, D., Jud, W., Junninen, H., Kreissl, F., Kvashin, A., Laaksonen, A., Lehtipalo, K., Lima, J., Lovejoy, E. R., Makhmutov, V., Mathot, S., Mikkilä, J., Minginette, P., Mogo, S., Nieminen, T., Onnela, A., Pereira, P., Petäjä, T., Schnitzhofer, R., Seinfeld, J. H., Sipilä, M., Stozhkov, Y., Stratmann, F., Tomé, A., Vanhanen, J., Viisanen, Y., Vrtala, A., Wagner, P. E., Walther, H., Weingartner, E., Wex, H., Winkler, P. M., Carslaw, K. S., Worsnop, D. R., Baltensperger, U., and Kulmala, M.: Role of sulphuric acid, ammonia and galactic cosmic rays in atmospheric aerosol nucleation, *Nature*, 476, 429–433, <https://doi.org/10.1038/nature10343>, 2011.
- Kürten, A., Rondo, L., Ehrhart, S., and Curtius, J.: Calibration of a Chemical Ionization Mass Spectrometer for the Measurement of Gaseous Sulfuric Acid, *The Journal of Physical Chemistry A*, 116, 6375–6386, <https://doi.org/10.1021/jp212123n>, 2012.
- 1040 Lagg, A., Taucher, J., Hansel, A., and Lindinger, W.: Applications of proton transfer reactions to gas analysis, *International Journal of Mass Spectrometry and Ion Processes*, 134, 55–66, [https://doi.org/10.1016/0168-1176\(94\)03965-8](https://doi.org/10.1016/0168-1176(94)03965-8), 1994.
- Laskin, J., Laskin, A., and Nizkorodov, S. A.: Mass Spectrometry Analysis in Atmospheric Chemistry, *Analytical Chemistry*, 90, 166–189, <https://doi.org/10.1021/acs.analchem.7b04249>, 2018.
- Lee, B. H., Lopez-Hilfiker, F. D., Mohr, C., Kurtén, T., Worsnop, D. R., and Thornton, J. A.: An Iodide-Adduct High-Resolution Time-of-Flight Chemical-Ionization Mass Spectrometer: Application to Atmospheric Inorganic and Organic Compounds, *Environmental Science & Technology*, 48, 6309–6317, <https://doi.org/10.1021/es500362a>, 2014.

- Liao, J., Huey, L. G., Liu, Z., Tanner, D. J., Cantrell, C. A., Orlando, J. J., Flocke, F. M., Shepson, P. B., Weinheimer, A. J., Hall, S. R., Ullmann, K., Beine, H. J., Wang, Y., Ingall, E. D., Stephens, C. R., Hornbrook, R. S., Apel, E. C., Riemer, D., Fried, A., Mauldin, R. L., Smith, J. N., Staebler, R. M., Neuman, J. A., and Nowak, J. B.: High levels of molecular chlorine in the Arctic atmosphere, *Nature Geoscience*, 7, 91–94, <https://doi.org/10.1038/ngeo2046>, 2014.
- 1050 Liu, L., Li, S., Zu, H., and Zhang, X.: Unexpectedly significant stabilizing mechanism of iodic acid on iodine acid nucleation under different atmospheric conditions, *Science of The Total Environment*, 859, 159832, <https://doi.org/10.1016/j.scitotenv.2022.159832>, 2023.
- Lopez-Hilfiker, F. D., Iyer, S., Mohr, C., Lee, B. H., D'Ambro, E. L., Kurtén, T., and Thornton, J. A.: Constraining the sensitivity of iodide adduct chemical ionization mass spectrometry to multifunctional organic molecules using the collision limit and thermodynamic stability of iodide ion adducts, *Atmospheric Measurement Techniques*, 9, 1505–1512, <https://doi.org/10.5194/amt-9-1505-2016>, 2016.
- 1055 Mielke, L. H., Furgeson, A., and Osthoff, H. D.: Observation of ClNO<sub>2</sub> in a Mid-Continental Urban Environment, *Environmental Science & Technology*, 45, 8889–8896, <https://doi.org/10.1021/es201955u>, 2011.
- Mishra, S., Singh, V., Jain, A., and Verma, K. K.: Determination of iodide by derivatization to 4-iodo-N,N-dimethylaniline and gas chromatography–mass spectrometry, *The Analyst*, 125, 459–464, <https://doi.org/10.1039/a908363d>, 2000.
- 1060 Munson, M. S. B. and Field, F. H.: Chemical Ionization Mass Spectrometry. I. General Introduction, *Journal of the American Chemical Society*, 88, 2621–2630, <https://doi.org/10.1021/ja00964a001>, 1966.
- Neese, F.: The ORCA program system: The ORCA program system, *Wiley Interdisciplinary Reviews: Computational Molecular Science*, 2, 73–78, <https://doi.org/10.1002/wcms.81>, 2012.
- O'Dowd, C. D., Jimenez, J. L., Bahreini, R., Flagan, R. C., Seinfeld, J. H., Hämeri, K., Pirjola, L., Kulmala, M., Jennings, S. G., and Hoffmann, T.: Marine aerosol formation from biogenic iodine emissions, *Nature*, 417, 632–636, <https://doi.org/10.1038/nature00775>, 2002.
- 1065 O'Meara, S. P., Xu, S., Topping, D., Alfarra, M. R., Capes, G., Lowe, D., Shao, Y., and McFiggans, G.: PyCHAM (v2.1.1): a Python box model for simulating aerosol chambers, *Geoscientific Model Development*, 14, 675–702, <https://doi.org/10.5194/gmd-14-675-2021>, 2021.
- Pan, Y., Zhang, Q., Zhou, W., Zou, X., Wang, H., Huang, C., Shen, C., and Chu, Y.: Detection of Ketones by a Novel Technology: Dipolar Proton Transfer Reaction Mass Spectrometry (DP-PTR-MS), *Journal of the American Society for Mass Spectrometry*, 28, 873–879, <https://doi.org/10.1007/s13361-017-1638-7>, 2017.
- 1070 Passananti, M., Zapadinsky, E., Zanca, T., Kangasluoma, J., Mylly, N., Rissanen, M. P., Kurtén, T., Ehn, M., Attoui, M., and Vehkamäki, H.: How well can we predict cluster fragmentation inside a mass spectrometer?, *Chemical Communications*, 55, 5946–5949, <https://doi.org/10.1039/C9CC02896J>, 2019.
- 1075 Peterson, K. A., Figgen, D., Goll, E., Stoll, H., and Dolg, M.: Systematically convergent basis sets with relativistic pseudopotentials. II. Small-core pseudopotentials and correlation consistent basis sets for the post-*d* group 16–18 elements, *The Journal of Chemical Physics*, 119, 11113–11123, <https://doi.org/10.1063/1.1622924>, 2003.
- Riplinger, C. and Neese, F.: An efficient and near linear scaling pair natural orbital based local coupled cluster method, *The Journal of Chemical Physics*, 138, 034106, <https://doi.org/10.1063/1.4773581>, 2013.
- 1080 Riplinger, C., Sandhoefer, B., Hansen, A., and Neese, F.: Natural triple excitations in local coupled cluster calculations with pair natural orbitals, *The Journal of Chemical Physics*, 139, 134101, <https://doi.org/10.1063/1.4821834>, 2013.
- Rissanen, M. P., Mikkilä, J., Iyer, S., and Hakala, J.: Multi-scheme chemical ionization inlet (MION) for fast switching of reagent ion chemistry in atmospheric pressure chemical ionization mass spectrometry (CIMS) applications, *Atmospheric Measurement Techniques*, 12, 6635–6646, <https://doi.org/10.5194/amt-12-6635-2019>, 2019.

- 1085 Saiz-Lopez, A., Fernandez, R. P., Ordóñez, C., Kinnison, D. E., Gómez Martín, J. C., Lamarque, J.-F., and Tilmes, S.: Iodine chemistry in the troposphere and its effect on ozone, *Atmospheric Chemistry and Physics*, 14, 13 119–13 143, <https://doi.org/10.5194/acp-14-13119-2014>, 2014.
- Sanchez, J., Tanner, D. J., Chen, D., Huey, L. G., and Ng, N. L.: A new technique for the direct detection of HO<sub>2</sub> radicals using bromide chemical ionization mass spectrometry (Br-CIMS): initial characterization, *Atmospheric Measurement Techniques*, 9, 3851–3861, <https://doi.org/10.5194/amt-9-3851-2016>, 2016.
- 1090 Saunders, S. M., Jenkin, M. E., Derwent, R. G., and Pilling, M. J.: Protocol for the development of the Master Chemical Mechanism, MCM v3 (Part A): tropospheric degradation of non-aromatic volatile organic compounds, *Atmospheric Chemistry and Physics*, 3, 161–180, <https://doi.org/10.5194/acp-3-161-2003>, 2003.
- Shen, J. and He, X.-C.: MARFORCE-Flowtube model, <https://github.com/momo-catcat/MARFORCE-flowtube>, 2023.
- 1095 Sherwen, T., Evans, M. J., Carpenter, L. J., Andrews, S. J., Lidster, R. T., Dix, B., Koenig, T. K., Sinreich, R., Ortega, I., Volkamer, R., Saiz-Lopez, A., Prados-Roman, C., Mahajan, A. S., and Ordóñez, C.: Iodine’s impact on tropospheric oxidants: a global model study in GEOS-Chem, *Atmospheric Chemistry and Physics*, 16, 1161–1186, <https://doi.org/10.5194/acp-16-1161-2016>, 2016.
- Sipilä, M., Sarnela, N., Jokinen, T., Henschel, H., Junninen, H., Kontkanen, J., Richters, S., Kangasluoma, J., Franchin, A., Peräkylä, O., Rissanen, M. P., Ehn, M., Vehkamäki, H., Kurten, T., Berndt, T., Petäjä, T., Worsnop, D., Ceburnis, D., Kerminen, V.-M., Kulmala, M., and O’Dowd, C.: Molecular-scale evidence of aerosol particle formation via sequential addition of HIO<sub>3</sub>, *Nature*, 537, 532–534, <https://doi.org/10.1038/nature19314>, 2016.
- 1100 Smith, D. and Španěl, P.: Selected ion flow tube mass spectrometry (SIFT-MS) for on-line trace gas analysis, *Mass Spectrometry Reviews*, 24, 661–700, <https://doi.org/10.1002/mas.20033>, 2005.
- Tham, Y. J., He, X.-C., Li, Q., Cuevas, C. A., Shen, J., Kalliokoski, J., Yan, C., Iyer, S., Lehmusjärvi, T., Jang, S., Thakur, R. C., Beck, L., Kempainen, D., Olin, M., Sarnela, N., Mikkilä, J., Hakala, J., Marbouti, M., Yao, L., Li, H., Huang, W., Wang, Y., Wimmer, D., Zha, Q., Virkanen, J., Spain, T. G., O’Doherty, S., Jokinen, T., Bianchi, F., Petäjä, T., Worsnop, D. R., Mauldin, R. L., Ovadnevaite, J., Ceburnis, D., Maier, N. M., Kulmala, M., O’Dowd, C., Dal Maso, M., Saiz-Lopez, A., and Sipilä, M.: Direct field evidence of autocatalytic iodine release from atmospheric aerosol, *Proceedings of the National Academy of Sciences*, 118, e2009951 118, <https://doi.org/10.1073/pnas.2009951118>, 2021.
- 1110 Thornton, J. A., Kercher, J. P., Riedel, T. P., Wagner, N. L., Cozic, J., Holloway, J. S., Dubé, W. P., Wolfe, G. M., Quinn, P. K., Middlebrook, A. M., Alexander, B., and Brown, S. S.: A large atomic chlorine source inferred from mid-continental reactive nitrogen chemistry, *Nature*, 464, 271–274, <https://doi.org/10.1038/nature08905>, 2010.
- Veres, P., Roberts, J. M., Warneke, C., Welsh-Bon, D., Zahniser, M., Herndon, S., Fall, R., and de Gouw, J.: Development of negative-ion proton-transfer chemical-ionization mass spectrometry (NI-PT-CIMS) for the measurement of gas-phase organic acids in the atmosphere, *International Journal of Mass Spectrometry*, 274, 48–55, <https://doi.org/10.1016/j.ijms.2008.04.032>, 2008.
- 1115 Wang, M., He, X.-C., Finkenzeller, H., Iyer, S., Chen, D., Shen, J., Simon, M., Hofbauer, V., Kirkby, J., Curtius, J., Maier, N., Kurtén, T., Worsnop, D. R., Kulmala, M., Rissanen, M., Volkamer, R., Tham, Y. J., Donahue, N. M., and Sipilä, M.: Measurement of iodine species and sulfuric acid using bromide chemical ionization mass spectrometers, *Atmospheric Measurement Techniques*, 14, 4187–4202, <https://doi.org/10.5194/amt-14-4187-2021>, 2021a.
- 1120 Wang, S., McNamara, S. M., Moore, C. W., Obrist, D., Steffen, A., Shepson, P. B., Staebler, R. M., Raso, A. R. W., and Pratt, K. A.: Direct detection of atmospheric atomic bromine leading to mercury and ozone depletion, *Proceedings of the National Academy of Sciences*, 116, 14 479–14 484, <https://doi.org/10.1073/pnas.1900613116>, 2019.

- Wang, X., Jacob, D. J., Downs, W., Zhai, S., Zhu, L., Shah, V., Holmes, C. D., Sherwen, T., Alexander, B., Evans, M. J., Eastham, S. D., Neuman, J. A., Veres, P. R., Koenig, T. K., Volkamer, R., Huey, L. G., Bannan, T. J., Percival, C. J., Lee, B. H., and Thornton, J. A.:  
1125 Global tropospheric halogen (Cl, Br, I) chemistry and its impact on oxidants, *Atmospheric Chemistry and Physics*, 21, 13 973–13 996, <https://doi.org/10.5194/acp-21-13973-2021>, 2021b.
- Weigend, F. and Ahlrichs, R.: Balanced basis sets of split valence, triple zeta valence and quadruple zeta valence quality for H to Rn: Design and assessment of accuracy, *Physical Chemistry Chemical Physics*, 7, 3297, <https://doi.org/10.1039/b508541a>, 2005.
- Westmore, J. B. and Alauddin, M. M.: Ammonia chemical ionization mass spectrometry, *Mass Spectrometry Reviews*, 5, 381–465,  
1130 <https://doi.org/10.1002/mas.1280050403>, 1986.
- Wine, P. H., Thompson, R. J., Ravishankara, A. R., Semmes, D. H., Gump, C. A., Torabi, A., and Nicovich, J. M.: Kinetics of the reaction  $\text{OH} + \text{SO}_2 + \text{M} \rightarrow \text{HOSO}_2 + \text{M}$ . Temperature and pressure dependence in the fall-off region, *The Journal of Physical Chemistry*, 88, 2095–2104, <https://doi.org/10.1021/j150654a031>, 1984.
- Woodward-Massey, R., Taha, Y. M., Moussa, S. G., and Osthoff, H. D.: Comparison of negative-ion proton-transfer with iodide ion  
1135 chemical ionization mass spectrometry for quantification of isocyanic acid in ambient air, *Atmospheric Environment*, 98, 693–703, <https://doi.org/10.1016/j.atmosenv.2014.09.014>, 2014.
- Zellner, R., Ewig, F., Paschke, R., and Wagner, G.: Pressure and temperature dependence of the gas-phase recombination of hydroxyl radicals, *The Journal of Physical Chemistry*, 92, 4184–4190, <https://doi.org/10.1021/j100325a038>, 1988.
- Zhang, R., Xie, H.-B., Ma, F., Chen, J., Iyer, S., Simon, M., Heinritzi, M., Shen, J., Tham, Y. J., Kurtén, T., Worsnop, D. R., Kirkby, J.,  
1140 Curtius, J., Sipilä, M., Kulmala, M., and He, X.-C.: Critical Role of Iodous Acid in Neutral Iodine Oxoacid Nucleation, *Environmental Science & Technology*, 56, 14 166–14 177, <https://doi.org/10.1021/acs.est.2c04328>, 2022.